2019-06

A SYSTEM ARCHITECTURE OF A MIMO OPTICAL SYSTEM TO RAPIDLY STREAM ENCODED DATA IN THE TACTICAL AND MARITIME ENVIRONMENT

Stewart, Eric R.

Monterey, CA; Naval Postgraduate School

NAVAL POSTGRADUATE SCHOOL

MONTEREY, CALIFORNIA

THESIS

A SYSTEM ARCHITECTURE OF A MIMO OPTICAL SYSTEM TO RAPIDLY STREAM ENCODED DATA IN THE TACTICAL AND MARITIME ENVIRONMENT

by

Eric R. Stewart

June 2019

Thesis Advisor: Raymond R. Buettner Jr.
Co-Advisor: Gregory A. Miller
Second Reader: Peter R. Ateshian

Approved for public release. Distribution is unlimited.

THIS PAGE INTENTIONALLY LEFT BLANK

REPORT DOCUMENTATION PAGE				*Form Approved OMB No. 0704-0188*
Public reporting burden for this collection of information is estimated to average 1 hour per response, including the time for reviewing instruction, searching existing data sources, gathering and maintaining the data needed, and completing and reviewing the collection of information. Send comments regarding this burden estimate or any other aspect of this collection of information, including suggestions for reducing this burden, to Washington headquarters Services, Directorate for Information Operations and Reports, 1215 Jefferson Davis Highway, Suite 1204, Arlington, VA 22202-4302, and to the Office of Management and Budget, Paperwork Reduction Project (0704-0188) Washington, DC 20503.				
1. AGENCY USE ONLY ***(Leave blank)***	**2. REPORT DATE** June 2019	**3. REPORT TYPE AND DATES COVERED** Master's thesis		
4. TITLE AND SUBTITLE A SYSTEM ARCHITECTURE OF A MIMO OPTICAL SYSTEM TO RAPIDLY STREAM ENCODED DATA IN THE TACTICAL AND MARITIME ENVIRONMENT				**5. FUNDING NUMBERS**
6. AUTHOR(S) Eric R. Stewart				
7. PERFORMING ORGANIZATION NAME(S) AND ADDRESS(ES) Naval Postgraduate School Monterey, CA 93943-5000				**8. PERFORMING ORGANIZATION REPORT NUMBER**
9. SPONSORING / MONITORING AGENCY NAME(S) AND ADDRESS(ES) N/A				**10. SPONSORING / MONITORING AGENCY REPORT NUMBER**
11. SUPPLEMENTARY NOTES The views expressed in this thesis are those of the author and do not reflect the official policy or position of the Department of Defense or the U.S. Government.				
12a. DISTRIBUTION / AVAILABILITY STATEMENT Approved for public release. Distribution is unlimited.				**12b. DISTRIBUTION CODE** A

13. ABSTRACT (maximum 200 words)

The National Defense Strategy (NDS) has highlighted the need to be prepared to compete with near-peer competitors. Specifically, the Marine Corps has a critical requirement for resilient and survivable networks capable of operating in contested and denied environments. The free space optical communication (FSOC) channel provides opportunity to mitigate many electronic attack (EA) threats. This thesis describes a system architecture that is capable of mitigating the challenging effects of the FSOC channel. Model-based systems engineering (MBSE) tools and a discrete event simulation are used to model the operation of a multiple-input, multiple-output (MIM) FSOC system. A full factorial design of experiments is used to explore the breadth of the design space. Statistical analysis is applied to the simulation's outputs to identify the design decisions that are most critical. This study employs a tradeoff analysis between the bit error rate (BER), transmission rate, and power consumption to identify candidate architectures. There are two main conclusions in this thesis. Firstly, the error correction capacity of the coding scheme must increase as atmospheric turbulence increases. Secondly, as the laser array increases beyond eight independent channels, the system is capable of mitigating the negative effects of the FSOC channel. This concept merits further development to provide critical communications capabilities in a contested environment.

14. SUBJECT TERMS systems engineering, information sciences, free space optics, MIMO, systems architecture, low probability of detection, LPD, LPI			**15. NUMBER OF PAGES** 141
			16. PRICE CODE
17. SECURITY CLASSIFICATION OF REPORT Unclassified	**18. SECURITY CLASSIFICATION OF THIS PAGE** Unclassified	**19. SECURITY CLASSIFICATION OF ABSTRACT** Unclassified	**20. LIMITATION OF ABSTRACT** UU

NSN 7540-01-280-5500

Standard Form 298 (Rev. 2-89)
Prescribed by ANSI Std. 239-18

THIS PAGE INTENTIONALLY LEFT BLANK

Approved for public release. Distribution is unlimited.

A SYSTEM ARCHITECTURE OF A MIMO OPTICAL SYSTEM TO RAPIDLY STREAM ENCODED DATA IN THE TACTICAL AND MARITIME ENVIRONMENT

Eric R. Stewart
Major, United States Marine Corps
BS, Northwestern University, 2001
MA, Webster University, 2013

Submitted in partial fulfillment of the
requirements for the degrees of

MASTER OF SCIENCE IN INFORMATION WARFARE SYSTEMS ENGINEERING

and

MASTER OF SCIENCE IN SYSTEMS ENGINEERING

from the

NAVAL POSTGRADUATE SCHOOL
June 2019

Approved by: Raymond R. Buettner Jr.
Advisor

Gregory A. Miller
Co-Advisor

Peter R. Ateshian
Second Reader

Dan C. Boger
Chair, Department of Information Sciences

Ronald E. Giachetti
Chair, Department of Systems Engineering

THIS PAGE INTENTIONALLY LEFT BLANK

ABSTRACT

The National Defense Strategy (NDS) has highlighted the need to be prepared to compete with near-peer competitors. Specifically, the Marine Corps has a critical requirement for resilient and survivable networks capable of operating in contested and denied environments. The free space optical communication (FSOC) channel provides opportunity to mitigate many electronic attack (EA) threats. This thesis describes a system architecture that is capable of mitigating the challenging effects of the FSOC channel. Model-based systems engineering (MBSE) tools and a discrete event simulation are used to model the operation of a multiple-input, multiple-output (MIM) FSOC system. A full factorial design of experiments is used to explore the breadth of the design space. Statistical analysis is applied to the simulation's outputs to identify the design decisions that are most critical. This study employs a tradeoff analysis between the bit error rate (BER), transmission rate, and power consumption to identify candidate architectures. There are two main conclusions in this thesis. Firstly, the error correction capacity of the coding scheme must increase as atmospheric turbulence increases. Secondly, As the laser array increases beyond eight independent channels, the system is capable of mitigating the negative effects of the FSOC channel. This concept merits further development to provide critical communications capabilities in a contested environment.

THIS PAGE INTENTIONALLY LEFT BLANK

TABLE OF CONTENTS

THIS PAGE INTENTIONALLY LEFT BLANK

LIST OF FIGURES

THIS PAGE INTENTIONALLY LEFT BLANK

LIST OF TABLES

LIST OF ACRONYMS AND ABBREVIATIONS

ANOVA	analysis of variance
BER	bit error rate
BPPM	binary pulse position modulation
C2	command and control
CSI	channel state information
D2E2	denied, degraded, and exploited environments
DARPA	Defense Advanced Research Projects Agency
DOD	Department of Defense
DOE	design of experiments
DON	Department of the Navy
DRM	design reference mission
DSE	design space exploration
EAB	expeditionary advanced base
EABO	Expeditionary Advanced Base Operations
EM	electromagnetic
FOC	fiber optic communications
FOCAL	free-space optical communications airborne link
FSO	free space optics
FSOC	free space optics communication
HF	high frequency
JLTV	Joint Light Tactical Vehicle
Kbps	kilo-bits per second
LAR	light armored reconnaissance
LAV	Light Armored Vehicle
LOCE	Littoral Operations in a Contested Environment
LOS	line-of-sight
LPD	low probability of detection
LPE	low probability of exploitation
LPI	low probability of interception

Mbps	mega-bits per second
MCCDC	Marine Corps Combat Development Command
MIMO	multiple-input multiple-output
MISO	multiple-input single-output
MIT	Massachusetts Institute of Technology
MOC	Marine Corps Operating Concept
MOE	measures of effectiveness
MOP	measures of performance
NDS	National Defense Strategy
NIWC	Naval Information Warfare Center
NLOS	non-line-of-sight
NMS	National Military Strategy
OOK	on-off keying
ORCA	Optical RF Communications Adjunct
OSI	Open Systems Interconnection
PAT	pointing, acquisition, and tracking
PPM	pulse position modulation
RF	radio frequency
ROMO	range of military operations
SATCOM	satellite communications
SE	systems engineering
SECDEF	Secretary of Defense
SI	scintillation index
SIMO	single-input multiple-output
SISO	single-input single-output
SM	spatial modulation
SNR	signal-to-noise ratio
SSK	space shift keying
TALON	Tactical Line-of-Sight Optical communications Network
TCP/IP	transmission control protocol/internet protocol
UHF	ultra high frequency

USA	United States Army
USAF	United States Air Force
USMC	United States Marine Corps
USN	United States Navy
VHF	very high frequency

THIS PAGE INTENTIONALLY LEFT BLANK

EXECUTIVE SUMMARY

Technological developments, increasing requirements for command and control (C2) networks, and the growing reliance on sensors have increased bandwidth usage in support of military operations. Advanced electronic warfare threats have spread beyond major state actors and must be accounted for across the range of military operations (ROMO). Newly developed United States Marine Corps (USMC) and United States Navy (USN) operational concepts, Expeditionary Advanced Base Operations (EABO) and Littoral Operations in a Contested Environment (LOCE) identify several proposed capabilities that are required for successful concept implementation. Specifically, the Commandant of the Marine Corps (CMC) and Chief of Naval Operations (CNO) identify the "[a]bility to command and control naval task organizations in denied, degraded, and exploited environments (D2E2)" (Chief of Naval Operations and Headquarters, U.S. Marine Corps 2017, 15).

For decades, lasers have been explored as an option for communication due to wavelength and spectrum availability advantages. The significant effects of the atmosphere on optical wave propagation have been extensively studied (Andrews and Phillips 2005; Tatarskii 1961). The atmospheric channel imposes significant negative effects on optical beams, often resulting in deep fades that can last multiple milliseconds. As transmission speeds can operate at multiple gigabits per second, this can result in the "loss of potentially up to [1 billion] consecutive bits" (Chan 2006, 4754). Typical error correction codes are not capable of overcoming this level of signal corruption. Interleaving the transmitted symbols attempts to spread the concentration of errors due to channel fading across multiple codewords. Even at modest transmission speeds of 100 MB per second, the required interleaving depth would be over 1 GB. The memory requirements and computational overhead would introduce significant latency and complications when integrating with standard upper-level Open Systems Interconnection (OSI) stack protocols.

While recent advances in hardware capabilities for fiberoptic communications has facilitated renewed interest in FSOC system development, there remains significant hurdles to implement a dependable communication system. These challenges cannot be overcome by merely applying increased power to the transmitter. Mathematical coding algorithms and modulation schemes must be employed in concert to mitigate the atmospheric effects.

The simulation explored the effects and interactions between several key systems architecture design points: number of lasers, coding scheme, modulation scheme, laser wavelength, irradiance threshold, and SNR. The number of lasers was varied at 4, 8, 16, and 32-laser array sizes. Error correction capabilities in the form of algebraic codes were applied to mitigate the negative effects of the optical channel. Three levels of Reed-Solomon (RS) codes were employed to provide error correction: RS(233,255), RS(191,255), and RS(127,255). The second error correction approach that was employed was transmitting the same information across multiple independent channels. This will mitigate the effect of channel outages but comes at the cost of decreased transmission rates.

The modulation schemes this experiment employed were on-off-keying (OOK), binary pulse position modulation (BPPM), 2-ary modulation, and 4-ary modulation. These schemes offer different levels of power and spectral efficiency. The laser wavelength, system SNR, and the detector’s irradiance threshold directly impact the probability of detection at the receiver, and the probability of fades in the optical channel.

The simulation results highlighted the difficulty in using the optical channel in high turbulence environments. Increasing the SNR beyond 30 decibels did not provide additional benefits in terms of improved bit error rate (BER). In weak turbulence conditions, the RS(191, 255) code with OOK modulation is sufficient to overcome the optical channel effects. In moderate turbulence, the RS(127,255) code with BPPM modulation was the candidate architecture. In strong turbulence, the half repetition code with BPPM performed best in terms of minimizing BER and maximizing the transmission rate and power efficiency.

The thesis explored the ability of Reed-Solomon codes to mitigate the devastating effects of deep fades. Due to the distinct architecture requirements at different turbulence levels, the ability to adapt the system to the environment is critical. The development of an adaptive protocol is essential to leveraging this emerging technology. In addition to adaptive protocols at the physical layer, protocols controlling the upper layers of the OSI stack must be modified to increase resiliency. Free space optics communication offers the potential to ensure communications capability in a contested operational environment, but additional development is essential to ensuring that the warfighter's needs are met.

References

Andrews, Larry C., and R. L. Phillips. 2005. *Laser Beam Propagation through Random Media*. 2nd ed. Bellingham, WA.: SPIE Press.

Chan, V. W. S. 2006. "Free-Space Optical Communications." *Journal of Lightwave Technology* 24, no. 12 (December): 4750–62.

Chief of Naval Operations and Headquarters, U.S. Marine Corps. 2017. *Littoral Operations in a Contested Environment*. Washington, DC: Office of the Chief of Naval Operations and Headquarters, U.S. Marine Corps.

Tatarskii, V.I. 1961. *Wave Propagation in a Turbulent Medium*. New York, NY: McGraw-Hill.

THIS PAGE INTENTIONALLY LEFT BLANK

ACKNOWLEDGMENTS

I would like to thank my advisor group, Dr. Buettner, Professor Miller, and Professor Ateshian. Thank you for your guidance and support throughout this process. Any shortfalls are mine alone. I could not have done this without your guidance.

Most importantly, I must thank my wife, Ashley. Without your love and support, I would not be where I am today. I am grateful for every day that we are together. I can never say enough how I appreciate all of your sacrifices that often seem to go unnoticed. Thank you for everything that you do.

THIS PAGE INTENTIONALLY LEFT BLANK

I. INTRODUCTION

The National Defense Strategy (NDS) has highlighted the need to be prepared to compete with near-peer competitors. Specifically, the Secretary of Defense (SECDEF) determined that "[i]nvestments will prioritize developing resilient, survivable, federated networks… from the tactical level up to strategic planning" (Secretary of Defense 2018, 6). A sober assessment of the operational environment leads to questioning the assumption of reliable use of the electromagnetic (EM) spectrum for communications. Most existing communication systems require unfettered access to radio frequencies which the enemy has the ability to deny. Free space optical communication systems should be developed to support Marine Corps operations.

A. BACKGROUND

Technological developments, increasing requirements for command and control (C2) networks, and the growing reliance on sensors have increased bandwidth usage in support of military operations. Advanced electronic warfare threats have spread beyond major state actors and must be accounted for across the range of military operations (ROMO). Newly developed United States Marine Corps (USMC) and United States Navy (USN) operational concepts, Expeditionary Advanced Base Operations (EABO) and Littoral Operations in a Contested Environment (LOCE) identify several proposed capabilities that are required for successful concept implementation. Specifically, the Commandant of the Marine Corps (CMC) and Chief of Naval Operations (CNO) identify the "[a]bility to command and control naval task organizations in denied, degraded, and exploited environments (D2E2)" (Chief of Naval Operations and Headquarters, U.S. Marine Corps 2017, 15).

These distributed forces must be capable of focusing combat power at decisive points. This capability will require a highly networked force of sensors and shooters capable of sharing information while managing signatures (Chief of Naval Operations and Headquarters, U.S. Marine Corps 2018). Existing systems, such as the Tactical Line-of-Sight Optical Network (TALON) employ single input, single output (SISO) methods for free space optical (FSO) communications. The SISO FSO communication method operates with restrictive line of sight (LOS) requirements and is highly susceptible to atmospheric conditions. These systems mitigate atmospheric losses through employing high-powered optical transmitters. Multiple input, multiple output (MIMO) FSO systems have demonstrated the potential to overcome these restrictions by reducing atmospheric effects, offering wider transmission angles for LOS communications, and potential non-line of sight (NLOS) capabilities. This thesis explores potential system architectures to support MIMO FSO communications and evaluate these architectures against relevant performance metrics and system characteristics.

B. GOALS AND OBJECTIVES

When designing the architecture of a MIMO FSO system, there are several key questions to consider. The systems engineering process will result in:

1. Determining the most significant decisions for architecting a MIMO FSO system.
2. Determining the most significant interactions amongst the architecture decisions.
3. Determining the best combination for communication across the free space optical channels with weak turbulence.
4. Determining the best combination for communication across the free space optical channels with strong turbulence.
5. Proposing an architecture for an engineering prototype proof of concept.

C. BENEFITS OF THE STUDY

Achieving the goal of identifying the critical architecture decisions will support the USN and USMC in meeting critical capability gaps identified in current concepts (CNO and HQMC 2017; CNO and HQMC 2018). Proposing a systems architecture that is capable of meeting requirements will support development of an engineering prototype.

DARPA and ONR efforts have focused on meeting the communication requirements of larger headquarter units. This system has the potential to provide LPD/LPI/LPE communication paths to critical tactical units. This research can provide capability developers and requirements writers at the Marine Corps Combat Development Command (MCCDC) a glimpse at the potential for FSOC systems for small units.The science and technology communities can leverage these results to aid in tackling the challenges of optical communication in the free space channel.

D. SCOPE AND ASSUMPTIONS

This thesis focuses on the systems architecture decisions required to develop an engineering prototype proof of concept. This thesis does not deal with any data communication systems outside of the physical layer of the Open Systems Interconnection (OSI) model. The coding, modulation, and laser transmitter choices have been chosen from commercially available and common coding and modulation choices for FSOC systems.

The effective implementation of a FSOC system will require additional research outside the scope of this thesis. For the purposes of this study, the following assumptions were made:

1. The pointing, acquisition, and tracking (PAT) system is outside the scope of the study.

2. Power sources will be able to support laser transmitter requirements.

E. THESIS STRUCTURE

Chapter II is a review of the current literature for the problem. It provides the necessary awareness of current research efforts.

Chapter III presents the methodology of this study. It describes the development of the model and the design of experiments that were used to collect the data. The systems engineering effort to develop the functional flow block diagram is presented. A numerical simulation tool provides the primary measure of effectiveness for the FSOC system.

Chapter IV is the analysis and interpretation of the data from the experiment runs. Statistical and analytical interpretation of the results is presented. It provides an overview of the data analysis and leverages statistical evidence to identify significant architectural decisions and explore their interactions.

Chapter V contains a summary of the findings and results, the conclusions, and recommendations for follow-on research to support this topic.

II. EXPLORATORY RESEARCH

This chapter reviews the current literature covering systems engineering and free space optical communication systems research. It provides insight into recent efforts to codify more robust systems engineering efforts during the exploration of systems architecture decisions. The history of digital communications theory, and applicable research on laser propagation provide insight into the challenges from a physics perspective. A survey of major military research programs leveraging FSOC systems highlights previous efforts to implement a solution. Finally, an explanation of current efforts to improve coding algorithms and modulation schemes to mitigate FSO channel impacts.

A. SYSTEM ARCHITECTING

While there are differing views on system architecture development, there is agreement that it must be done early in the systems engineering efforts. With the increasing complexity of new systems, new research has highlighted the critical nature of system architecture decisions on system performance. System architecture is simply the "basis for the preparation of all lower-level specifications" (Blanchard and Fabrycky 2011, 58). But, this does not highlight how simple changes for one architectural element can cause outsized effects on performance. In contrast, a competing definition holds that system architecture is "an abstract description of the entities of a system and the relationships between those entities" (Crawley et al. 2004, 2), which better focuses systems engineers on exploring the interactions within system elements (Ulrich and Eppinger 2012). The Defense Acquisition University (DAU) even separates architecture development into its own separate architecture design process. The DAU specifically highlights modeling, trade-off studies, and decision analysis to capture the interdependent elements of the system architecture (DAU 2017).

The purpose of developing the system architecture is to identify critical decisions early in system development that will have significant effects on key system attributes throughout the life-cycle. These early architecture and design decisions significantly impact the final design and its performance (Crawley, Cameron, and Selva 2015; Maier and Rechtin 2009; Selva, Cameron, and Crawley 2009).

Levis and Wagenhals explored the process of developing DOD information systems architectures to meet Command, Control, Communications, Computer, Intelligence, Surveillance, and Reconnaissance (C4ISR) requirements (2000). They present the process in three phases: Analysis Phase, Synthesis Phase, and Evaluation Phase. An overview of the architecture development process from operational concept through architecture evaluation is presented in Figure 1.

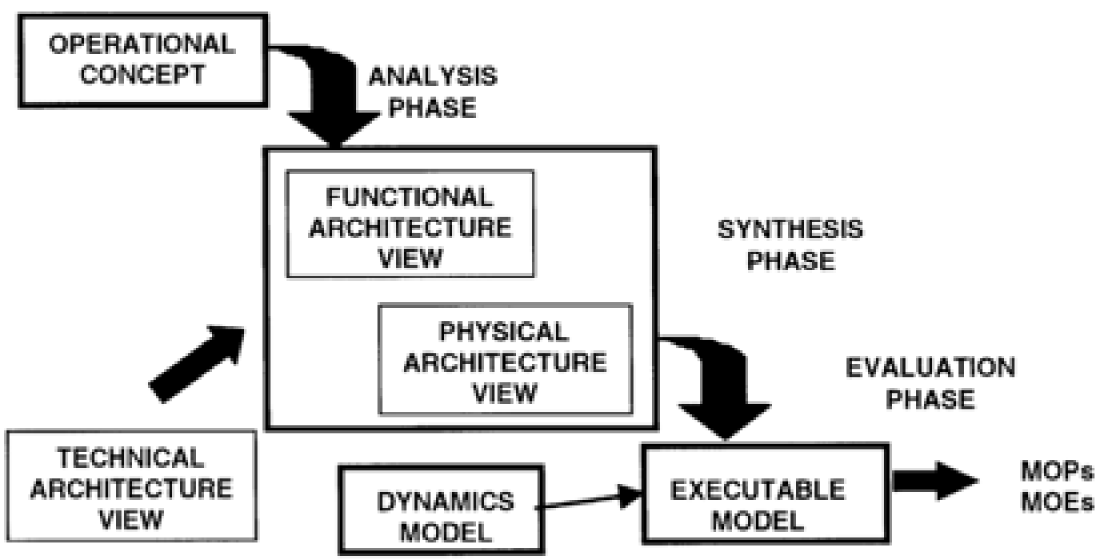

Figure 1. The Three Phases of Architecture Development. Source: Levis and Wagenhals (2000).

Systems architecture decisions must often balance competing requirements: the need for better insight when making design trade-offs, greater focus on solving the problem, and better management of requirements (Haveman and Bonnema 2013). This section presents the current state of research focused on architecting through discussion of the analysis phase, synthesis phase, evaluation phase, and tradeoff studies.

1. Analysis Phase

The analysis phase focuses on the development of the static architecture views: functional architecture view, and physical architecture view. The clearly described operational concept supports the development of functional and physical architectures that meet stakeholder operational and suitability requirements. "[The] operational concept is based on a simple idea of how the over-riding goal is to be met" (Levis and Wagenhals 2000, 228). Levis and Wagenhals describe the technical architecture view as the "minimal set of rules governing the arrangement, interaction and interdependence of the parts or elements" (Levis and Wagenhals 2000, 229).

Kang, Jackson, and Shulte (2011) describe this process of exploring alternative designs early in the SE process as design space exploration (DSE). The system architecture's design space encompasses the critical decisions that must be made to system development. Engineers must develop a robust set of potential alternative architectures that can be evaluated via simulation.

Classic systems engineering texts discuss functional architecture development in detail. Buede discusses the development of the configuration items that will compose the physical solution. He discusses that the "intent of systems engineers should not be to design these components but rather to state representative instantiations for the generic components" (Buede 2009, 252).

2. Synthesis Phase

The synthesis phase leverages the static architecture views developed in the analysis phase and incorporates a dynamics model to develop an executable simulation model. The dynamics model characterizes the behavior of the architecture as the system's state changes. The executable model integrates the operational concept, technical architecture view, functional and physical architectures views, and the dynamics model to support evaluation. The model outputs include the measures of performance (MOPs) and measures of effectiveness (MOEs) to support further analysis and evaluation of competing requirements.

Fricke and Schulz explored the requirement for changeability in system architectures, "systems and their architectures have to offer changeability throughout their life cycle not only within themselves but also towards their environments" (Fricke and Schulz 2005, 15). Specifically, they discuss the need to incorporate robustness, flexibility, agility, and adaptability (Fricke and Schulz 2005). This concept is especially important in the design of military communications systems. Adversaries have developed capabilities to affect the EM spectrum and DOD communication channel capacity requirements have exploded resulting in congestion throughout the EM spectrum. The output from the synthesis phase is the conversion of the static architecture representations into a dynamic model to support additional analysis.

3. Evaluation Phase

At this point in the systems engineering process, the goal of modeling and simulation is to provide response results that allow engineers to gain insight into system performance. To support effective design space exploration, "the systems engineer should choose the most efficient lowest fidelity model and simulation that answers the design problem or question" (Hebert et al. 2016, 378). Hebert (2016) discusses the use of surrogate models in place of detailed physics-based models to provide the level of detail required for insight. "If a surrogate model is selected, the physics-based code is run a few times to generate a limited number of sample basis points that are selected by a design of experiments" (Hebert et al. 2016, 380). This is the same concept described by Levis and Wagenhals (2000) as the Dynamics Model. This reduces computational workload and allows for deeper exploration of the design space.

Sanchez and Wan highlight that the goals of simulation experiments include: "develop[ing] a basic understanding of a particular simulation model or system, [finding] robust decisions or policies, or [comparing] the merits of various decisions or policies" (Sanchez and Wan 2015, 1796). The goal of Design of Experiments (DOE) is to create an efficient plan to develop design points that allow the simulation to efficiently explore the design space. The statistical analysis identifies design factors that have statistically significant effects on system performance. An executable model allows the design team to gain insight into what impact decisions may have. Within the design, there are input parameters and environmental assumptions that are labeled factors. The simulation responses represent the output performance measures (Law 2014).

4. Tradeoff Analysis

Tradeoff analyses present system stakeholders with insight into the effect design decisions will have on system performance. The analysis uses the MOE and MOP output from the evaluation phase. Statistical analysis of the simulation or experimentation results can identify if any factors impart statistically significant responses to the system's performance. "By identifying important factors, interactions, and nonlinear effects, the experimenter can improve their understanding of the simulation's behavior, find robust solutions, or raise questions to be explored in subsequent experiments" (Sanchez and Won 2015, 1805).

Raz, Kenley, and DeLaurentis (2018) highlighted the importance of coupling design space characterization with identifying important architectural decisions. Their approach "emphasizes the importance of holistic design space characterization by taking into account the interactions between different decisions" (Raz, Kenley, and DeLaurentis 2018, 14). As system complexity increases, simple design decisions can affect the system performance disproportionately. A common thread throughout the research is the difficulty in characterizing and assessing the consequences of choosing between alternative architectures (Haveman and Bonnema 2013; Torry-Smith et al. 2011).

Tradeoff studies are well-suited to evaluate measures of performance. Challenges arise, however, when performance characteristics such as safety and ease of use must be analyzed. The inherent tension between safety measures, functionality, and ease of use can be hard to quantify when evaluating simulation results (Haveman and Bonnema 2013). Failure to account for these tensions will merely delay the resolution of these conflicts until later in the process after key decisions may have been made.

B. COMMUNICATIONS THEORY

The main purpose of any communication system is to transfer information from a source to a destination. Claude Shannon laid out the theoretical foundations of digital communications in his seminal paper "A Mathematical Theory of Communication," Shannon (1948) described the fundamental challenge for communication systems as the identification of the information source from the received signal in the presence of noise. A communication system with the essential five parts is presented in Figure 2. The information source produces the message. The transmitter manipulates the message to make it suitable for transmission. The channel is "merely the medium used to transmit the signal from transmitter to receiver. It may be… a beam of light, etc." (Shannon 1948, 2). The destination is the intended recipient of the message. The receiver inverses the manipulations conducted by the transmitter (Shannon 1948).

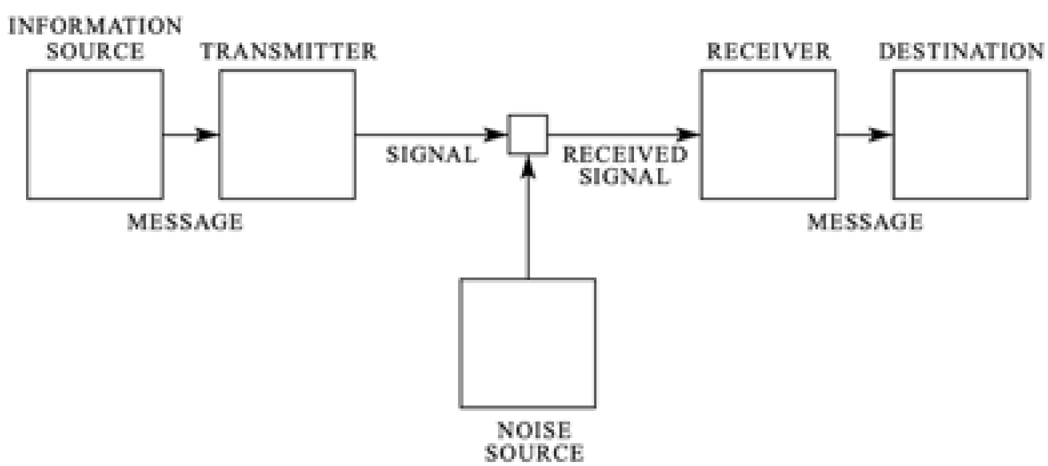

Figure 2. Schematic Diagram of a General Communication System. Source: Shannon (1948).

Efficient transmission of information is the characteristic of well-designed communication systems. Two primary resources will limit system performance: power and channel capacity (Haykin and Moher 2007). Successful development of a communication system relies upon leveraging a strong understanding of technical components and theoretical underpinnings (Haykin and Moher 2007). The key mathematical theories that will allow for adequate resolution in the system model are modulation theory, Fourier analysis, and detection theory (Haykin and Moher 2007; Karp and Stotts 2012; Majumdar 2015; Stotts 2017).

C. MIMO COMMUNICATIONS RESEARCH

The focus of effort for much commercial civilian communication research is on improving the performance of cellular and broadband networks. From the systems engineering perspective, spectral efficiency, channel capacity, energy efficiency, and minimizing complexity are the relevant measures of performance for tradeoff studies (Renzo et al. 2014). A diagram of the general single-input single-output (SISO), single-input multiple-output (SIMO), multiple-input single-output (MISO), and multiple-input multiple-output (MIMO) techniques in wireless networks is presented in Figure 3. Special cases of single-user MIMO (SU-MIMO) and multiple-user MIMO (MU-MIMO) are also examined.

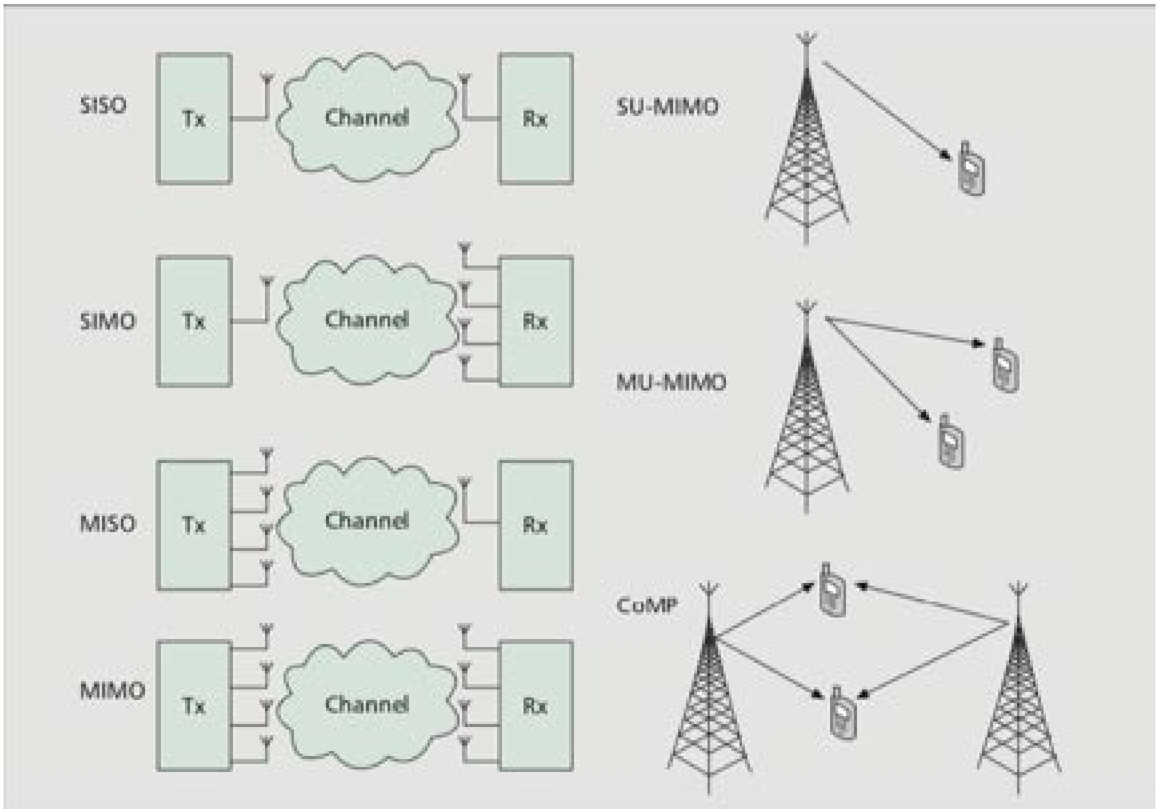

Figure 3. Diagram of MIMO Schemes. Source: Lie et al. (2011).

The number of transmitters and receivers distinguishes the schemes from each other. The information source is on the left side of the channel, while the destination is on the right side of the channel in Figure 3. The general schemes imply that there is one single user. While MIMO techniques are useful in improving the capacity and reliability of wireless channels, this comes at the sacrifice of decreased energy efficiency. The SISO scheme is completely dependent on the channel effects of the single transmitter and receiver. The SIMO employs several receivers to increase the system's ability to detect the transmitted signal. The MISO seeks to overcome the channel effects by employing multiple transmitters. These transmitters are often separated either spatially or by frequency deconfliction. Finally, the MIMO schemes employ multiple transmitters and multiple receivers. This offers several different channels that can be separated both spatially and by frequency. This method is commonly employed in modern cellular telephones that are able to transmit and receive at multiple frequencies.

Lit et al. (2011) explore the tradeoff between the schemes and the penalties in terms of spectral efficiency and energy efficiency. The MIMO schemes require additional power requirements at the transmitter and receiver nodes, and additional signaling overhead. Based on the channel state information (CSI), adaptive modulation and adaptively changing the number of transmitting antennas has proven effective at mitigating the negative effects of employing MIMO techniques (Li et al. 2011).

Renzo et al. (2014) gave the most in-depth treatment of MIMO techniques leveraging spatial modulation (SM). While Figure 3 presents the generic MIMO approach where each antenna transmits an independent data stream, the spatial modulation technique attempts to improve energy efficiency by mapping additional information implicitly based on which transmitting antenna is active (Renzo et al. 2014).

While Renzo et al. (2014) focused on employing RF antennas to transmit information, Popoola, Poves, and Haas (2012) explored SM schemes for optical wireless communication systems. They explored combining space shift keying (SSK) based on the general SM technique with pulse position modulation (PPM) to create spatial pulse position modulation (SPPM). Four independent optical transmitters (white LEDs) were employed using SPPM. An example of SPPM employment is presented in Figure 4. The transmitted information is derived from which laser transmits a rectangular pulse in the time slot.

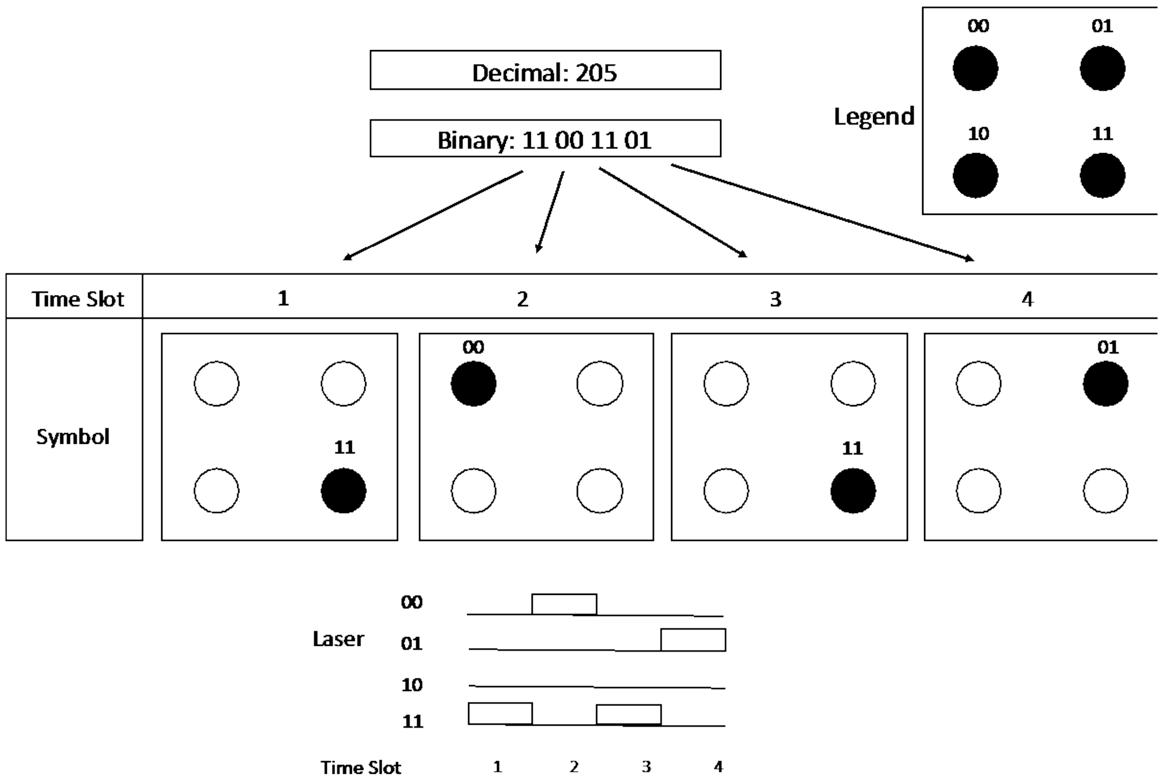

Figure 4. Diagram of Spatial Pulse Position Modulation Implementation

The performance of the SPPM scheme showed that it "combines the energy efficiency of the PPM with the high spectral efficiency of the SSK" (Popoola, Poves, and Haas 2012, 2953). Experimental results demonstrated transmission rates 18.75 Mbps with low error rates (Olanrewaju, Thompson, and Popoola 2016).

D. VISUAL CODES

In contrast to the SM schemes discussed above, visual codes seek to transmit information based on some combination of visual indicators. Lucas explored the historical use of semaphore by naval vessels to transmit messages with flags (Lucas 2013). In an attempt to develop modern implementations of semaphore, several Naval Postgraduate School (NPS) white papers and theses that have explored the tactical employment of visual codes to transmit information. The suitability of using static Quick Response (QR) codes to support ship-to-ship communications at tactical distances was explored (Lucas 2013 and

Richter 2013). Streaming QR code communication, improved detection capabilities, and modifications to the QR code for security purposes are identified for further research (Lucas 2013).

Streaming QR codes to achieve higher data rates was explored using a light emitting diode (LED) array and a camera receiver. The concept of employment was validated at the physical and link layer as an avenue for further exploration (Felder 2018). Additionally, QR codes were evaluated to support wireless data transmission within a passenger aircraft cabin. Due to hardware restrictions, the frame rate was limited to 13 frames per second resulting in a transmission rate of 120 kbit/second (Fath, Schubert, and Haas 2014).

E. MILITARY RESEARCH PROGRAMS

Current command and control doctrine within the Joint Force implicitly assumes unfettered access to the electromagnetic spectrum. The proliferation of information requirements, distributed operations, and the migration of data to cloud-based solutions has stressed DOD communication networks. Increased use of existing channel capacities in the radio frequency has been the purpose of several research efforts. Major research efforts throughout the DoD have focused on creating the backbone to support communications requirements. The United States Air Force (USAF), Defense Advanced Research Projects Agency (DARPA), and the Office of Naval Research (ONR) have explored several different avenues to meet these communication requirements through the use of optical channels.

The USAF sponsored the Free-Space Optical Communications Airborne Link (FOCAL) program to explore the development of airborne FSOC systems in support of persistent surveillance missions. Massachusetts Institute of Technology's (MIT) Lincoln Laboratory conducted research focused on this effort. Karp and Stotts (2012) summarize their efforts focused on two techniques: optical diversity and coding with interleaving. The physical separation of the apertures for the optical diversity technique is presented in Figure 5.

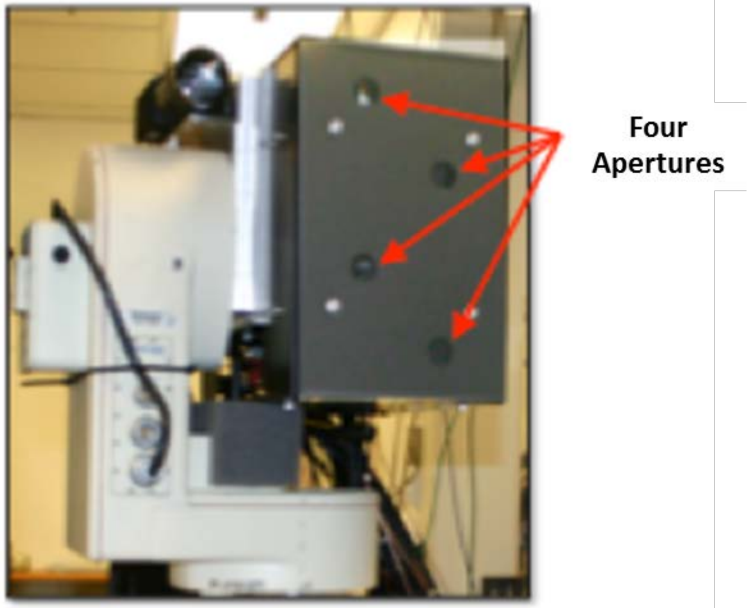

Figure 5. Optical Diversity Implementation in a Ground-Based Optical Module. The Four Ground-Based Receivers Are Independently Pointed by Separate Tracking Units. Adapted from Frederick et al. (2010).

The optical diversity technique leverages the fact that the channels are statistically independent if separated by more than 10 centimeters (Karp and Stotts 2012). This implementation of spatial diversity was implemented by summing the measured power in the plane of the photodetector across the available apertures. This mitigates the effect of a single channel's non-availability. The second effort leveraged forward error correction (FEC) coding and interleaving. The research was able to establish links at a 50 km range (Frederick et al. 2010).

DARPA's Optical RF Communications Adjunct (ORCA) program explored the potential to mitigate several critical problems FSOC systems face: cloud obscuration and atmospheric turbulence. These two problems have limited successful implementation to short range networks. The ORCA system implemented a hybrid FSO/RF system to improve reliability of the communication link. When the FSO link was untenable due to the state of the optical channel, the RF transmitter was available for transmission. The experimental results were favorable due to the adaptive mechanisms that allowed for low bit error rates (Stotts et al. 2009).

Unlike the hybrid RF approach that ORCA explored, the 100GB/s RF backbone program explored spatial multiplexing of millimeter wavelength RF frequencies, starting in 2013, to offer DoD the ability to replicate the capacity of fixed communications links (Woodward 2017). The program implemented spatial multiplexing to achieve stream information rates of 1 GB/s for each link, which aggregated to a 4 GB/s overall information rate (Woodward 2017). "[U]sing [the] RF spectrum rather than the optical spectrum can increase the availability of these links for transmission through rain, fog, dust, and cloud conditions that can impair free-space optical links" (Woodward 2017, 1).

The ONR's TALON project tackled the long-range communication backbone problem through employing optical communications that lie outside the RF spectrum. "Ultimately, FSO is an enabling technology that allows users to operate in environments where RF-spectrum is constrained or unavailable" (Mann et al. 2018, 9). The implementation challenges include pointing, acquisition, and tracking (PAT) between transmitter and receiver and development of a system "tailored for robust operations, useable, and satisfy cost and size, weight, and power needs" (Mann et al. 2018, 9).

F. FREE SPACE OPTICAL COMMUNICATION

For decades, lasers have been explored as an option for communication due to wavelength and spectrum availability advantages. The effects of the atmosphere on optical wave propagation has been extensively studied (Andrews and Phillips 2005; Tatarskii 1961). Recent advances in hardware capabilities has facilitated renewed interest in FSOC system development. Fiber Optic Communications (FOC) technologies in the form of optical detectors with 100 GBps bandwidth and solid-state laser sources have allowed FSOC developments to resume (Karp and Stotts 2013; Stotts et al. 2008). Figure 6 presents a general functional flow block diagram of a FSOC communication system.

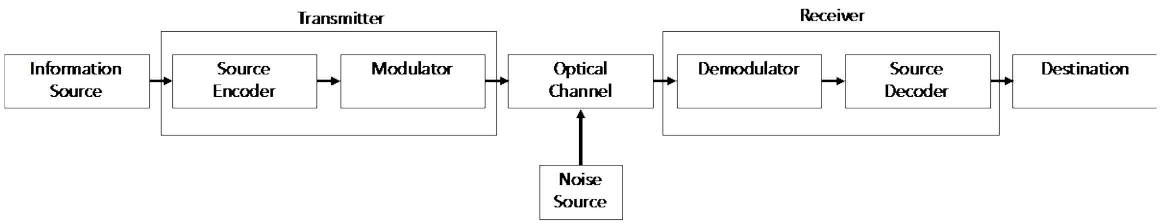

Figure 6. Block Diagram of a Free Space Optical Communication System. Adapted from: Majumdar (2015) and Shannon (1948).

Encoding encompasses all of the required message manipulation to translate the message into bits. This includes encryption, error encoding, and interleaving. Modulation translates the encoded information onto a carrier signal. Common modulation schemes vary the amplitude, frequency, phase, and quadrature of the carrier signal according to the message. Effective modulation requires the ability to detect the manipulations executed at the transmitter. With technological improvements, industry has developed practical solutions to the fundamental limitations of the free-space optical channel (Majumdar 2015; Karp and Stotts 2013; Stotts 2017; Kartalopoulos 2011). This block diagram will guide the development of the functional flow block diagram and potential physical architectures. The optical channel characteristics will require different employment considerations compared to typical RF military communications.

1. Electromagnetic Spectrum

The free space optical communication channel lies within the visible spectrum of the EM spectrum. Andrews and Phillips deliver the most in-depth treatment of how laser beams propagate through the atmosphere. The most useful lasers for communication systems generate coherent radiation within the ultraviolet, visible, and infrared bands. The wavelengths for useful lasers are between 850 and 1550 nm (Andrews and Phillips 2005). These wavelengths fall within the visible and infrared range in Figure 7.

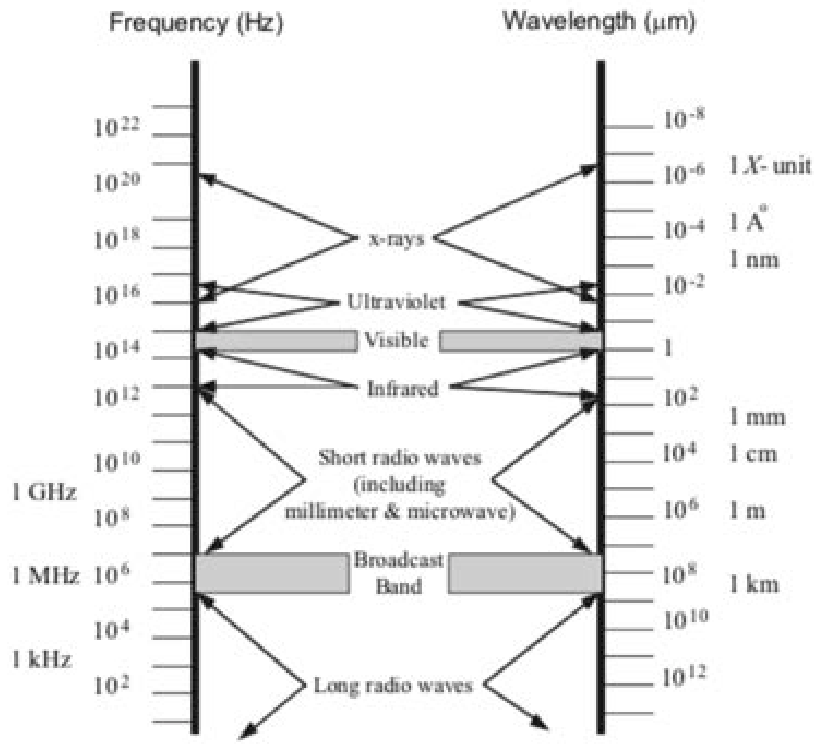

Figure 7. The Electromagnetic Spectrum.
Source: Andrews and Phillips (2005).

2. Laser Beam Propagation

Typical lasers for FSOC systems are beam waves, which suffer from several fundamental phenomena as they travel through the atmosphere: diffraction, atmospheric turbulence, and atmospheric attenuation (Andrews and Phillips 2005). The effects of diffraction are due to the physical characteristics of the laser source. A generic laser source is presented in Figure 8 to illustrate the dependence of the beam spot in the plane of the receiver on the initial beam radius at the waist, the beam divergence angle, and distance from the laser source.

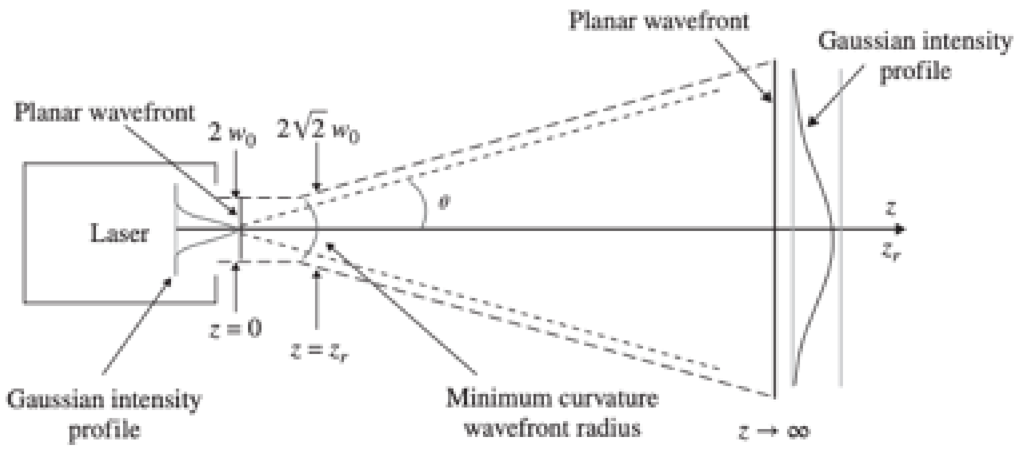

Figure 8. Growth in Beam Diameter as a Function of Distance from the Laser. Source: Stotts (2017).

The typical laser source transmits energy characterized by a Gaussian distribution about the transmission axis. The transmission axis is typically in the positive direction in the z-plane. In FSO communication systems, the size of the beam spot at any point in time is dependent on several beam parameters. The beam waist, w_0, is the radius of the beam in the plane of the transmitter, where $z = 0$. The divergence angle, θ, is a function of the laser's wavelength and the beam waist. The laser's beam waist and divergence angle should be matched with the area of the receiver to ensure that the receiver is capable of detecting the most transmitted power possible.

3. Atmospheric Effects

While diffraction is largely dependent on the laser source characteristics, atmospheric effects significantly influence laser beam propagation. These effects vary based on geographic location, weather conditions, and time of day (Andrews and Phillips 2005; Stotts 2017). "In the marine and atmospheric channels, turbulence is associated with the random velocity fluctuations of the 'viscous fluid' comprising that channel" (Stotts 2017, 256). Turbulence in the atmospheric channel is characterized by two separate ranges of discrete eddies. The atmospheric turbulence is described with the outer scale of turbulence, L_0, and the inner scale of turbulence, ℓ_0. Propagation of energy through a turbulent environment is presented in Figure 9.

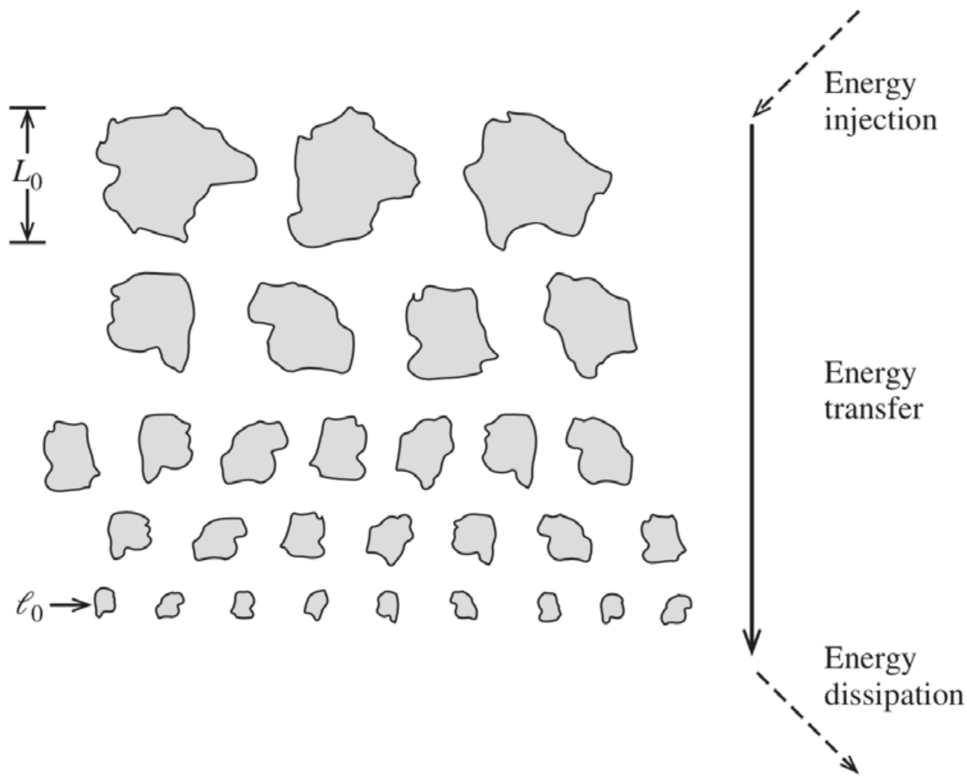

Figure 9. Geometry for Propagation through a Turbulent Environment. Source: Stotts (2017).

Atmospheric conditions are typically categorized as weak turbulence, medium turbulence, and strong turbulence. As the atmospheric turbulence increases from weak to strong turbulence, the concentration of eddies increases. Andrews and Phillips (2005) derived a distribution model from earlier work by Nakagami (1964) that adequately models the atmospheric effects in all atmospheric conditions. There are four major effects that a particulate medium, such as the atmosphere, has on optical beams: angular spreading, spatial spreading, temporal spreading, and transmission loss (Stotts 2017). The effects are presented in Figure 10.

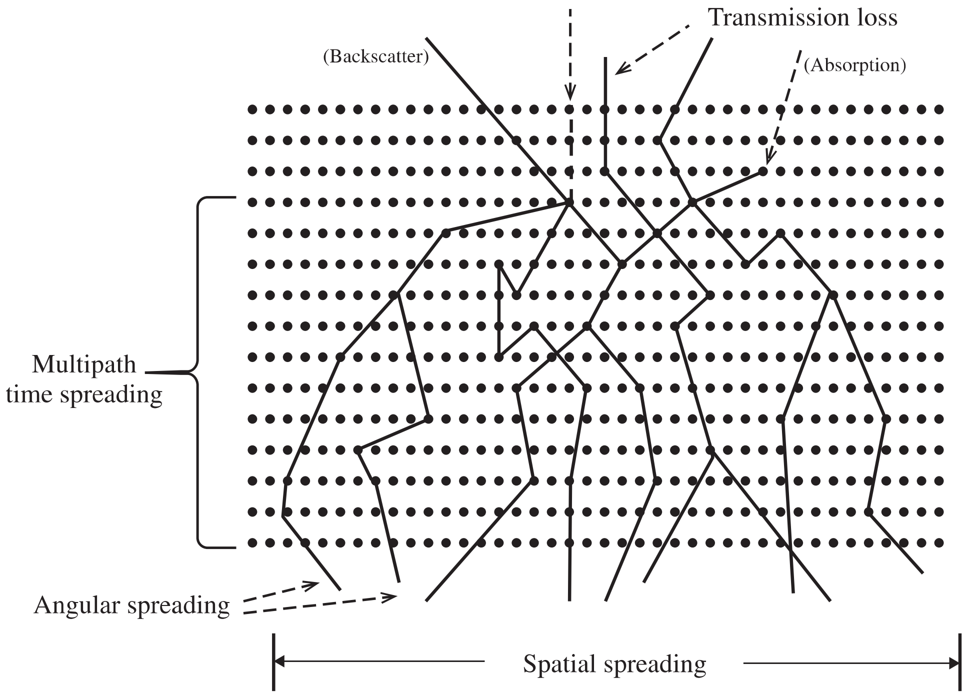

Figure 10. Various Light Beam Effects from Particulate Scattering Process. Source: Stotts (2017).

Several key components of the atmosphere cause atmospheric absorption and scattering, including molecules, aerosols, and turbulence. Stotts (2017) derived functions to model laser beam propagation in the total atmosphere due to each component. These functions are uncorrelated, and the overall atmospheric effect was modeled as the product of each component's effect (Stotts 2017). The effects on the received power in the plane of the receiver at a distance of 1000 meters from the transmitting laser is presented in Figure 11.

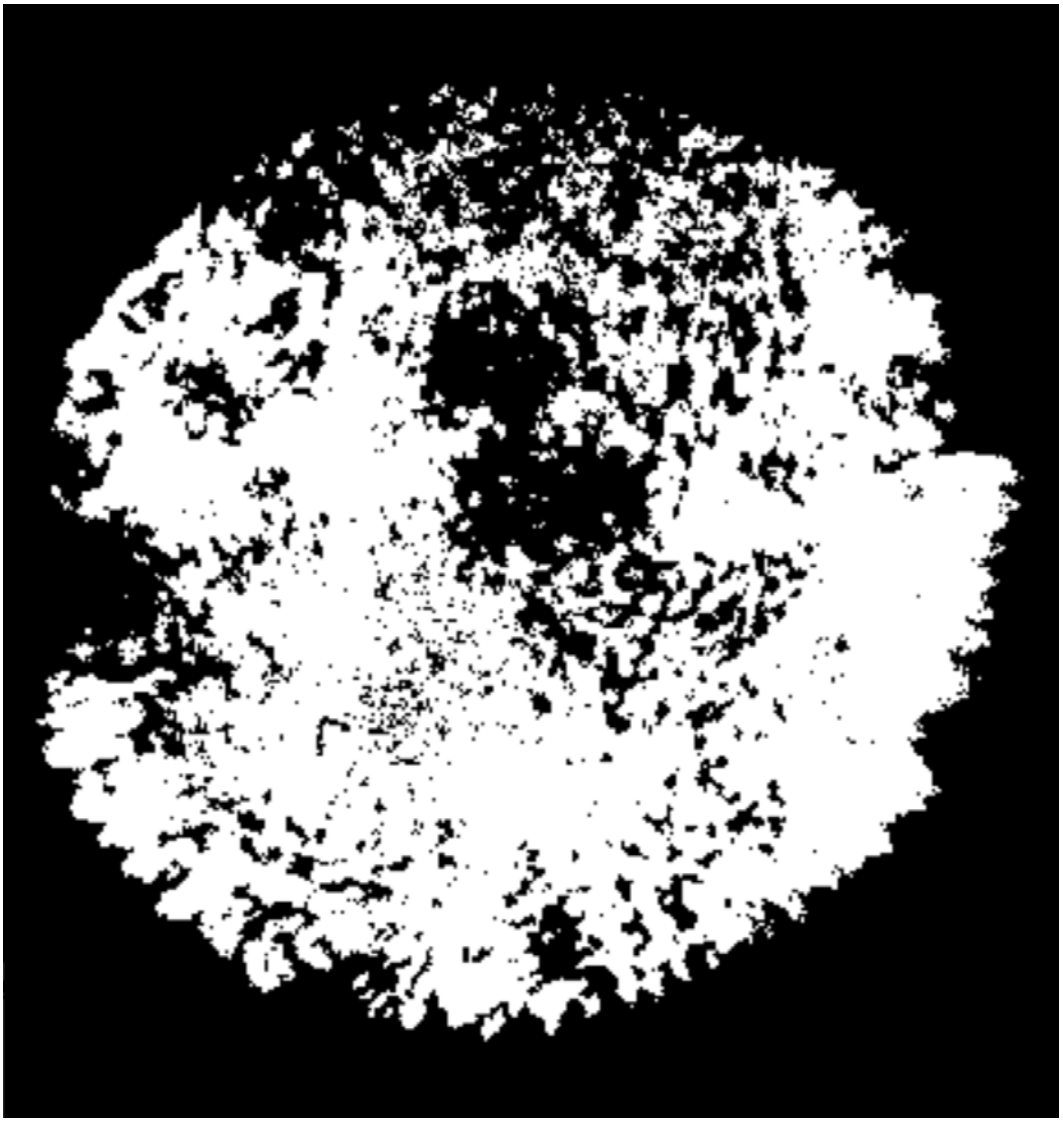

Figure 11. Still Photo of Laser Beam after Propagating 1000 Meters. Source: Andrews and Phillips (2001).

In the plane of the transmitter, the laser beam irradiance is described by a Gaussian distribution about the axis of transmission. Before accounting for the atmospheric effects from the particulate scattering process, the beam spot in the plane of the receiver would be a clearly defined shape with the irradiance that has a Gaussian distribution about the axis of transmission.

The random processes of the turbulent fluctuations contribute to the refractive structure parameter in the optical channel. Refractive-index fluctuations are induced by the randomness of the atmospheric turbulence. While Figure 11 presents an instantaneous view of the laser beam spot, over time it is constantly changing due to randomness in the optical channel. The effect of this is the beam spot's irradiance is constantly fluctuating, resulting in randomness in the received power in the plane of the receiver. "The twinkling of the stars at night is a manifestation of the dynamic nature of the refractive index changes induced by the [eddies]" (Stotts 2017, 256). The dark spots presented in Figure 11 represent fading in the laser irradiance in the plane of the receiver. Deep fading occurs when the spatial distribution and concentration of the eddies reduce the received energy below the detector's threshold. The deep fades would present themselves as increased concentration of black spots within the beam spot and decreased power at the receiver. This effect can last multiple milliseconds (Andrews and Phillips 2005; Chan 2006).

Deep fades, especially at high transmission rates, can cause significant and devastating effects on communication networks. Increasing the SNR at the detector cannot overcome the effects. Physically separating the MIMO transmission paths, however, can mitigate the effects of fades. "Multiple transmitters and receivers only need to be placed centimeters apart to see approximately independent channel fades" (Chan 2006, 4754). This research path has shown promise because typical coding techniques alone are generally not sufficient to counteract the fading effects (Chan 2006).

G. CODING

Coding in digital communications encompasses all steps required to translate the source information into bits at the transmission side and retrieve those bits at the receiver side (Hoykin and Moher 2007). It provides the ability to correct errors that appear during the transmission. The level of coding employed should be matched to the expected channel state and the number of errors expected to be incurred. Codes protect against transmission errors at the cost of additional computational load at both the transmission and receiving ends.

The Jet Propulsion Laboratory has tackled the problem of coding for optical channels in NASA's Deep Space Network (DSN). The DSN established two-way communication with its unmanned spacecraft conducting deep space exploration. Baumert, McEliece and Rumsey (1978) laid the groundwork for exploring the application of error correcting codes to mitigate the significant effects of outages, latency, and erasures on the channel. Later, McEliece (1981) further developed the concept of matching modulation schemes with Reed-Solomon encoding to achieve improved error rates on the channel. The efforts at NASA and JPL laid the groundwork for mitigating the effects in the optical channel.

Djordjevic, Ryan, and Vasic (2010) provide the most in-depth recent treatment of coding for optical channels. They discuss the rapid development of static FOC networks by commercial providers. The constant demand for greater transmission capacity has fueled interest in squeezing out the best performance possible from networks. Their research showed coded repetition MIMO was sufficient to deal with some levels of atmospheric turbulence. When the channel suffers from deep fades, coded orthogonal frequency division multiplexing (OFDM) with bit interleaving was required to overcome channel impairments (Djordevic, Ryan, and Vasic 2010). As the channel state degrades, different modulation and coding schemes will be optimal at different times. To maximize performance, they "discussed the possibility of using the adaptive modulation and coding to tolerate deep fades due to scintillation" (Djordevic, Ryan, and Vasic 2010, 350).

H. MODULATION

The choice of modulation schemes within a system will have significant effects on the performance measures. "For digital data transmission, digital modulation provides source coding (data compression), channel coding (error detection/correction), and easy multiplexing of multiple information streams" (Majumdar 2015, 74). Optical transmitters can be modulated in respect to amplitude, frequency, phase, and polarization. The most common and currently practical modulation scheme involves intensity modulation of the transmitting beam and direct detection at the receive side. Majumdar (2015) identified that the modulation decision significantly impacts system performance in terms of power efficiency, bandwidth efficiency, and simplicity. Common modulation formats for FSOC systems include on-off keying, pulse-position modulation, binary phase-shift keying modulation, and pulse amplitude modulation (Stotts 2017).

I. PERFORMANCE MEASURES

Stotts, along with Haykin and Moher, gives in-depth discussions of relevant performance measures for optical communication systems (Stotts 2017; Haykin and Hoher 2007). These performance measures are specifically related to the architecture decisions for the transmitter and receiver and the effects that receiver sensitivity can have on the bit error rates. The atmospheric effects on the optical waves result in deep fades, regardless of the amount of transmitted power. "This implies that techniques other than a mere increase in transmitted power will be required to mitigate atmospheric turbulence beyond the very weak regime" (Ghassemlooy 2011, 386). While typical RF communication systems increase link availability with increased power, current research on FSOC systems seeks systems architecture designs that maximize performance. For general communication systems, Haykin and Moher (2007) noted that improving channel capacity often increases the complexity of the system. Stotts (2017) discusses several common measures: signal-to-noise ratio, minimum detectable power, probability of false alarm, probability of bit error, and receiver sensitivity.

J. OPERATIONAL CONCEPT

The operational concept for this thesis supports the LOCE and EABO concepts. The concepts' requirement for distributed operations and effective C2 in a D2E2 enemy threat scenario drives the need for low probability of detection (LPD), low probability of interception (LPI), and low probability of exploitation (LPE) communications.

1. Friendly Forces

The friendly forces will employ the FSOC system from fixed positions or stationary mobile platforms. The representative fixed positions support the C2 and security of expeditionary advanced bases (EABs). The stationary mobile platforms can include the Light Armored Vehicle (LAV), a joint light tactical vehicle (JLTV) platform, or the M777 howitzer within the USMC artillery battery. These platforms are capable of providing adequate power for the FSOC system. The dispersion between individual systems will be approximately 1,000 meters.

The LAV family of vehicles (FOV) includes six different variants. The LAV-25 represents the majority of the combat power and is equipped with a 25mm Bushmaster cannon. The LAV-Logistics and LAV-Recovery variant provide the logistical and maintenance support internal to the Light Armored Reconnaissance (LAR) company. The LAR company has two LAV-81mm mortar variants that provide internal fire support for the LAR platoons. The LAV-Command and Control variant provides the company's communication with higher headquarters. It is capable of communicating on high frequency (HF), very high frequency (VHF), ultra-high frequency (UHF), and satellite communications (SATCOM) frequency bands.

The LAR company often screens forward of a Marine Infantry Regiment. One critical task within the screen mission is to "[g]ain and maintain contact with the enemy and report their activity" (HQMC 2009, 3-7). Upon identification of enemy lead reconnaissance elements, the LAV company will "destroy or repel units within its capability" (HQMC 2009, 3-7).

2. Enemy Threat

The projected enemy threat is patterned from the 2018 NDS. The enemy forces will employ a variety of electronic support (ES) sensors capable of identifying EM emissions and the C2 to employ kinetic fires on identified positions. Additionally, the threat of electronic attack (EA) is constantly present. The enemy EA threat is expected to target friendly force RF bands to degrade command and control capabilities.

3. Vignette

The LAR company has set up an engagement area to target the lead elements of an enemy motorized reconnaissance unit. As the lead elements of the enemy unit enter the engagement area, the LAV-25s begin to engage with their 25mm cannons. As the lead vehicles of the enemy reconnaissance units are destroyed, the trail elements seek cover and report the LAR company positions.

The enemy conducts EA targeting the VHF band typically employed by USMC units. Leveraging the FSOC system, the LAR company is able to maintain communications internal to the company. LAV-25 crews, serving as forward observers, communicate with the LAV-81mm section to request fire support. They are able to adjust 81mm mortar fires onto the remainder of the enemy reconnaissance unit. This forces the enemy to maneuver, allowing the LAV-25s to destroy them.

With internal communications, the LAR company is able to maneuver to alternate positions and continue conducting its security operations. The appropriate combat reporting is sent back to the Marine Infantry Regiment via traditional communication pathways: high frequency (HF) radio systems or satellite communications (SATCOM).

III. EXPERIMENTAL METHODOLOGY

A. OVERVIEW

This chapter will discuss the methodology for this study. It will describe the systems engineering approach taken to develop the MIMO FSOC system architecture. The approach will include the system measures of effectiveness (MOE), modeling and simulation tools employed, and the DOE. The experimental parameters derived from the architecture decisions will be presented during the discussion of the simulation DOE.

B. DEFINING THE MEASURES OF EFFECTIVENESS

Digital communication systems support the transmission of information in the presence of noise. The quality of the information received is the primary purpose of this system. The primary MOE is the bit error rate (BER) for digital communication systems (Haykin and Moher 2007, 395). The system measures of performance (MOPs) include the transmission rate, measured in bits per second, and power requirements. The MOE and MOPs are presented in Table 1.

Table 1. System Measures

Description	Type
Bit Error Rate	MOE
Transmission Rate (bit/sec)	MOP
Power Consumption (pulse/bit)	MOP
Probability of Detection	MOP
Probability of False Alarm	MOP

The BER will be derived from the number of received bits in error divided by total number of bits transmitted. The transmission rate will be derived from the coding efficiency, modulation scheme, and laser modulation speed. The power consumption will be derived from the laser transmitter power and the modulation scheme. Finally, the number of lasers will be a proxy for the size attribute of the system. Fewer lasers will result in a smaller system size. The critical assumption allowing the use of number of lasers as a proxy for size is that they will be placed as close together as possible. The lasers must be spaced a few centimeters apart to achieve statistically independent channel states (Chan 2006). The MOP assumes that laser dispersion will be minimized.

C. SIMULATION DESIGN

The simulation to support evaluation of the systems architecture will use the Monte-Carlo simulation approach. This approach is traditionally used to model digital radio communication system. The functional flow block diagram (FFBD) provides the framework for the architecture decisions for this system. The FFBD is presented in Figure 12.

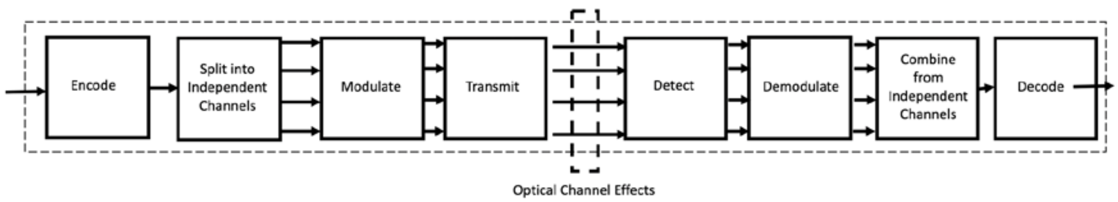

Figure 12. Free Space Optical Communication System Functional Diagram

The following sections will develop the detailed architecture decisions within each function. The dotted line represents the system boundary and the scope of the system architecture exploration.

a. Encode Function

The most common code used for FSOC systems is the Reed-Solomon (RS) code. It is a linear block code that is capable of dealing with burst errors. The message frame contains a block of eight-bit symbols, sized to be manipulated by the Reed-Solomon encoder. The Message Frame input, Encode function, Split into Independent Channels function, and the output Codeword Frame are detailed in Figure 13.

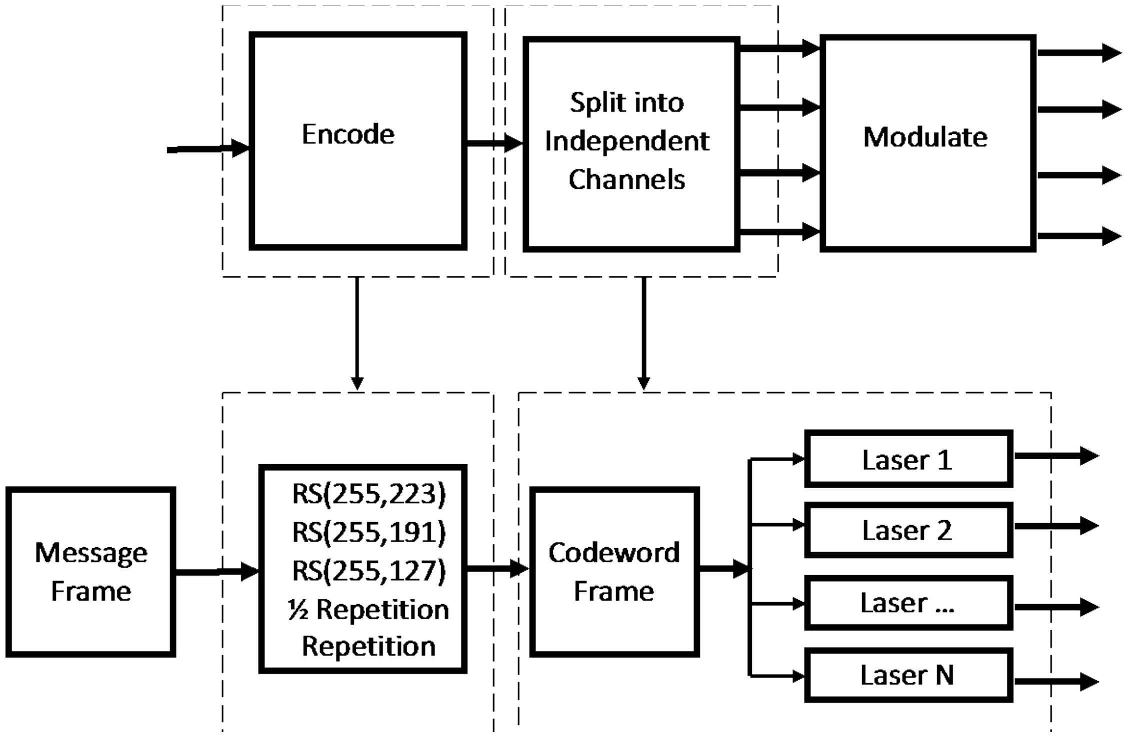

Figure 13. Simulated Encoding and Split into Independent Channels Functions

There are three Reed-Solomon options explored in the simulation. The Reed-Solomon encoding algorithm receives a frame of 8-bit message words. The output of the encoding function is a frame of 255 different 8-bit codewords. The 8-bit codewords from the RS codes are fed sequentially into the buffer for the architecture's number of lasers. The RS and repetition schemes are presented in Figure 14.

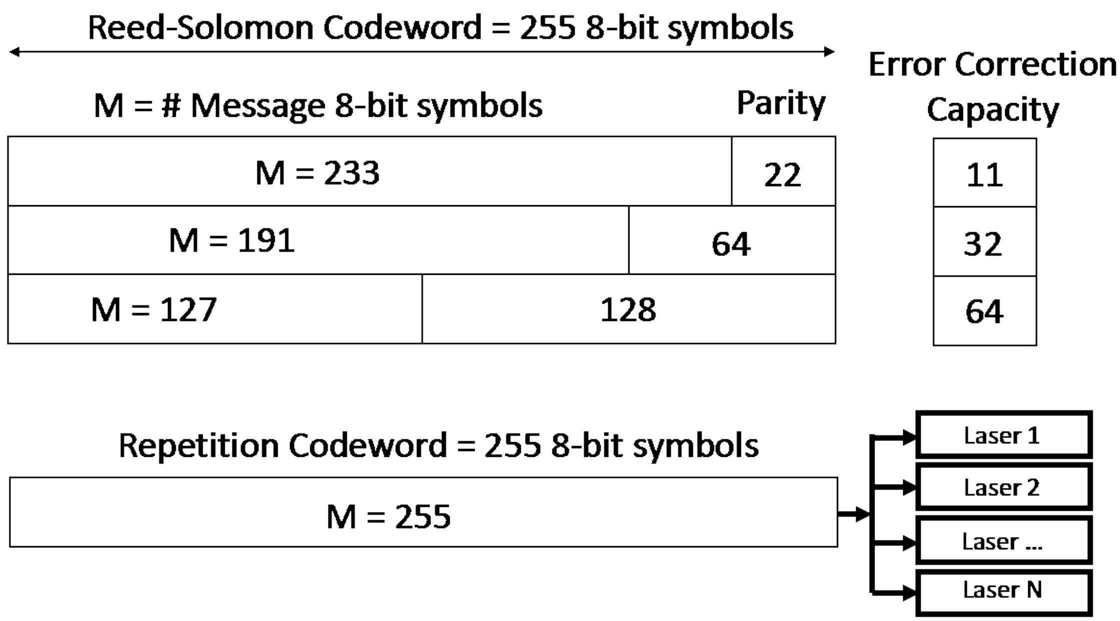

Figure 14. Encoding Functions

The RS codes offer error correction capacity. Error correction capacity describes the ability to receive a number of incorrect symbols within the codeword and still decode the correct message. This error correction capacity is dependent on the number of parity symbols added to the message symbols. Huffman (2003) defines the rate of the code as the ratio of message information within the transmitted codewords. Increased error correction capacity results in decreased message transmission rates since the parity symbols must also be transmitted.

The repetition coding scheme leverages the aperture averaging approach. The half-rate repetition coding scheme transmits the same information across half of the lasers, and a second stream of information over the other half of the lasers. The full repetition coding scheme transmits the same stream of information across all channels.

b. Split into Independent Channels Function

The system will split the codewords into independent channels associated with the number of lasers. The simulation explores the effect of the architecture incorporating 4, 8, 16, and 32 laser transmitters. Increased numbers of lasers in the system have the potential to increase transmission rates, but increase system size, weight, and power consumption.

c. Modulation Function

The purpose of signal modulation is to impart information into the pulses of the laser beam. The chosen modulation schemes employ variations of pulse-position modulation. The laser beam pulses in an assigned time slot in order to transmit the message information. Figure 15 presents a representative modulation by each of the four modulation schemes: On-off-keying (OOK), binary pulse-position modulation (BPPM), 2-ary pulse position modulation (PPM), and 4-ary PPM.

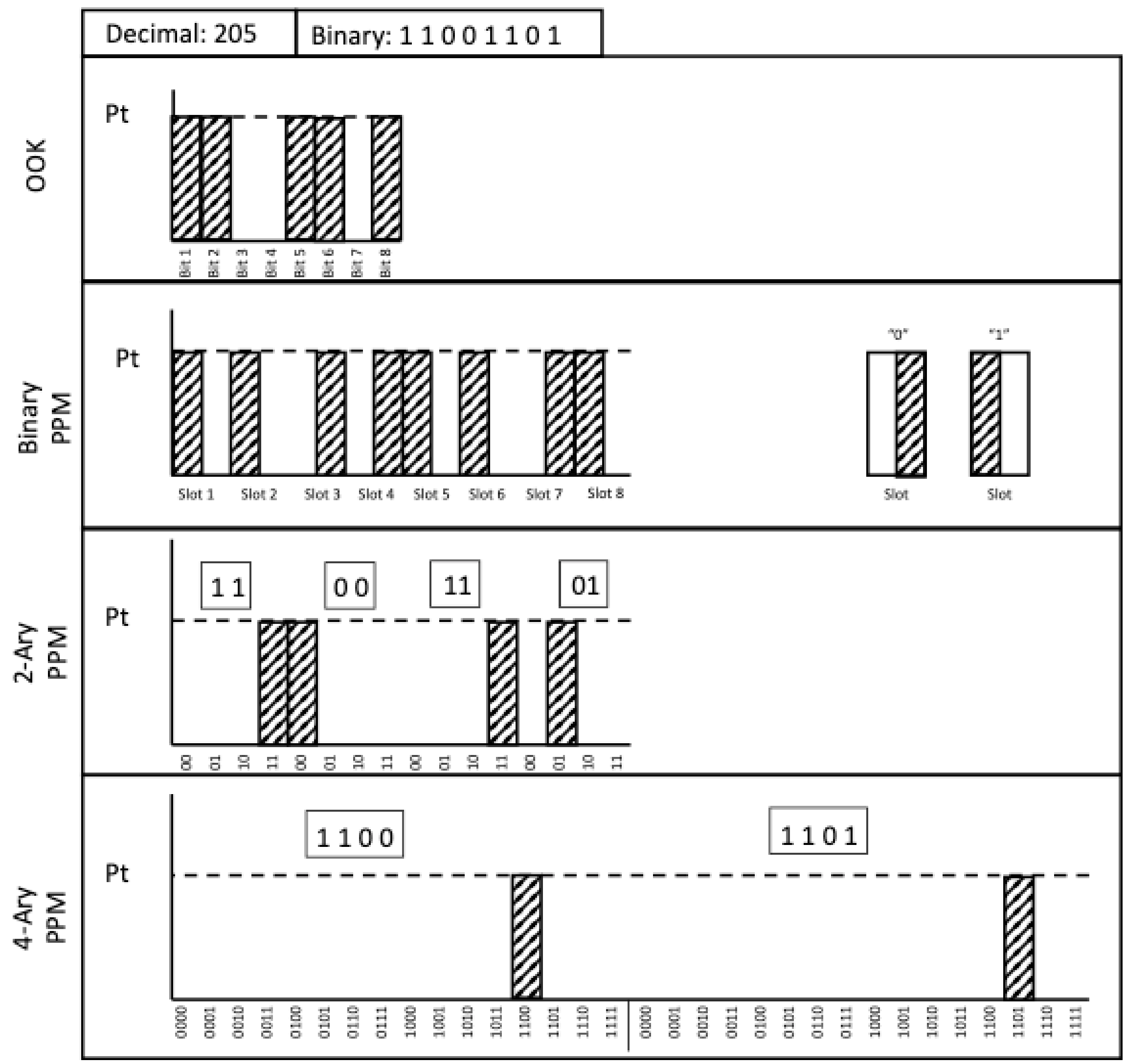

Figure 15. Modulation Schemes

Lasers within the FSOC systems are modulated at a consistent speed to allow the detector to extract the information from received optical waves. OOK is the simplest modulation scheme. Each 8-bit codeword is split into eight time slots. A pulse represents a "1" and the absence of a pulse represents a "0." If the system fails to detect a transmitted pulse, there is only the loss of a single bit.

The BPPM scheme introduces redundancy. Each bit requires a duration of two time slots. The BPPM implementation of the 1 and 0 bits are presented on the right side of the BPPM section in Figure 15. The power consumption is increased for the BPPM but allows for the ability to identify bit errors during the demodulation step. If a bit window receives two pulses or fails to detect any pulse, then there is an identified error.

The 2-ary and 4-ary PPM schemes assign a time slot to either a 2-bit or 4-bit sequence. The 2-ary PPM scheme splits an 8-bit codeword into four 2-bit sections. The pulse is then assigned to the time slot corresponding to its value. The 4-ary PPM scheme splits an 8-bit codeword into two 4-bit fragments and assigns the laser pulse to the appropriate time slot. As the power efficiency of the modulation scheme increases, the amount of information transmitted within each pulse also increases. The effects of the optical channel volatility combined with the modulation scheme choice will be analyzed following the experiment.

d. Transmit Function

The final critical decision in the systems architecture are the laser specifications. The simulation will receive the signal to noise ratio (SNR) as a proxy for the laser power. During the analysis of the simulated system performance, the appropriate laser power to achieve the system's SNR requirement will be derived. The transmitter function parameters are presented in Table 2.

Table 2. Transmitter Function Parameters

Transmitter Variable	Parameter Value	Unit
Signal-to-Noise Ratio	15, 30, 45	dB
Wavelength	850, 1550	nm

Under normal conventions, the signal-to-noise ratio is "defined as the ratio of signal power to the noise power" (Stotts 2017, 336). Both Stotts (2017) and Andrews and Phillips (2005) develop equations for the optical SNR at the receiver. Assuming that the noise current after the output filter has a mean of zero, they define the output optical SNR as the ratio of the detector current, i_S, to the root-mean-square (RMS) noise current, σ_N.

$$SNR_{Optical} = \frac{i_S}{\sigma_N} \tag{1}$$

The noise current represents all noise sources and is modeled as a Gaussian distribution with a zero mean (Andrews and Phillips 2005). For a given SNR parameter, the required detector signal current will be derived. The effect of the laser's wavelength is also explored. First generation FSOC system lasers typically operate at 1550 nm wavelength, while newer vertical-cavity surface-emitting laser (VCSEL) are widely available with an operating wavelength of 850 nm.

There were several critical beam parameters that were held constant to allow for consistent comparison across the architecture decisions. The beam is modeled as a collimated transverse electro-magnetic (TEM) Gaussian-beam wave. The wave number, k, is derived from the wavelength in Equation 2.

$$k = \frac{2\pi}{\lambda} \text{ [m}^{-1}\text{]} \tag{2}$$

e. Optical Channel

This section will develop the key optical channel effects within the model. The effects of the weak, moderate, and strong turbulence level effects on the laser beam will be captured with the Rytov Variance. The duration of deep fades within the channel will be developed. Finally, the probabilistic characteristics of the laser beam irradiance after traveling through the atmospheric channel will be developed.

(1) Channel Turbulence

The strength of atmospheric turbulence is represented by the refractive index structure parameter C_n^2 [$m^{-2/3}$]. The turbulence effects on the beam are described using the Rytov variance, σ_R^2 (Andrews and Phillips 2001). The link distance, L [m], will be held constant at 1000 meters to support architecture comparisons. The development of this value is presented in Equation 3.

$$\sigma_R^2 = 1.23 C_n^2 k^{7/6} L^{11/6} \text{ [unitless]} \quad (3)$$

The refractive index structure parameter varies significantly over the course of the day, showing a diurnal cycle (Stotts et al. 2010; Andrews and Phillips 2005). Additionally, the parameter varies due to geographic location and weather effects. Typical refractive index levels presented in Table 3 were described by Andrews and Philips (2005). Typical Rytov variance parameter values are calculated using Equations 2 and 3. The typical values are categorized by the qualitative turbulence levels presented in Table 3.

Table 3. Channel Turbulence Parameters

Turbulence Level	C_n^2	σ_R^2 $\lambda = 1550nm$	σ_R^2 $\lambda = 850nm$
Weak	$1\times10^{-15} m^{-2/3}$	0.02	0.04
Moderate	$1\times10^{-13} m^{-2/3}$	1	1
Strong	$5\times10^{-13} m^{-2/3}$	9.95	20.06

The turbulence levels correspond to typical qualitative optical channel descriptions discussed in the literature (Andrews and Phillips 2005). The Rytov variance parameter significantly affects the irradiance present at the receiver and directly impacts the probability of detecting the beam in the plane of the photodetector.

(2) Irradiance

Irradiance is the measure of power divided by area. The FSO system's laser beam irradiance is described by a randomly fading signal that follows the gamma distribution for both small-scale, α, and large-scale, β, turbulence effects. This effect is also referred to as scintillation. Equation 4 presents the derivation of the parameter for small-scale turbulence effects. Equation 5 presents the derivation of the parameter for large-scale turbulence effects.

$$\frac{1}{\alpha} = \exp\left(\frac{0.49\sigma_R^2}{\left(1+1.11\sigma_R^{12/5}\right)^{7/6}}\right) - 1 \text{ [unitless]} \quad (4)$$

$$\frac{1}{\beta} = \exp\left(\frac{0.51\sigma_R^2}{\left(1+0.69\sigma_R^{12/5}\right)^{5/6}}\right) - 1 \text{ [unitless]} \quad (5)$$

The small-scale and large-scale turbulence effect parameters derived in Equations 4 and 5 support the derivation of the gamma-gamma distribution for irradiance in the plane of the receiver. Equation 6 presents the probability distribution function (PDF) (Andrews and Phillips 2005). The irradiance, *I*, is any positive value. Additional functions present within the probability function are the gamma function, *Γ*, and the Bessel function, *K*.

$$p_I(I) = \frac{2(\alpha\beta)^{(\alpha+\beta)/2}}{\Gamma(\alpha)\Gamma(\beta)I} I^{(\alpha+\beta)/2-1} K_{\alpha-\beta}\left(2\sqrt{\alpha\beta I}\right), I > 0 \text{ [unitless]} \quad (6)$$

Equation 7 presents the total scintillation index developed from the parameters in Equations 4 and 5 (Andrews and Phillips 2001).

$$\sigma_I^2 = \frac{1}{\alpha} + \frac{1}{\beta} + \frac{1}{\alpha\beta} \text{ [unitless]} \quad (7)$$

The total scintillation index describes the irradiance fluctuations that the optical wave will experience across the link distance.

f. Detect Function

The model employs a direct detection scheme. The purpose of the photodetector is to detect the transmitted optical energy and translate that into the same information in the original message. The generic PDF function for measured irradiance in the plane of the photodetector is presented in Figure 16.

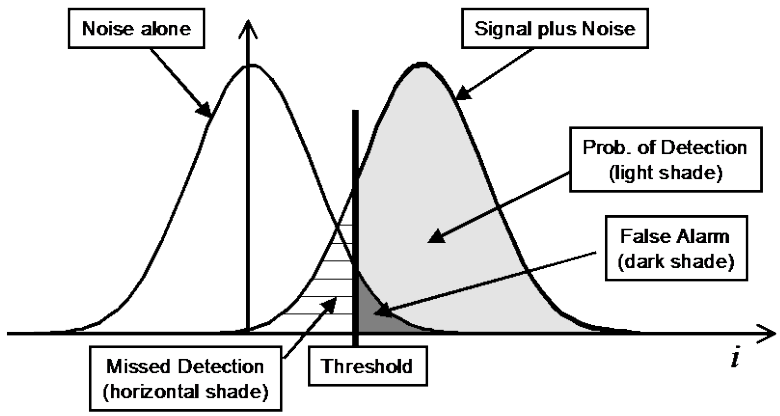

Figure 16. Probability of Detection and False Alarm. Source: Andrews and Phillips (2005).

The probabilistic nature of the irradiance was derived in Equation 6. As the laser power increases, the signal plus noise curve will move to the right of the figure. This allows the threshold irradiance for detection to be optimally placed to minimize the probability of missed detection and the probability of false alarm. Utilizing the PDF for the irradiance in the plane of the photodetector from Equation 6, the probability of detection is defined in Equation 8 and probability of false alarm in Equation 9 (Andrews and Phillips 2005). To simplify the model calculations, the received signal's irradiance, i_S, is normalized to 1. The threshold irradiance for detection of the signal varies between 0.125 and 0.5.

$$P_d \equiv \Pr(i > i_T) = \int_{i_T}^{\infty} p_{s+n}(i)\,di = \frac{1}{2} erfc\left(\frac{i_T - i_S}{\sqrt{2}\sigma_N}\right) \text{ [unitless]} \quad (8)$$

$$P_{fa} \equiv \Pr(i_N > i_T) = \int_{i_T}^{\infty} p_N(i)\,di \text{ [unitless]} \quad (9)$$

The mean fade time represents the average length of time, measured in seconds that the irradiance measured at the receiver is below the threshold. Equation 10 presents the derived number of threshold crossings for a gamma-gamma distributed irradiance in one second (Andrews and Phillips 2005). The quasi-frequency, v_0 [Hz], represents the frequency of irradiance threshold crossings. In order to simplify the model and facilitate consistency across the architectural decisions, it is held constant at 550 Hz. This frequency is representative of an appropriate frequency based on common system parameters. (Andrews and Phillips 2005). The parameter I_T, represents the irradiance threshold set by the detector.

$$\langle n(I_T)\rangle = \frac{2\sqrt{2\pi\alpha\beta}\,v_0\sigma_I}{\Gamma(\alpha)\Gamma(\beta)}\left(\frac{\alpha\beta I_T}{\langle I\rangle}\right)^{(\alpha+\beta-1)/2} K_{\alpha-\beta}\left(2\sqrt{\frac{\alpha\beta I_T}{\langle I\rangle}}\right) \text{ [crossings / second]} \quad (10)$$

Equation 11 presents the probability of fade (Andrews and Phillips 2005). This represents the probability that the irradiance distribution in the plane of the receiver falls below the set irradiance threshold.

$$\mathrm{P}_{Fade} = P(I \le I_T) = \int_0^{I_T} p_I(I)\,dI = 1 - P_d \text{ [unitless]} \quad (11)$$

Equation 12 presents the mean fade time in seconds that the signal irradiance will spend below the set threshold level (Andrews and Phillips 2005).

$$\langle t(I_T)\rangle = \frac{\Pr(I \le I_T)}{\langle n(I_T)\rangle} \text{ [seconds]} \quad (12)$$

With the mean fade time developed, the model is capable of closely representing the challenges that deep fades present to FSOC system performance.

g. Decoding Function

The decoding function executes the inverse of the assigned encoding function. The Reed-Solomon codes will correct errors up to the correction capacity of the code. The error code capacity was derived from the Reed-Solomon parameters and presented in Figure 14. The repetition codes will compare the channels that repeated the original message. The output from this function is the highest frequency bit across the optical channels.

h. Design Decisions

The functional flow block diagram was presented in Figure 12. This section has explored the development of the architectural decisions. A comprehensive presentation of the decisions is presented in Figure 17. The environmental parameter, the refractive index, is set apart from the design decisions in the top of the figure. While this parameter is not a part of the design, it interacts with the SNR, laser wavelength, and the irradiance threshold to determine the probability of detection, probability of fade, and the mean fade time.

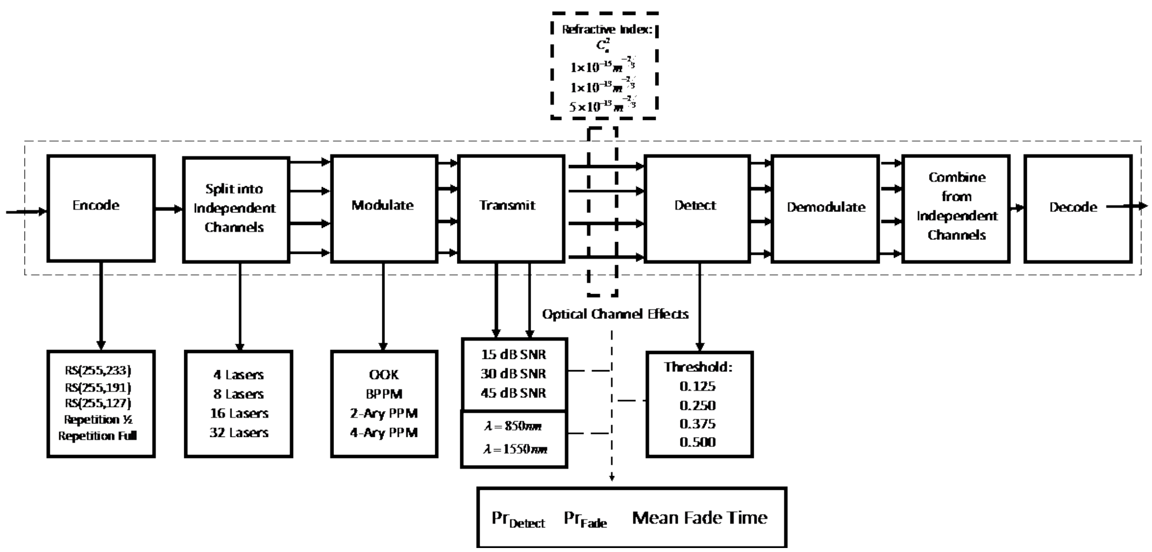

Figure 17. Architecture Design Decisions

The architectural decisions that are under control within the system design are presented in the bottom of Figure 17. In the Encode function, the design decision is between the three RS coding schemes and the two repetition coding schemes. In the Split into Independent Channels function, the design decision is the number of lasers the system employs. In the Modulate function, the design decision is between the OOK, BPPM, 2-ary PPM, and 4-ary PPM. In the Transmit function, there are two design decision: system SNR and laser wavelength. The system SNR parameter is 15, 30, and 45 decibels. The laser wavelengths are 850 and 1550 nm. In the Detect function, the design decision is the irradiance Threshold for detecting the transmitted signal. The thresholds are 0.125, 0.250, 0.375, and 0.500.

D. DESIGN OF EXPERIMENTS

The experimental design is a full factorial that examines the limits of the design space and explores the interactions between architecture decisions. The experiment parameters are presented in Table 4.

Table 4. Design of Experiment Parameter Values

Parameter	Values
Number of Lasers	4, 8, 16, 32
Coding Scheme	RS(233,255), RS(191,255), RS(127,255), Half Repetition, Full Repetition
Modulation Scheme	OOK, BPPM, 2-Ary PPM, 4-Ary PPM
Laser Wavelength	850 nm, 1550 nm
Irradiance Threshold	0.125, 0.250, 0.375, 0.500
SNR	15, 30, 45 dB
Refractive Structure Parameter (Optical Channel)	$1\times10^{-15}m^{-2/3}$, $1\times10^{-13}m^{-2/3}$, $5\times10^{-13}m^{-2/3}$

Each replication of the experiment will simulate the transmission of 2 megabits across the free space channel. There are 1,920 different candidate architectures. Each experimental design will include a candidate architecture at one of three different atmospheric turbulence conditions. The experiment will have four replications of each experimental design resulting in 23,040 runs. The experimental results are analyzed using analysis of variance (ANOVA) methods. The focus of the analysis is on determining the main effects and factor interactions.

THIS PAGE INTENTIONALLY LEFT BLANK

IV. ANALYSIS OF SIMULATED PERFORMANCE

The experiment was conducted using MATLAB scripts and the Communications Toolbox package. MATLAB R2018b was used for this simulation. The full factorial experimental design was leveraged to fully explore the interactions from the design decisions presented in Chapter III, Figure 17. This chapter begins with a detailed presentation of the simulation model. The chapter then presents a two-way analysis of variance (ANOVA) with interaction analysis for BER. The derivation of the transmission rate and power efficiency follows. The chapter concludes with a tradeoff analysis for the design space architectures amongst the BER, transmission rate, and power efficiency.

A. DETAILED SIMULATION MODEL

The detailed MATLAB code is presented in Appendix A. This section will present the conceptual overview of how the simulations were conducted.

1. Design Parameters

For each simulated experiment, the design parameters for a candidate architecture include the coding scheme, number of lasers, modulation scheme, refractive index, laser wavelength, detector irradiance threshold, and the system SNR. The key channel effects that support the simulation are the probability of detection, probability of false alarm, probability of fade, and mean fade time in seconds. These effects were derived for all combinations of the atmospheric refractive index, laser wavelength, detector irradiance threshold, and the SNR.

2. Simulation Time Step

The base time unit for the simulation is the laser modulation speed. Each time step in the Monte Carlo simulation is based on the 100 MHz laser modulation speed. The duration of the atmospheric deep fades is converted into the number of time steps by multiplying the mean fade time in seconds by the laser modulation speed. This results in the mean fade time in number of time steps.

3. Encode Function

The output of this section is a stream of codewords aligned to each laser in the candidate architecture. The information source's message consists of approximately 2 million bits, or approximately 250,000 8-bit message words. The original message words consist of random integers between 0 and 255. The message length is derived from the candidate architecture coding scheme. The RS codes have potential message lengths of 127, 191, and 223. The matrix manipulation is presented in Figure 18. The algorithm starts with a message composed of approximately 250,000 random 8-bit message words.

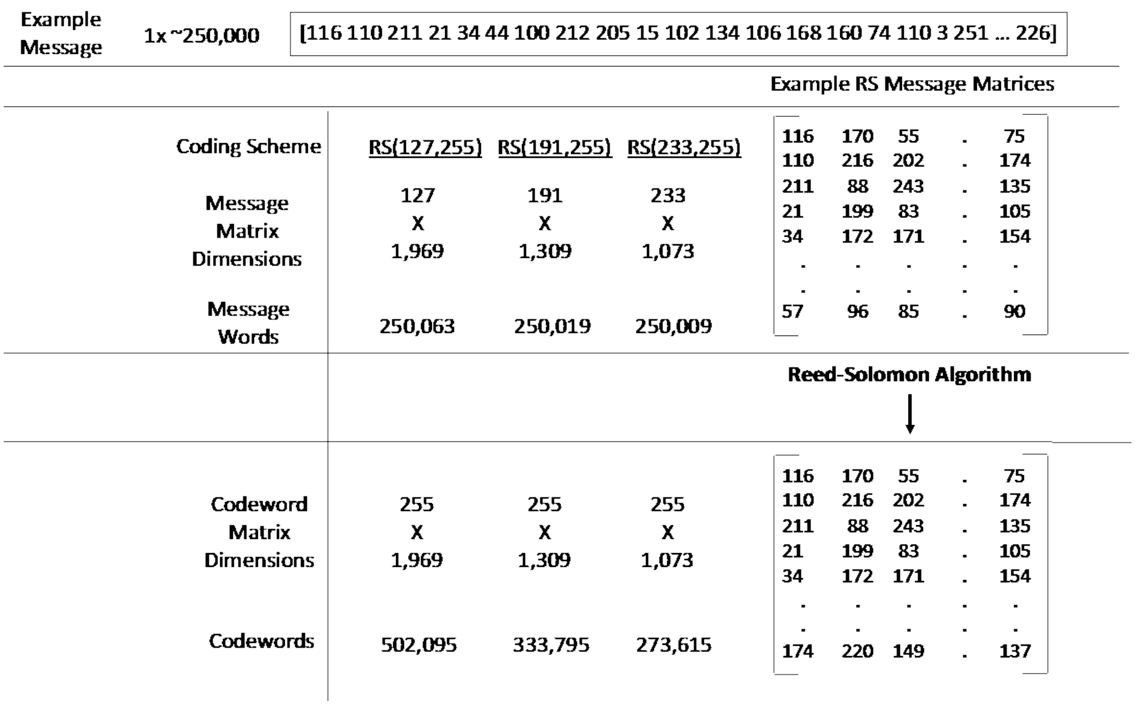

Figure 18. Example Simulation Information Source Encoding, Reed-Solomon Codes

The repetition codes have a message length of 255. The matrix manipulations for the repetition codes are presented in Figure 19.

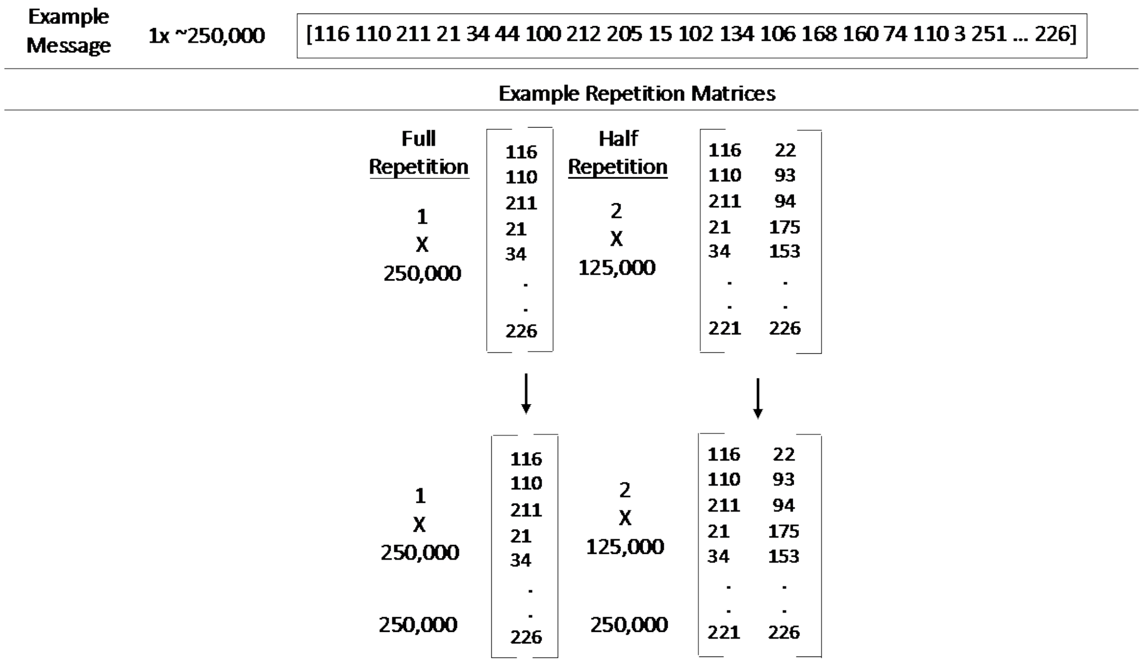

Figure 19. Example Simulation Information Source Encoding, Repetition Codes

The message words are then reshaped into a matrix appropriately dimensioned to support RS encoding. The dimensions of the message matrices are presented in the upper section of Figure 18. Each column in the RS message matrix is a frame of the appropriate message length for the RS code. Each column is manipulated using the Reed-Solomon encoding object within the MATLAB Communications Toolbox. The output of this function is the codeword matrix. Each column of the codeword matrix is 255 codewords long. At this point in the simulation, the cost of increased error correction capacity in the RS codes is evident in the growth in number of codewords.

4. Split into Independent Channels

After encoding, the codewords are split into independent channels. In the simulation, this is accomplished by reshaping the codewords matrices into a matrix with the number of rows equal to the architecture's number of lasers. An example implementation with 8 lasers is presented in Figure 20. The matrix dimensions are presented on the left side of the figures, while the example codeword matrix and laser stream matrices are presented on the right side.

Coding Scheme	RS(127,255)	RS(191,255)	RS(233,255)
Codeword Matrix Dimensions	255 X 1,969	255 X 1,309	255 X 1,073
Codewords	502,095	333,795	273,615

Example RS Codeword Matrix

116	170	55	.	75
110	216	202	.	174
211	88	243	.	135
21	199	83	.	105
34	172	171	.	154
.	.	.	.	.
.	.	.	.	.
174	220	149	.	137

8 Lasers	RS(127,255)	RS(191,255)	RS(233,255)
Symbols	502,096	333,800	273,616

RS Independent Channels

Laser 1	116	205	110	.	168
Laser 2	110	15	3	.	56
Laser 3	211	102	251	.	31
Laser 4	21	134	42	.	39
Laser 5	34	106	27	.	77
Laser 6	44	168	95	.	139
Laser 7	100	160	50	.	72
Laser 8	212	74	125	.	137

Figure 20. Split into Independent Channels Matrix Manipulation, Reed-Solomon Codes

The simulation padded the codeword matrix with additional random integers to complete a matrix with the number of rows equal. The number of padding symbols is derived from Equation 13 using the modulo function.

$$Padding = \left(CodeWords\right)\mathrm{mod}\left(numLasers\right) \text{ [\# codewords]} \qquad (13)$$

An example of the matrix manipulations with eight lasers is presented in Figure 21. The full repetition code repeats the message across each independent channel. The half repetition code alternates the message across two independent channels.

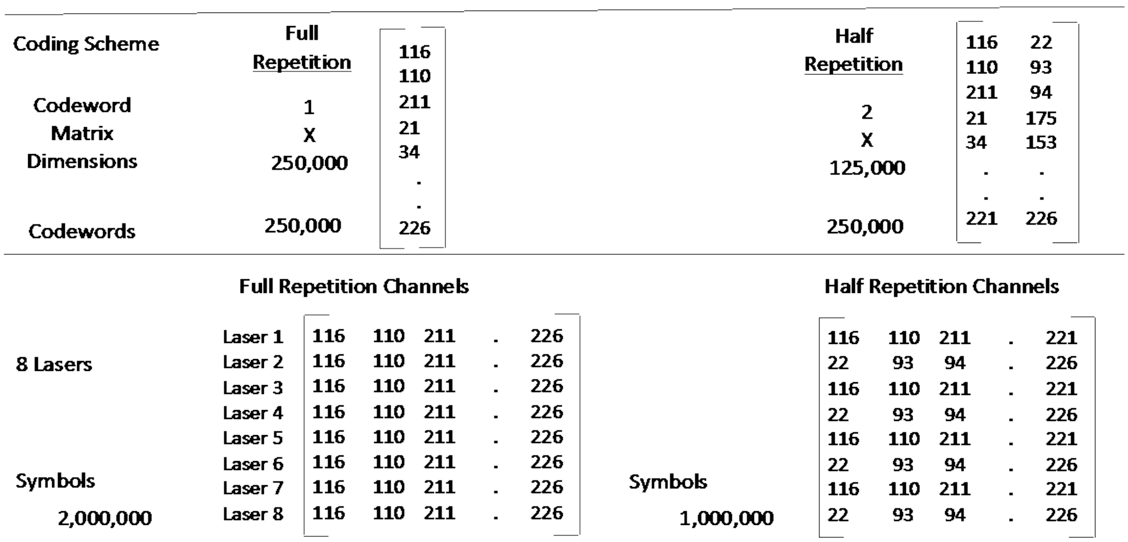

Figure 21. Split into Independent Channels Matrix Manipulation, Repetition Coding

These symbols are added to the last column of the independent channel matrix to allow MATLAB to conduct the required matrix manipulations. The stream of symbols transmitted through the lasers is labeled *laserStream* in the MATLAB script.

5. Channel States

The independent channels are modeled as either available or in a fade. The state of the channel is dependent on the probability of fade due to the atmospheric conditions. The initial state of each independent channel for the lasers is determined prior to the first transmission. The channel state matrix that tracked the status of the independent channels is presented in Figure 22.

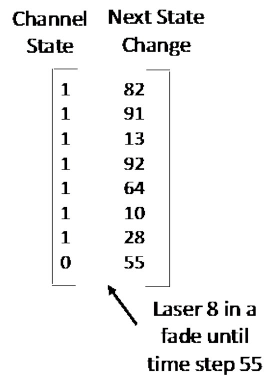

Figure 22. Channel State Matrix

The duration of the current channel state was tracked in terms of simulation time steps. The channel state cannot change until the designated simulation time step. The next state change is dependent on the mean fade time and the laser modulation speed. Based on Chan's (2006) research on fade times, the fade time was uniformly distributed. The mean fade time was determined from the atmospheric conditions. The maximum fade time was set at double the mean fade time. The minimum fade time was set at 1% of the maximum fade time. This captures the probabilistic nature of the fading effects (Chan 2006).

6. Global Variable Initialization

There are three global variables that support calculating the MOE and MOPs: *currentTime*, *totalPulses*, and *receivedLaserStream*. The *currentTime* for the simulation begins at 0 after the source encoding is complete. The simulation time increase by *1* each time slot during the transmit function. The *totalPulses* is initially set to *0*. This variable will increase with each laser pulse during the simulation. Finally, the *receivedLaserStream* variable is set as an empty matrix in MATLAB.

7. Modulate Function

The modulate function translates the 8-bit symbols into a sequence of laser pulses. The location of the laser pulses is dependent on the candidate architecture's modulation scheme. The simulation manipulates one column of the *laserStream* at a time. The simulated modulation function with OOK and BPPM outputs is presented in Figure 23.

	Laser Stream	OOK	BPPM
Laser 1	116	0 1 1 1 0 1 0 0	0 1 1 0 1 0 1 0 0 1 1 0 0 1 0 1
Laser 2	110	0 1 1 0 1 1 1 0	0 1 1 0 1 0 0 1 1 0 1 0 1 0 0 1
Laser 3	211	1 1 0 1 0 0 1 1	1 0 1 0 0 1 1 0 0 1 0 1 1 0 1 0
Laser 4	21	0 0 0 1 0 1 0 1	0 1 0 1 0 1 1 0 0 1 1 0 0 1 1 0
Laser 5	34	0 0 1 0 0 0 1 0	0 1 0 1 1 0 0 1 0 1 0 1 1 0 0 1
Laser 6	44	0 0 1 0 1 1 0 0	0 1 0 1 1 0 0 1 1 0 1 0 0 1 0 1
Laser 7	100	0 1 1 0 0 1 0 0	0 1 1 0 1 0 0 1 0 1 1 0 0 1 0 1
Laser 8	212	1 1 0 1 0 1 0 0	1 0 1 0 0 1 1 0 0 1 1 0 0 1 0 1

Figure 23. Simulation Modulation Function, OOK and BPPM

The first frame of symbols for the eight lasers is the input for Figure 23. The *1* denotes a laser pulse in that time slot, and the *0* denotes the lack of a laser pulse in that time slot.

8. Transmit and Receive Functions

The transmit function receives the modulated signal matrix as the input. The relevant system parameters are the probability of detection and probability of false alarm. These values are determined from the design parameters and the calculated atmospheric effects. The conditional probabilities of detecting irradiance above the receiver's threshold given a pulse or no pulse are presented in Equations 14-17.

$$\Pr(Rx = 1 \mid Tx = 1) = \Pr_{Detect} \text{ [unitless]} \quad (14)$$

$$\Pr(Rx = 0 \mid Tx = 1) = 1 - \Pr_{Detect} \text{ [unitless]} \quad (15)$$

$$\Pr(Rx = 1 \mid Tx = 0) = \Pr_{FalseAlarm} \text{ [unitless]} \quad (16)$$

$$\Pr(Rx = 0 \mid Tx = 0) = 1 - \Pr_{FalseAlarm} \text{ [unitless]} \quad (17)$$

The simulation time increases by a time unit per each laser pulse. If any independent channel is due for a state change, then the channel states are updated as discussed in Section 5.

9. Demodulate Function

The simulation inverses the modulation manipulations during this step. If the coding scheme is a variant of the RS code, the output from this simulation step is a column matrix of 8-bit symbols. This column matrix is concatenated with the previously received and demodulated signals. It is stored in the *receivedLaserStream* matrix variable. The modulate, transmit and receive, and demodulate steps iterate through the entire *laserStream* matrix.

If either the half or full repetition code is used, a hard decision is implemented at this step. For each time slot, if more than one pulse is received, a *1* is assigned to that time slot. Otherwise, a *0* is assigned to that time slot. The single modulated signal is then demodulated, and a single 8-bit symbol is appended to the *receivedLaserStream*.

10. Decode Function

At this point in the simulation, the padding symbols are removed from the *receivedLaserStream* matrix. If the RS coding scheme is used, the matrix is then reshaped in preparation for decoding. The RS decoder object within the Communication Toolbox in MATLAB executes the RS decoding algorithm. The simulation iterates through each column of the *receivedLaserStream* and outputs the *receivedMessage* matrix.

11. Simulation Outputs

The system BER is calculated using the biterr function in MATLAB. This function compares the number of bits received in error between the *inputMessage* and the *receivedMessage* matrices. Equation 18 converts the currentTime variable, representing the simulation time, into seconds.

$$Time_{Total} = \left(laserModulation\right)\left(currentTime\right) \text{ [seconds]} \tag{18}$$

Equation 19 calculates the transmission rate from the size of the message and the total simulation time.

$$Rate_{Transmission} = \frac{totalBits}{Time_{Total}} = \frac{2 \times 10^6}{Time_{Total}} \text{ [bits/second]} \tag{19}$$

Equation 20 calculates the power efficiency of the system in terms of laser pulses per message bit transmitted.

$$pulsesPerBit = \frac{totalPulses}{totalBits} = \frac{totalPulses}{2 \times 10^6} \text{ [pulses/bit]} \quad (20)$$

These three variables are the MOE and MOP that support the analysis of system performance.

B. IMPACT OF DESIGN ALTERNATIVES, BIT ERROR RATE ANALYSIS

The simulation results were analyzed using the JMP Pro statistical program. A regression model was fit to the simulation results using the JMP Pro 14 statistical program. The Fit Model function was used with the BER set as the response variable. The independent variables for the model are the modulation scheme, coding scheme, irradiance threshold, and SNR. These variables were coded as descriptive variables. The final independent variable was the number of lasers. It was encoded as a numerical continuous variable.

The analysis seeks to understand the main effects and interaction effects of the architecture decisions on system performance. Main effects are defined as the effect on performance that an architecture decision has by itself. Interaction effects are denoted as main effect * main effect. Interaction effects are the impact on system performance that two main effects have when they are present together. The purpose of identifying these interactions is to identify certain combinations of design decisions that have a synergistic positive or negative effect on system performance.

Initial analysis of the system performance was conducted assessing the main factors and the second-degree interactions identified that the SNR and atmospheric turbulence were most significant. The SNR and atmospheric turbulence significantly impact the probability of detection and the length of deep fades. The system will perform differently based on the atmospheric conditions in the channel. To focus on the changing system requirements due to the optical channel, the simulated performance was separately analyzed under each turbulence condition. The effect analysis for BER across all of the atmospheric turbulence conditions is presented in Appendix B. The high influence of the atmospheric turbulence led to the exploration of the system's performance in each turbulence level separately.

Each turbulence condition will present the regression model summary of fit, an analysis of the main effects, and an analysis of the significant interaction effects. The R^2 statistic measures the proportion of the variance within the system response that is explained by the independent variables. The output of each regression model was the identification of the architectural decisions or interaction between decisions that had the most impact on system performance. A significance level of 0.05 was the statistical threshold for effect significance. The 95% confidence level is presented for the main effects. If the confidence intervals for design decisions overlap, there is no statistically significant difference. If there is no overlap between design decisions, there is a statistically significant difference in the model’s response variable at the 95% confidence level.

1. Weak Turbulence

a. Regression Model.

The regression model developed for the weak turbulence condition explains 87% of the variance in BER. The summary of fit for the regression model for the BER system response in weak turbulence is presented in Figure 24.

Summary of Fit	
RSquare	0.873253
RSquare Adj	0.871716
Root Mean Square Error	0.03811
Mean of Response	0.050878
Observations (or Sum Wgts)	7680

Figure 24. Weak Turbulence Summary of Fit, BER

The effect summary is presented in Figure 25. The dotted line box highlights the statistically significant effects. The relative strength of the effect on the system BER is represented by the LogWorth. A higher LogWorth value indicates a stronger effect on the system's response variable. The remainder of this section will explore the BER response for each of the statistically significant main effects. Following the main effects, significant interaction effects will be explained.

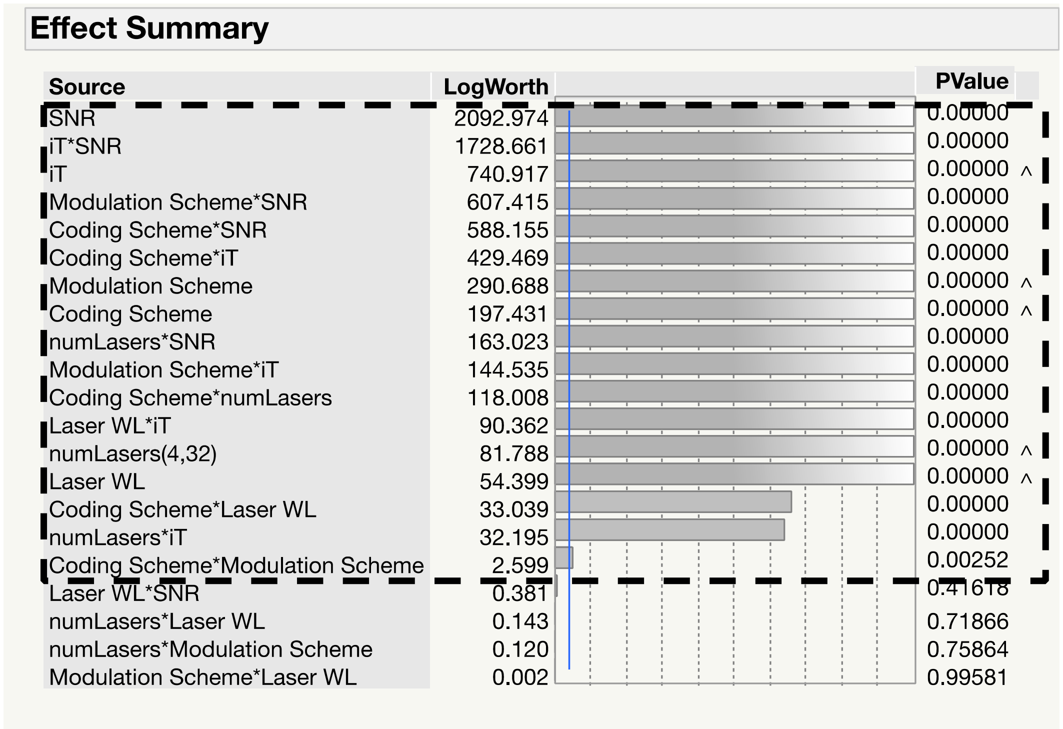

Effect Summary

Source	LogWorth	PValue
SNR	2092.974	0.00000
iT*SNR	1728.661	0.00000
iT	740.917	0.00000 ^
Modulation Scheme*SNR	607.415	0.00000
Coding Scheme*SNR	588.155	0.00000
Coding Scheme*iT	429.469	0.00000
Modulation Scheme	290.688	0.00000 ^
Coding Scheme	197.431	0.00000 ^
numLasers*SNR	163.023	0.00000
Modulation Scheme*iT	144.535	0.00000
Coding Scheme*numLasers	118.008	0.00000
Laser WL*iT	90.362	0.00000
numLasers(4,32)	81.788	0.00000 ^
Laser WL	54.399	0.00000 ^
Coding Scheme*Laser WL	33.039	0.00000
numLasers*iT	32.195	0.00000
Coding Scheme*Modulation Scheme	2.599	0.00252
Laser WL*SNR	0.381	0.41618
numLasers*Laser WL	0.143	0.71866
numLasers*Modulation Scheme	0.120	0.75864
Modulation Scheme*Laser WL	0.002	0.99581

Figure 25. Weak Turbulence Effect Summary for BER

b. Main Effects

The achievement of an adequate SNR at the receiver and setting an appropriate irradiance threshold for that SNR are the most significant effects on the system performance. While the modulation scheme and coding scheme have an effect on the system, it is not as pronounced. The atmospheric effects are mild when the turbulence is weak. The effects on the optical channel are able to be mitigated with additional power.

- SNR. There is a statistically significant improvement in the system BER when the SNR increases from 15 dB to 30 dB. The system's mean BER improves by a factor of 15. After 30 dB, however, there was no statistically significant improvement at the 95% confidence level. The 95% confidence interval for the mean BER is presented in Table 5.

Table 5. Mean BER by SNR, 95% Confidence Interval in Weak Turbulence

SNR	Mean	Std Dev	95% Confidence Interval
15 dB	0.1351	0.1491	[0.1293, 0.1409]
30 dB	0.0088	0.0249	[0.0078, 0.0098]
45 dB	0.0088	0.0229	[0.0079, 0.0097]

- <u>Irradiance Threshold.</u> The 0.375 irradiance threshold outperformed the other three thresholds. It performed the best by maximizing the probability of detection and minimizing the probability of false alarm. The 95% confidence interval for the mean BER is presented in Table 6.

Table 6. Mean BER by Irradiance Threshold, 95% Confidence Interval in Weak Turbulence

Irradiance Threshold	Mean	Std Dev	95% Confidence Interval
0.125	0.0968	0.1618	[0.0895, 0.1040]
0.250	0.0533	0.1098	[0.0484, 0.0582]
0.375	0.0205	0.0476	[0.0184, 0.0227]
0.500	0.0329	0.0377	[0.0313, 0.0346]

- <u>Modulation Scheme.</u> The BPPM and OOK modulation schemes outperform the 2-ary and 4-ary modulation schemes in terms of BER. These two schemes have no statistical difference in mean BER. The 95% confidence intervals for the mean BER are presented in Table 7.

Table 7. Mean BER by Modulation Scheme, 95% Confidence Interval in Weak Turbulence

Modulation Scheme	Mean	Std Dev	95% Confidence Interval
2ARY	0.0491	0.1001	[0.0446, 0.0536]
4ARY	0.0799	0.1438	[0.0735, 0.0863]
BPPM	0.0372	0.0818	[0.0336, 0.0409]
OOK	0.0372	0.0818	[0.0336, 0.0409]

- Coding Scheme. In low turbulence conditions, there was no statistically significant difference between the three potential RS coding schemes. The repetition half scheme performed the worst. While there was no statistically significant difference between the RS(255,233) and the full repetition scheme, the RS(255,127) and RS(255,191) both performed better than the full repetition scheme with a lower mean BER response. The 95% confidence intervals for the mean BER by coding scheme is presented in Table 8.

Table 8. Mean BER by Coding Scheme, 95% Confidence Interval in Weak Turbulence

Coding Scheme	Mean	Std Dev	95% Confidence Interval
Rep Full	0.0553	0.1346	[0.0486, 0.0620]
Rep Half	0.0714	0.1445	[0.0642, 0.0786]
RS(255,127)	0.0383	0.0764	[0.0345, 0.0421]
RS(255,191)	0.0438	0.0748	[0.0401, 0.0475]
RS(255,233)	0.0456	0.0741	[0.0419, 0.0493]

- Number of Lasers. As the number of lasers increases, the mean BER also increases. The increase is not statistically significant until the number of lasers increases by a factor of 4. When the lasers increased from 4 to 8, 8 to 16, and 16 to 32, there was no statistically significant difference in the mean BER. There was, however, a statistically significant difference between the 4 and 16 laser arrays, the 4 and 32 laser arrays, and the 8 and

32 laser arrays. The 95% confidence intervals for the mean BER by number of lasers is presented in Table 9.

Table 9. Mean BER by Number of Lasers, 95% Confidence Interval in Weak Turbulence

Number of Lasers	Mean	Std Dev	95% Confidence Interval
4	0.0393	0.0801	[0.0357, 0.0428]
8	0.0466	0.0966	[0.0422, 0.0509]
16	0.0550	0.1139	[0.0499, 0.0601]
32	0.0627	0.1275	[0.0570, 0.0684]

- Laser Wavelength. The 1550 nm laser has a better mean BER at a 95% confidence level. This is likely due to the increased probability of detection and decreased probability of fade for the atmospheric channel. The 95% confidence intervals for the mean BER by laser wavelength is presented in Table 10.

Table 10. Mean BER by Laser Wavelength, 95% Confidence Interval in Weak Turbulence

Laser Wavelength	Mean	Std Dev	95% Confidence Interval
1550 nm	0.0437	0.1057	[0.0404, 0.0471]
850 nm	0.0580	0.1066	[0.0547, 0.0614]

c. Interaction Effects

Significant interaction effects amongst the main factors are evident when the response lines are not parallel. The interaction plots explore the interactions between the coding scheme, number of lasers, modulation scheme, laser wavelength, irradiance threshold, and the system SNR. The interaction plots for the mean BER in weak turbulence are presented in Figure 26.

The only significant interaction is between the irradiance threshold and the system SNR. This is interaction is highlighted by the bold box in the figure. When the SNR is 30 dB or 45 dB, increasing irradiance threshold increases the BER. When the SNR is only 15 dB, however, the BER reduces as the irradiance threshold increases. This is likely due to the changing probability of detection and probability of false alarm.

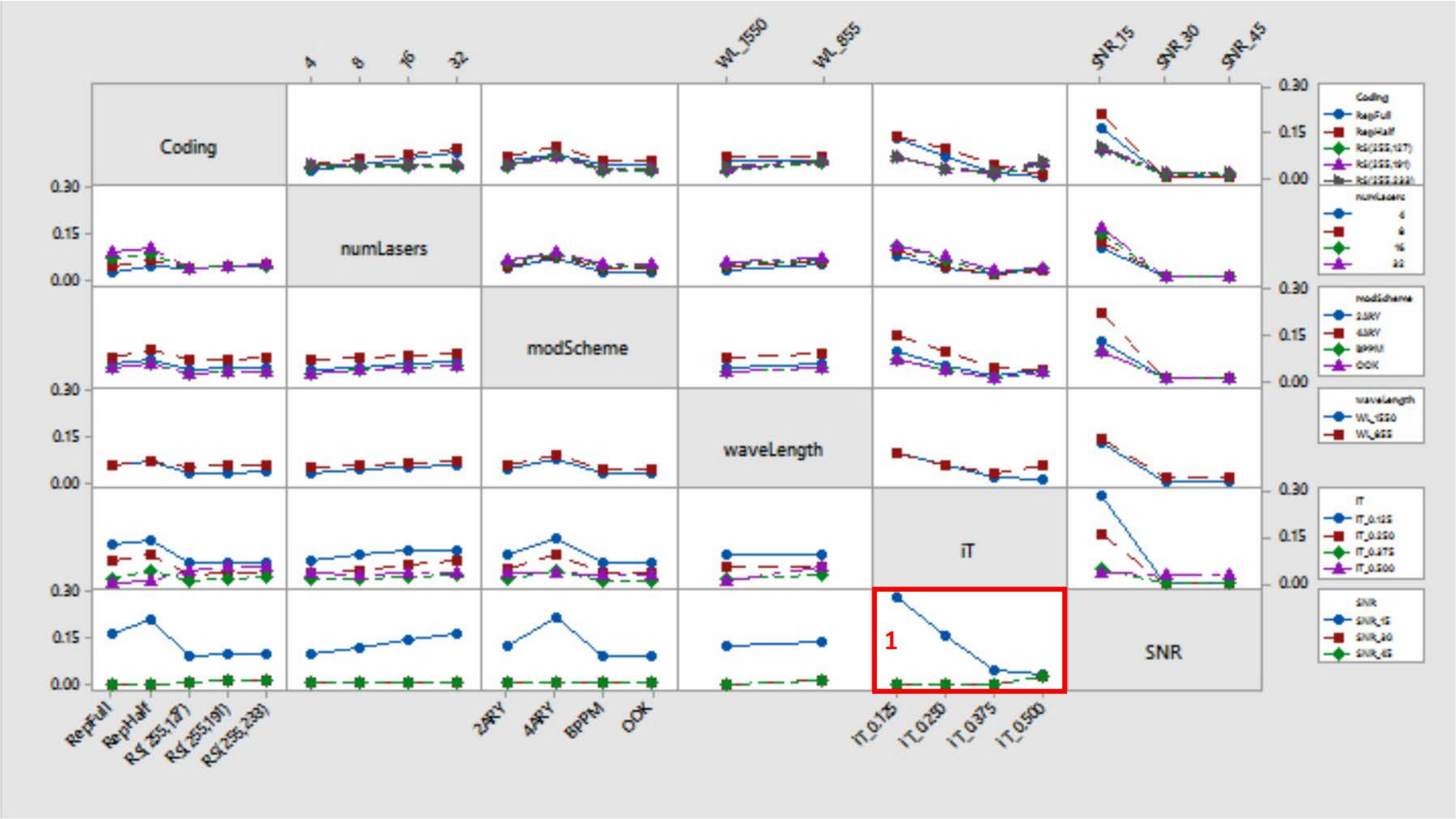

Figure 26. Weak Turbulence Interaction Plot for BER, Data Means

2. Moderate Turbulence

This section will analyze the system's response to architecture decisions when atmospheric turbulence is described as moderate. The regression model statistics, the main effects, and the interaction effects will be presented.

a. Regression Model

The model for the moderate turbulence condition explains 87% of the variability in the BER. The summary of fit for the model is presented in Figure 27.

Summary of Fit	
RSquare	0.872004
RSquare Adj	0.870452
Root Mean Square Error	0.045002
Mean of Response	0.149475
Observations (or Sum Wgts)	7680

Figure 27. Moderate Turbulence Summary of Fit, BER

As in the weak turbulence condition, achieving 30 dB of SNR and setting an appropriate irradiance threshold at the receiver to maximize probability of detection and minimize probability of false alarm is the most critical decision. The statistically significant effects for the BER response variable are highlighted by the dashed line box and presented in Figure 28.

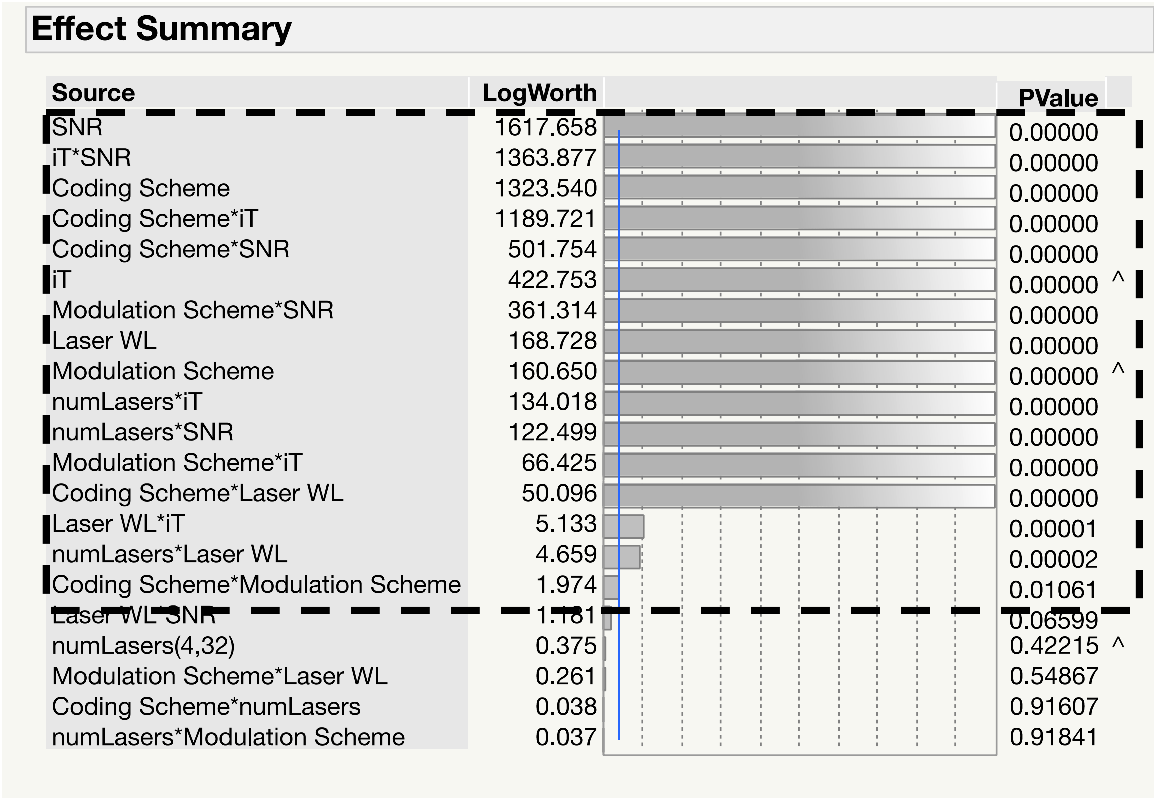

Effect Summary

Source	LogWorth	PValue
SNR	1617.658	0.00000
iT*SNR	1363.877	0.00000
Coding Scheme	1323.540	0.00000
Coding Scheme*iT	1189.721	0.00000
Coding Scheme*SNR	501.754	0.00000
iT	422.753	0.00000 ^
Modulation Scheme*SNR	361.314	0.00000
Laser WL	168.728	0.00000
Modulation Scheme	160.650	0.00000 ^
numLasers*iT	134.018	0.00000
numLasers*SNR	122.499	0.00000
Modulation Scheme*iT	66.425	0.00000
Coding Scheme*Laser WL	50.096	0.00000
Laser WL*iT	5.133	0.00001
numLasers*Laser WL	4.659	0.00002
Coding Scheme*Modulation Scheme	1.974	0.01061
Laser WL*SNR	1.181	0.06599
numLasers(4,32)	0.375	0.42215 ^
Modulation Scheme*Laser WL	0.261	0.54867
Coding Scheme*numLasers	0.038	0.91607
numLasers*Modulation Scheme	0.037	0.91841

Figure 28. Moderate Turbulence Effect Summary, BER

b. Main Effects

This section will explore the main effects in moderate turbulence. The number of lasers is the only architectural decision that is not statistically significant as a main effect. Its *p*-value is 0.42. The number of lasers does contribute to several interaction effects.

- <u>SNR.</u> The BER improvement due to increased SNR is less pronounced in under moderate turbulence conditions. The mean BER only improves by a factor of 2, compared to a factor of 15 in the weak turbulence condition. After the system SNR achieves 30 dB at the receiver, there is no statistically significant benefit to increased SNR. The 95% confidence intervals for the mean BER grouped by SNR is presented in Table 11.

Table 11. Mean BER by SNR, 95% Confidence Interval in Moderate Turbulence

SNR	**Mean**	**Std Dev**	**95% Confidence Interval**
15 dB	0.2294	0.1225	[0.2247, 0.2342]
30 dB	0.1095	0.1056	[0.1054, 0.1136]
45 dB	0.1095	0.1056	[0.1054, 0.1136]

- Coding Scheme. As the atmospheric turbulence increases, the error correction capability of the RS codes is stressed. They are unable to correct the increasing number of errors induced by the optical channel. The repetition codes outperformed the RS codes at the 95% confidence level. The full repetition code also outperformed the half repetition code at the 95% confidence level. The mean BER grouped by coding scheme is presented in Table 12.

Table 12. Mean BER by Coding Scheme, 95% Confidence Interval in Moderate Turbulence

Coding Scheme	**Mean**	**Std Dev**	**95% Confidence Interval**
Rep Full	0.0797	0.1365	[0.0736, 0.0858]
Rep Half	0.0935	0.1418	[0.0872, 0.0999]
RS(255,127)	0.1893	0.0970	[0.1849, 0.1936]
RS(255,191)	0.1922	0.0919	[0.1881, 0.1963]
RS(255,233)	0.1927	0.0909	[0.1886, 0.1967]

- Irradiance Threshold. There is no statistically significant difference in mean BER response between the 0.125 and 0.250 thresholds. As the irradiance threshold increased to 0.375 and 0.500, there is a statistically significant decrease in the mean BER under those thresholds. The mean BER grouped by irradiance threshold is presented in Table 13.

Table 13. Mean BER by Irradiance Threshold, 95% Confidence Interval in Moderate Turbulence

Irradiance Threshold	Mean	Std Dev	95% Confidence Interval
0.125	0.1195	0.1568	[0.1125, 0.1265]
0.250	0.1307	0.1066	[0.1259, 0.1355]
0.375	0.1530	0.0950	[0.1487, 0.1572]
0.500	0.1947	0.1193	[0.1893, 0.2000]

- Laser Wavelength. There is a similar effect on the BER as the laser wavelength decreases from 1550 nm to 850 nm. For the same reasons discussed in the weak turbulence analysis, the probability of detection and probability of false alarm are the most likely contributors to statistically significant difference in performance. The mean BER grouped by laser wavelength is presented in Table 14.

Table 14. Mean BER by Laser Wavelength, 95% Confidence Interval in Moderate Turbulence

Laser Wavelength	Mean	Std Dev	95% Confidence Interval
1550 nm	0.1337	0.1212	[0.1299, 0.1375]
850 nm	0.1653	0.1268	[0.1613, 0.1693]

- Modulation Scheme. The BPPM and OOK performances are indistinguishable from each other in terms of BER response. Both schemes result in a statistically significant improved performance over the 2-ary scheme. The 2-ary scheme is statistically different from the 4-ary scheme. Because the 2-ary and 4-ary schemes assign multiple bits to each time slot, the negative effects of missed detections or false alarms has greater effect than the BPPM or OOK modulations schemes. The mean BER grouped by modulation scheme is presented in Table 15.

Table 15. Mean BER by Modulation Scheme, 95% Confidence Interval in Moderate Turbulence

Modulation Scheme	**Mean**	**Std Dev**	**95% Confidence Interval**
2ARY	0.0491	0.1001	[0.0446, 0.0536]
4ARY	0.0799	0.1438	[0.0735, 0.0863]
BPPM	0.0372	0.0818	[0.0336, 0.0409]
OOK	0.0372	0.0818	[0.0336, 0.0409]

c. Interaction Effects

The interaction plots for the architectural decisions in moderate turbulence conditions are presented in Figure 29. The significant interactions are highlighted by the numbered, bold red boxes.

(1) <u>Irradiance threshold interaction with the coding scheme.</u>

There are two groups of interactions: RS codes with increasing irradiance threshold and repetition codes with increasing irradiance threshold. The RS code performance decreases as the irradiance threshold increases. The code’s performance is not robust enough to deal with the increased rate of missed detections that are associated with the increased threshold. The repetition codes offer a robust ability to mitigate the effects of increased irradiance thresholds. The repetition codes can miss multiple detections across the system’s independent channels and still decode the message from the information source.

(2) <u>Irradiance threshold with the system SNR.</u>

The interaction between increasing irradiance threshold and the SNR is the same interaction as in the weak turbulence environment.

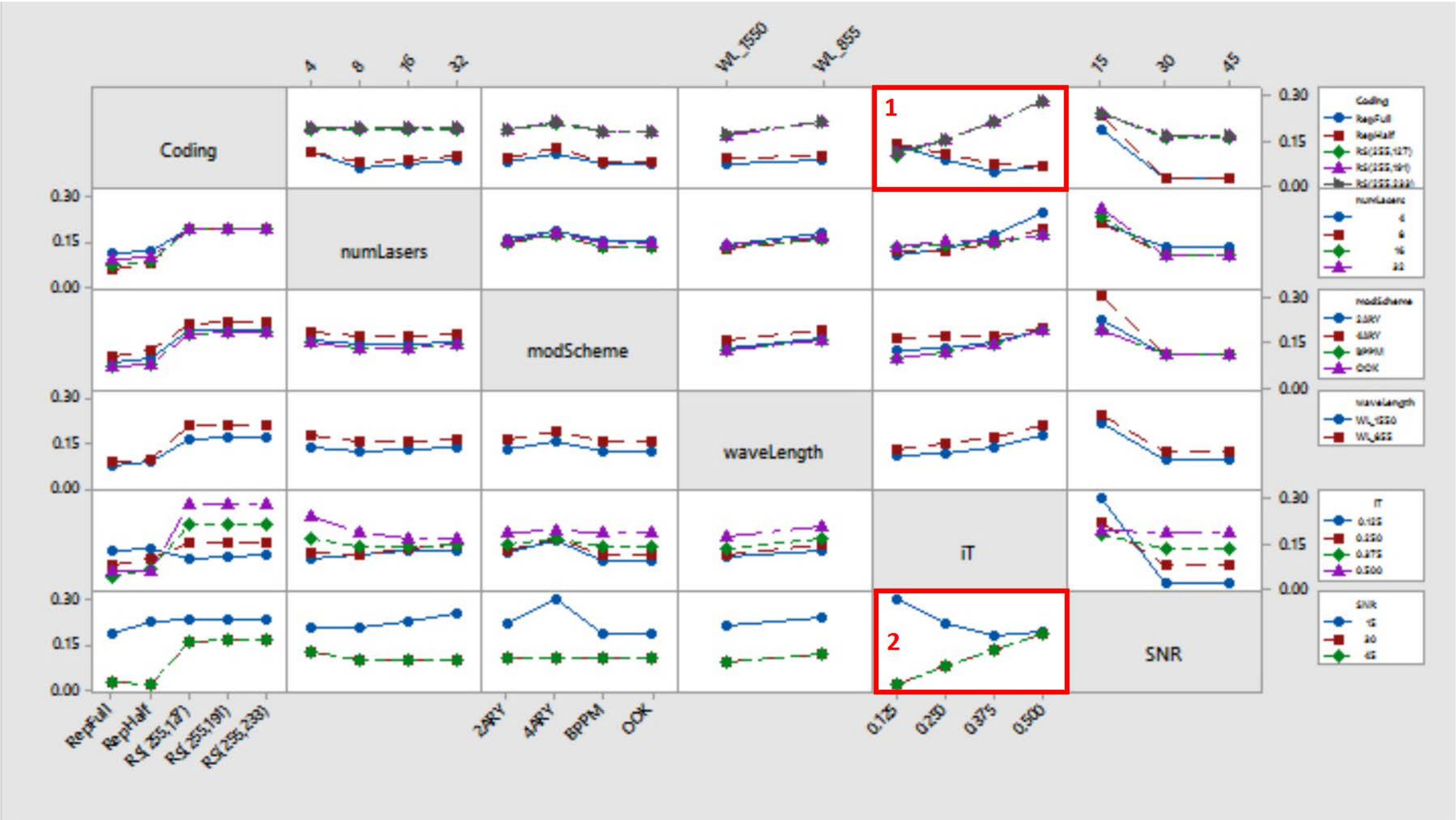

Figure 29. Moderate Turbulence Interaction Plot for BER, Data Means

3. Strong Turbulence.

This section will analyze the system's response to architecture decisions when atmospheric turbulence is described as strong. The regression model statistics, the main effects, and the interaction effects will be presented.

a. Regression Model

The model describes 86% of the variability in the BER response to the system architecture decisions. The summary of fit for the model is presented in Figure 30.

Summary of Fit	
RSquare	0.863045
RSquare Adj	0.861384
Root Mean Square Error	0.047845
Mean of Response	0.174857
Observations (or Sum Wgts)	7679

Figure 30. Strong Turbulence Summary of Fit, BER

The most significant effect in strong turbulence is the system’s coding scheme. The SNR’s effect is reduced

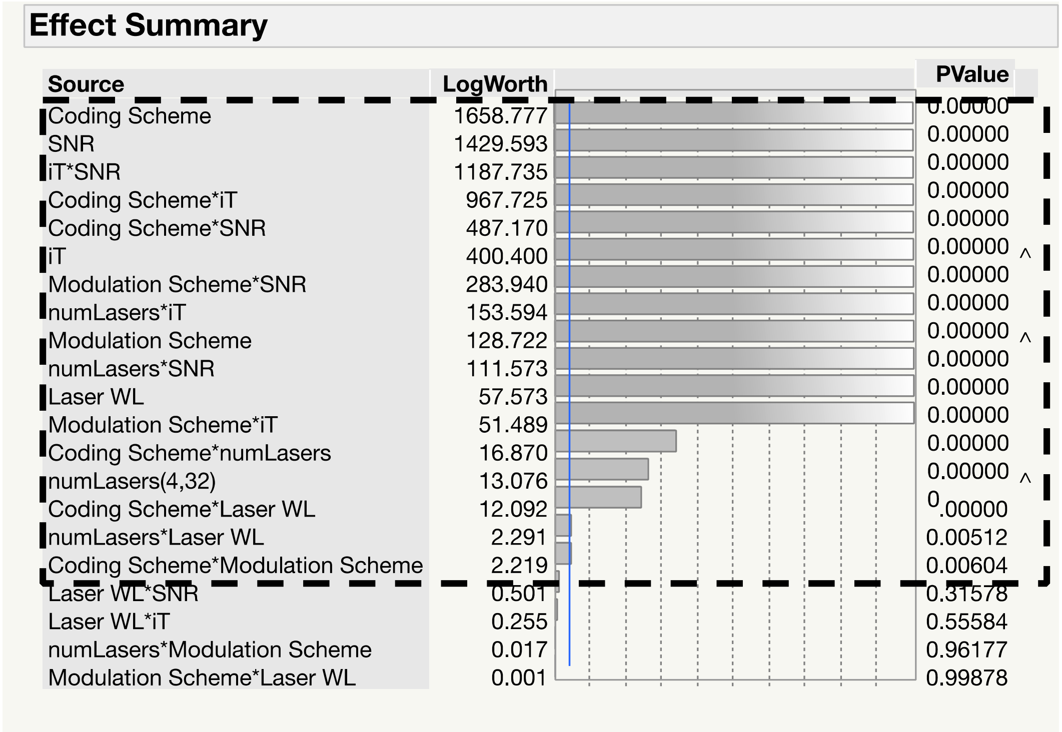

Effect Summary

Source	LogWorth	PValue
Coding Scheme	1658.777	0.00000
SNR	1429.593	0.00000
iT*SNR	1187.735	0.00000
Coding Scheme*iT	967.725	0.00000
Coding Scheme*SNR	487.170	0.00000
iT	400.400	0.00000 ^
Modulation Scheme*SNR	283.940	0.00000
numLasers*iT	153.594	0.00000
Modulation Scheme	128.722	0.00000 ^
numLasers*SNR	111.573	0.00000
Laser WL	57.573	0.00000
Modulation Scheme*iT	51.489	0.00000
Coding Scheme*numLasers	16.870	0.00000
numLasers(4,32)	13.076	0.00000 ^
Coding Scheme*Laser WL	12.092	0.00000
numLasers*Laser WL	2.291	0.00512
Coding Scheme*Modulation Scheme	2.219	0.00604
Laser WL*SNR	0.501	0.31578
Laser WL*iT	0.255	0.55584
numLasers*Modulation Scheme	0.017	0.96177
Modulation Scheme*Laser WL	0.001	0.99878

Figure 31. Strong Turbulence Effect Summary, BER

b. Main Effects

- <u>Coding Scheme.</u> The three RS codes' performance in terms of mean BER response is not statistically different at the 95% confidence level, but they are outperformed by both repetition codes. There is no statistically significant difference between the two repetition codes. The mean BER grouped by coding scheme in strong turbulence is presented in Table 16. The performance of the RS codes is also decreased in comparison to the RS codes in strong turbulence.

Table 16. Mean BER by Coding Scheme, 95% Confidence Interval in Strong Turbulence

Coding Scheme	Mean	Std Dev	95% Confidence Interval
Rep Full	0.0909	0.1394	[0.0839, 0.0979]
Rep Half	0.1030	0.1420	[0.0959, 0.1101]
RS(255,127)	0.2262	0.0883	[0.2217, 0.2306]
RS(255,191)	0.2272	0.0862	[0.2229, 0.2315]
RS(255,233)	0.2272	0.0861	[0.2229, 0.2315]

- SNR. Across all three turbulence levels, there is no statistically significant effect from increasing the SNR from 30 to 45 dB. The mean BER grouped by SNR is presented in Table 17.

Table 17. Mean BER by SNR, 95% Confidence Interval in Strong Turbulence

SNR	Mean	Std Dev	95% Confidence Interval
15 dB	0.2520	0.1190	[0.2473, 0.2566]
30 dB	0.1363	0.1150	[0.1319, 0.1408]
45 dB	0.1363	0.1151	[0.1319, 0.1408]

- Irradiance Threshold. Each threshold is statistically different from the other thresholds. The best irradiance threshold is the 0.125 irradiance threshold. The confidence intervals are presented in Table 18.

Table 18. Mean BER by Irradiance Threshold, 95% Confidence Interval in Strong Turbulence

Irradiance Threshold	Mean	Std Dev	95% Confidence Interval
0.125	0.1397	0.1515	[0.1330, 0.1465]
0.250	0.1580	0.1092	[0.1531, 0.1629]
0.375	0.1816	0.1059	[0.1769, 0.1863]
0.500	0.2202	0.1279	[0.2144, 0.2259]

- <u>Modulation Scheme.</u> At the 95% confidence level, there is no statistically significant difference between the 2-ary, BPPM, and the OOK modulation schemes. The 4-ary scheme performs the worst with the highest mean BER. The mean BER grouped by modulation scheme is presented in Table 19.

Table 19. Mean BER by Modulation Scheme, 95% Confidence Interval in Strong Turbulence

Modulation Scheme	Mean	Std Dev	95% Confidence Interval
2ARY	0.1740	0.1248	[0.1684, 0.1796]
4ARY	0.1984	0.1464	[0.1918, 0.2049]
BPPM	0.1635	0.1188	[0.1582, 0.1689]
OOK	0.1636	0.1188	[0.1582, 0.1689]

- <u>Laser Wavelength</u>. As with the other turbulence levels, the 1550 nm wavelength laser performs better than the 850 nm wavelength laser at a 95% statistical confidence level. The mean BER grouped by laser wavelength is presented in Table 20.

Table 20. Mean BER by Laser Wavelength, 95% Confidence Interval in Strong Turbulence

Number of Lasers	Mean	Std Dev	95% Confidence Interval
1550 nm	0.1653	0.1268	[0.1613, 0.1693]
850 nm	0.1845	0.1295	[0.1804, 0.1886]

- <u>Number of Lasers</u>. The system with only four lasers performed the worst amongst the four design choices. The 8, 16, and 32 laser arrays do not have different mean BER responses at a 95% confidence level. When the four-laser array sustains a deep fade in one of its channels, 25% of the transmitted symbols are not detected at the receiver. The eight-laser array is the smallest array that provides enough independent channels to mitigate the devastating effects of deep fades in conjunction with the forward error correction codes. The mean BER grouped by number of lasers is presented in Table 21.

Table 21. Mean BER by Number of Lasers, 95% Confidence Interval in Strong Turbulence

Number of Lasers	**Mean**	**Std Dev**	**95% Confidence Interval**
4	0.1926	0.1003	[0.1881, 0.1971]
8	0.1672	0.1233	[0.1617, 0.1727]
16	0.1664	0.1387	[0.1602, 0.1726]
32	0.1733	0.1452	[0.1668, 0.1798]

c. Interaction Effects

The interaction plots for the architectural decisions in moderate turbulence conditions are presented in Figure 32. Three specific interaction effects are explored for the mean BER response in strong turbulence conditions. The significant interactions are outlined in a bold red box and assigned a number that matches the following subsections.

(1) Irradiance threshold interaction with the coding scheme.

The interaction between the irradiance threshold and the coding scheme in strong turbulence conditions is the same as under weak and moderate conditions. Increasing irradiance threshold reduces the mean BER response for the repetition codes while increasing the mean BER response for the RS codes.

(2) Irradiance threshold with the system SNR.

The same interaction between the irradiance threshold and the system SNR is evident in the interaction plots in strong turbulence conditions.

(3) Number of Lasers and IT

When the irradiance threshold is 0.500 the BER decreases as the number of lasers increases. In contrast, when the irradiance threshold is 0.125 the BER increases as the number of lasers increase.

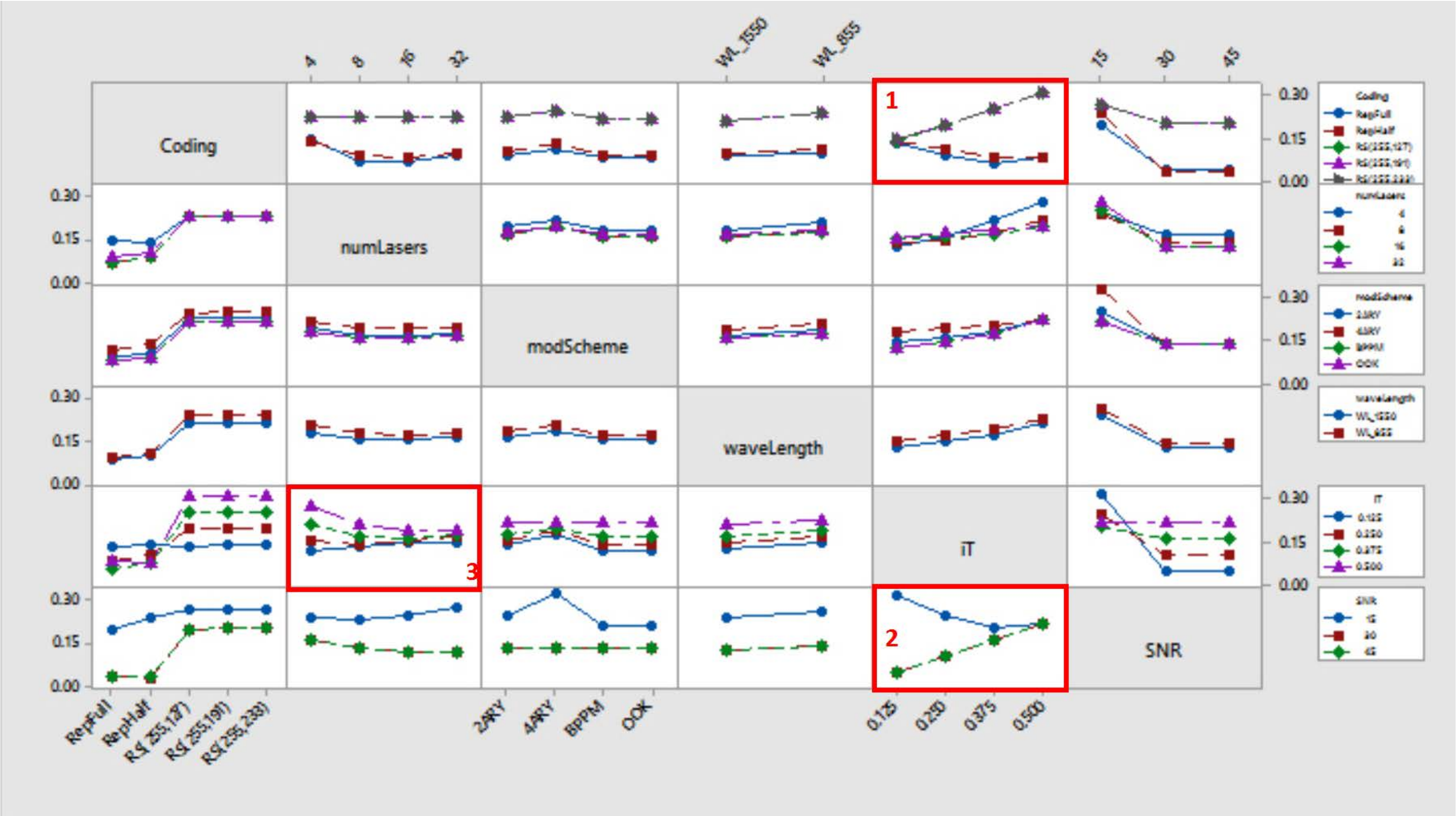

Figure 32. Strong Turbulence Interaction Plot for BER, Data Means

C. PREDICTED BER REGRESSION MODELS

This section will describe the derivation of the predicted BER MOE. The predicted BER will serve as a data point to explore the tradeoff between candidate architectures. The least squares regression models that provided the bases for the effect analysis in the previous section is used to support the tradeoff analysis.

The parameter estimates from the least squares regression model for the predicted BER under weak turbulence conditions is presented in Table 22. The parameter estimates for the predicted BER under moderate turbulence conditions is presented in Table 23. The parameter estimates for the predicted BER under strong turbulence conditions is presented in Table 24. The parameter estimates are used to evaluate predicted BER for each candidate architecture. The predicted BER rate is one MOE that will support the subsequent tradeoff analysis.

Table 22.   Low Turbulence Regression Parameter Estimates

Parameter Estimates				
Term	Estimate	Std Error	t Ratio	Prob>|t|
Intercept	0.0532481	0.000452	117.92	<.0001*
iT[0.125_iT]	0.0464558	0.000782	59.4	<.0001*
SNR[SNR_15DB]	0.0890386	0.000639	139.43	<.0001*
SNR[SNR_30DB]	-0.04451	0.000639	-69.70	<.0001*
Coding Scheme[RepHalf]*SNR[SNR_15DB]	0.0573342	0.00123	46.61	<.0001*
Modulation Scheme[4ARY]*SNR[SNR_15DB]	0.0598984	0.001065	56.23	<.0001*
iT[0.125_iT]*SNR[SNR_15DB]	0.109233	0.001065	102.55	<.0001*
iT[0.125_iT]*SNR[SNR_30DB]	-0.054581	0.001065	-51.24	<.0001*
iT[0.375_iT]*SNR[SNR_15DB]	-0.052631	0.001065	-49.41	<.0001*
iT[0.375_iT]	-0.030669	0.000782	-39.21	<.0001*
Modulation Scheme[4ARY]	0.0288123	0.000782	36.84	<.0001*
Modulation Scheme[4ARY]*SNR[SNR_30DB]	-0.029929	0.001065	-28.10	<.0001*
numLasers*SNR[SNR_15DB]	0.0225543	0.000803	28.09	<.0001*
Modulation Scheme[BPPM]*SNR[SNR_15DB]	-0.028057	0.001065	-26.34	<.0001*
Coding Scheme[RepHalf]	0.0235808	0.000903	26.11	<.0001*
iT[0.375_iT]*SNR[SNR_30DB]	0.0263113	0.001065	24.7	<.0001*
Coding Scheme[RS(255,127)]*SNR[SNR_15DB]	-0.028883	0.00123	-23.48	<.0001*
Coding Scheme[RepHalf]*SNR[SNR_30DB]	-0.028621	0.00123	-23.27	<.0001*
Coding Scheme[RS(255,191)]*SNR[SNR_15DB]	-0.027088	0.00123	-22.02	<.0001*
Coding Scheme[RepFull]*SNR[SNR_15DB]	0.0258174	0.00123	20.99	<.0001*
iT[0.25_iT]*SNR[SNR_15DB]	0.0223135	0.001065	20.95	<.0001*
Coding Scheme[RepFull]*iT[0.125_iT]	0.029727	0.001506	19.73	<.0001*
numLasers(4,32)	0.0110594	0.000568	19.48	<.0001*
Modulation Scheme[BPPM]	-0.013557	0.000782	-17.33	<.0001*
Coding Scheme[RepFull]*numLasers	0.0188124	0.001135	16.57	<.0001*
Coding Scheme[RS(255,127)]	-0.014953	0.000903	-16.56	<.0001*
Laser WL[WL_855]	0.0071192	0.000452	15.77	<.0001*
Modulation Scheme[4ARY]*iT[0.125_iT]	0.0202485	0.001305	15.52	<.0001*
Coding Scheme[RepHalf]*iT[0.125_iT]	0.0214967	0.001506	14.27	<.0001*
Coding Scheme[RepHalf]*iT[0.25_iT]	0.0214676	0.001506	14.25	<.0001*
numLasers*SNR[SNR_30DB]	-0.01127	0.000803	-14.04	<.0001*
Modulation Scheme[BPPM]*SNR[SNR_30DB]	0.0140177	0.001065	13.16	<.0001*
Coding Scheme[RepHalf]*numLasers	0.0143671	0.001135	12.65	<.0001*
Modulation Scheme[4ARY]*iT[0.25_iT]	0.0158785	0.001305	12.17	<.0001*
Coding Scheme[RS(255,191)]*iT[0.125_iT]	-0.018287	0.001506	-12.14	<.0001*
Coding Scheme[RS(255,127)]*SNR[SNR_30DB]	0.0144205	0.00123	11.72	<.0001*
Coding Scheme[RS(255,191)]*SNR[SNR_30DB]	0.0135353	0.00123	11	<.0001*
Coding Scheme[RepFull]*iT[0.25_iT]	0.016037	0.001506	10.65	<.0001*
Coding Scheme[RepFull]*SNR[SNR_30DB]	-0.012917	0.00123	-10.50	<.0001*
iT[0.25_iT]*SNR[SNR_30DB]	-0.011165	0.001065	-10.48	<.0001*
Coding Scheme[RS(255,191)]	-0.009451	0.000903	-10.46	<.0001*
Coding Scheme[RS(255,127)]*numLasers	-0.011074	0.001135	-9.75	<.0001*
Coding Scheme[RS(255,191)]*numLasers	-0.011056	0.001135	-9.74	<.0001*
Laser WL[WL_855]*iT[0.125_iT]	-0.007157	0.000753	-9.50	<.0001*
Coding Scheme[RepFull]	0.0084574	0.000903	9.36	<.0001*
numLasers*iT[0.25_iT]	0.0091586	0.000983	9.31	<.0001*
Laser WL[WL_855]*iT[0.25_iT]	-0.006799	0.000753	-9.03	<.0001*
Coding Scheme[RS(255,191)]*iT[0.25_iT]	-0.013515	0.001506	-8.97	<.0001*
Coding Scheme[RS(255,127)]*iT[0.125_iT]	-0.012802	0.001506	-8.50	<.0001*
Modulation Scheme[BPPM]*iT[0.125_iT]	-0.011072	0.001305	-8.49	<.0001*
Coding Scheme[RepFull]*Laser WL[WL_855]	-0.006881	0.00087	-7.91	<.0001*
Coding Scheme[RepHalf]*Laser WL[WL_855]	-0.006673	0.00087	-7.67	<.0001*
Modulation Scheme[4ARY]*iT[0.375_iT]	-0.009083	0.001305	-6.96	<.0001*
Coding Scheme[RepFull]*iT[0.375_iT]	-0.01002	0.001506	-6.65	<.0001*
Coding Scheme[RS(255,127)]*Laser WL[WL_855]	0.0050767	0.00087	5.84	<.0001*
Coding Scheme[RS(255,127)]*iT[0.25_iT]	-0.008701	0.001506	-5.78	<.0001*
iT[0.25_iT]	0.0043608	0.000782	5.58	<.0001*
Modulation Scheme[BPPM]*iT[0.25_iT]	-0.007162	0.001305	-5.49	<.0001*
Coding Scheme[RS(255,191)]*Laser WL[WL_855]	0.0045559	0.00087	5.24	<.0001*
Coding Scheme[RepFull]*Modulation Scheme[4ARY]	-0.006597	0.001506	-4.38	<.0001*
Modulation Scheme[BPPM]*iT[0.375_iT]	0.0053443	0.001305	4.1	<.0001*
Modulation Scheme[2ARY]*SNR[SNR_15DB]	-0.003789	0.001065	-3.56	0.0004*
Coding Scheme[RS(255,191)]*iT[0.375_iT]	0.0047446	0.001506	3.15	0.0016*
Coding Scheme[RepHalf]*Modulation Scheme[4ARY]	0.0044519	0.001506	2.96	0.0031*
numLasers*iT[0.125_iT]	0.0026672	0.000983	2.71	0.0067*
Modulation Scheme[2ARY]	-0.001699	0.000782	-2.17	0.0298*
Coding Scheme[RepHalf]*Modulation Scheme[BPPM]	-0.003183	0.001506	-2.11	0.0346*
Modulation Scheme[2ARY]*SNR[SNR_30DB]	0.0018925	0.001065	1.78	0.0757
Coding Scheme[RepFull]*Modulation Scheme[BPPM]	0.0024099	0.001506	1.6	0.1097
numLasers*iT[0.375_iT]	-0.001547	0.000983	-1.57	0.1158
Laser WL[WL_855]*iT[0.375_iT]	-0.001182	0.000753	-1.57	0.1166
Modulation Scheme[2ARY]*iT[0.125_iT]	0.0019098	0.001305	1.46	0.1433
Laser WL[WL_855]*SNR[SNR_15DB]	0.0008143	0.000615	1.32	0.1855
Coding Scheme[RepHalf]*Modulation Scheme[2ARY]	0.0019208	0.001506	1.28	0.2023
Modulation Scheme[2ARY]*iT[0.375_iT]	-0.001614	0.001305	-1.24	0.2162
Modulation Scheme[2ARY]*iT[0.25_iT]	-0.001569	0.001305	-1.20	0.2293
Coding Scheme[RepFull]*Modulation Scheme[2ARY]	0.0017848	0.001506	1.18	0.2361
numLasers*Modulation Scheme[4ARY]	-0.001065	0.000983	-1.08	0.2789
Coding Scheme[RS(255,127)]*iT[0.375_iT]	-0.00145	0.001506	-0.96	0.3357
Coding Scheme[RS(255,127)]*Modulation Scheme[2ARY]	-0.001419	0.001506	-0.94	0.3464
Coding Scheme[RS(255,127)]*Modulation Scheme[4ARY]	0.00112	0.001506	0.74	0.4572
Laser WL[WL_855]*SNR[SNR_30DB]	-0.000411	0.000615	-0.67	0.5035
Coding Scheme[RS(255,191)]*Modulation Scheme[2ARY]	-0.000988	0.001506	-0.66	0.5118
Coding Scheme[RS(255,191)]*Modulation Scheme[BPPM]	0.0009512	0.001506	0.63	0.5278
Coding Scheme[RS(255,191)]*Modulation Scheme[4ARY]	-0.000921	0.001506	-0.61	0.541
numLasers*Modulation Scheme[BPPM]	0.0003858	0.000983	0.39	0.6948
numLasers*Laser WL[WL_855]	-0.000205	0.000568	-0.36	0.7187
numLasers*Modulation Scheme[2ARY]	0.0002963	0.000983	0.3	0.7632
Modulation Scheme[4ARY]*Laser WL[WL_855]	0.0001896	0.000753	0.25	0.8013
Modulation Scheme[BPPM]*Laser WL[WL_855]	-0.00007	0.000753	-0.09	0.926
Coding Scheme[RS(255,127)]*Modulation Scheme[BPPM]	0.0001379	0.001506	0.09	0.9271
Modulation Scheme[2ARY]*Laser WL[WL_855]	-5.136e-5	0.000753	-0.07	0.9456
Coding Scheme[RepHalf]*iT[0.375_iT]	-1.964e-5	0.001506	-0.01	0.9896

Table 23. Moderate Turbulence Regression Parameter Estimates

Parameter Estimates				
Term	Estimate	Std Error	t Ratio	Prob>|t|
Intercept	0.1493594	0.000533	280.1	<.0001*
Coding Scheme[RepFull]	-0.069949	0.001066	-65.59	<.0001*
Coding Scheme[RepHalf]	-0.056128	0.001066	-52.63	<.0001*
SNR[SNR_15DB]	0.0848704	0.000754	112.55	<.0001*
SNR[SNR_30DB]	-0.042416	0.000754	-56.25	<.0001*
Coding Scheme[RepFull]*iT[0.125_iT]	0.0817084	0.001779	45.93	<.0001*
Coding Scheme[RepHalf]*iT[0.125_iT]	0.0762773	0.001779	42.88	<.0001*
Coding Scheme[RepHalf]*SNR[SNR_15DB]	0.0605117	0.001452	41.66	<.0001*
Modulation Scheme[4ARY]*SNR[SNR_15DB]	0.0524475	0.001258	41.7	<.0001*
iT[0.125_iT]*SNR[SNR_15DB]	0.1099379	0.001258	87.4	<.0001*
iT[0.125_iT]*SNR[SNR_30DB]	-0.054916	0.001258	-43.66	<.0001*
iT[0.375_iT]*SNR[SNR_15DB]	-0.051735	0.001258	-41.13	<.0001*
Coding Scheme[RS(255,191)]	0.0428347	0.001066	40.17	<.0001*
Coding Scheme[RS(255,127)]	0.0399271	0.001066	37.44	<.0001*
Coding Scheme[RS(255,127)]*iT[0.125_iT]	-0.058954	0.001779	-33.14	<.0001*
iT[0.125_iT]	-0.026997	0.000924	-29.23	<.0001*
Laser WL[WL_855]	0.0151797	0.000533	28.47	<.0001*
Coding Scheme[RS(255,191)]*iT[0.125_iT]	-0.050269	0.001779	-28.26	<.0001*
Modulation Scheme[4ARY]	0.0246776	0.000924	26.72	<.0001*
numLasers*SNR[SNR_15DB]	0.0229434	0.000948	24.2	<.0001*
Coding Scheme[RepFull]*iT[0.375_iT]	-0.039768	0.001779	-22.36	<.0001*
Coding Scheme[RS(255,191)]*SNR[SNR_15DB]	-0.030869	0.001452	-21.25	<.0001*
Modulation Scheme[4ARY]*SNR[SNR_30DB]	-0.026197	0.001258	-20.83	<.0001*
Coding Scheme[RepHalf]*SNR[SNR_30DB]	-0.030222	0.001452	-20.81	<.0001*
iT[0.375_iT]*SNR[SNR_30DB]	0.0258461	0.001258	20.55	<.0001*
Coding Scheme[RepFull]*SNR[SNR_15DB]	0.0296621	0.001452	20.42	<.0001*
Modulation Scheme[BPPM]*SNR[SNR_15DB]	-0.024825	0.001258	-19.74	<.0001*
Coding Scheme[RS(255,127)]*SNR[SNR_15DB]	-0.027943	0.001452	-19.24	<.0001*
Coding Scheme[RepHalf]*iT[0.375_iT]	-0.02948	0.001779	-16.57	<.0001*
iT[0.25_iT]	-0.015234	0.000924	-16.49	<.0001*
Coding Scheme[RepHalf]*iT[0.25_iT]	0.0292599	0.001779	16.45	<.0001*
numLasers*iT[0.25_iT]	0.0164533	0.001161	14.17	<.0001*
Coding Scheme[RS(255,127)]*iT[0.375_iT]	0.0251739	0.001779	14.15	<.0001*
iT[0.25_iT]*SNR[SNR_15DB]	0.0172996	0.001258	13.75	<.0001*
Modulation Scheme[BPPM]	-0.011864	0.000924	-12.85	<.0001*
Coding Scheme[RS(255,191)]*iT[0.375_iT]	0.0222816	0.001779	12.53	<.0001*
numLasers*SNR[SNR_30DB]	-0.011458	0.000948	-12.09	<.0001*
numLasers*iT[0.125_iT]	0.0138358	0.001161	11.92	<.0001*
Coding Scheme[RepFull]*iT[0.25_iT]	0.0203868	0.001779	11.46	<.0001*
Modulation Scheme[4ARY]*iT[0.125_iT]	0.0163772	0.001541	10.63	<.0001*
Coding Scheme[RS(255,191)]*SNR[SNR_30DB]	0.0154264	0.001452	10.62	<.0001*
Coding Scheme[RepFull]*SNR[SNR_30DB]	-0.014846	0.001452	-10.22	<.0001*
Coding Scheme[RepHalf]*Laser WL[WL_855]	-0.010344	0.001027	-10.07	<.0001*
Modulation Scheme[BPPM]*SNR[SNR_30DB]	0.012403	0.001258	9.86	<.0001*
Coding Scheme[RS(255,191)]*iT[0.25_iT]	-0.017342	0.001779	-9.75	<.0001*
Coding Scheme[RS(255,127)]*SNR[SNR_30DB]	0.0139531	0.001452	9.61	<.0001*
Coding Scheme[RepFull]*Laser WL[WL_855]	-0.009262	0.001027	-9.02	<.0001*

Parameter Estimates				
Term	Estimate	Std Error	t Ratio	Prob>|t|
Coding Scheme[RS(255,127)]*iT[0.25_iT]	-0.014453	0.001779	-8.12	<.0001*
Modulation Scheme[4ARY]*iT[0.25_iT]	0.012443	0.001541	8.08	<.0001*
Coding Scheme[RS(255,127)]*Laser WL[WL_855]	0.0072811	0.001027	7.09	<.0001*
iT[0.25_iT]*SNR[SNR_30DB]	-0.008664	0.001258	-6.89	<.0001*
Coding Scheme[RS(255,191)]*Laser WL[WL_855]	0.0064101	0.001027	6.24	<.0001*
Modulation Scheme[BPPM]*iT[0.125_iT]	-0.009358	0.001541	-6.07	<.0001*
Laser WL[WL_855]*iT[0.125_iT]	-0.004433	0.000889	-4.98	<.0001*
Modulation Scheme[4ARY]*iT[0.375_iT]	-0.007175	0.001541	-4.66	<.0001*
Coding Scheme[RepHalf]*Modulation Scheme[4ARY]	0.0077194	0.001779	4.34	<.0001*
numLasers*Laser WL[WL_855]	-0.002847	0.00067	-4.25	<.0001*
Modulation Scheme[BPPM]*iT[0.25_iT]	-0.005567	0.001541	-3.61	0.0003*
numLasers*iT[0.375_iT]	-0.00404	0.001161	-3.48	0.0005*
Laser WL[WL_855]*iT[0.375_iT]	0.0025822	0.000889	2.9	0.0037*
iT[0.375_iT]	0.0026503	0.000924	2.87	0.0041*
Modulation Scheme[BPPM]*iT[0.375_iT]	0.0043084	0.001541	2.8	0.0052*
Coding Scheme[RepHalf]*Modulation Scheme[BPPM]	-0.004518	0.001779	-2.54	0.0111*
Laser WL[WL_855]*SNR[SNR_15DB]	-0.001694	0.000726	-2.33	0.0197*
Modulation Scheme[2ARY]*SNR[SNR_15DB]	-0.002802	0.001258	-2.23	0.0260*
Coding Scheme[RS(255,127)]*Modulation Scheme[4ARY]	-0.003358	0.001779	-1.89	0.0591
Modulation Scheme[2ARY]*iT[0.125_iT]	0.0023588	0.001541	1.53	0.1258
Modulation Scheme[4ARY]*Laser WL[WL_855]	-0.00128	0.000889	-1.44	0.1502
Coding Scheme[RepFull]*Modulation Scheme[4ARY]	-0.002545	0.001779	-1.43	0.1526
Laser WL[WL_855]*SNR[SNR_30DB]	0.0008445	0.000726	1.16	0.2449
Modulation Scheme[2ARY]*SNR[SNR_30DB]	0.0013922	0.001258	1.11	0.2684
Laser WL[WL_855]*iT[0.25_iT]	0.0009467	0.000889	1.06	0.2872
Coding Scheme[RS(255,127)]*Modulation Scheme[BPPM]	0.0018392	0.001779	1.03	0.3012
Modulation Scheme[2ARY]	-0.000945	0.000924	-1.02	0.3061
Modulation Scheme[2ARY]*iT[0.375_iT]	-0.00145	0.001541	-0.94	0.3465
Coding Scheme[RS(255,191)]*Modulation Scheme[4ARY]	-0.001596	0.001779	-0.90	0.3696
Modulation Scheme[2ARY]*iT[0.25_iT]	-0.001312	0.001541	-0.85	0.3945
numLasers(4,32)	-0.000538	0.00067	-0.80	0.4221
Coding Scheme[RepHalf]*Modulation Scheme[2ARY]	0.0013054	0.001779	0.73	0.4631
numLasers*Modulation Scheme[4ARY]	-0.000823	0.001161	-0.71	0.4786
Coding Scheme[RepHalf]*numLasers	-0.000943	0.001341	-0.70	0.4821
Coding Scheme[RS(255,191)]*Modulation Scheme[BPPM]	0.0011958	0.001779	0.67	0.5015
Modulation Scheme[BPPM]*Laser WL[WL_855]	0.0005156	0.000889	0.58	0.5621
Coding Scheme[RepFull]*Modulation Scheme[2ARY]	0.0010293	0.001779	0.58	0.5628
Coding Scheme[RepFull]*numLasers	-0.000649	0.001341	-0.48	0.6286
Coding Scheme[RS(255,191)]*Modulation Scheme[2ARY]	-0.000797	0.001779	-0.45	0.6542
Coding Scheme[RepFull]*Modulation Scheme[BPPM]	0.0007548	0.001779	0.42	0.6714
Coding Scheme[RS(255,127)]*numLasers	0.0005346	0.001341	0.4	0.6901
Coding Scheme[RS(255,191)]*numLasers	0.0005274	0.001341	0.39	0.6941
Modulation Scheme[2ARY]*Laser WL[WL_855]	0.0002486	0.000889	0.28	0.7799
numLasers*Modulation Scheme[BPPM]	0.0002763	0.001161	0.24	0.8119
numLasers*Modulation Scheme[2ARY]	0.0002651	0.001161	0.23	0.8194
Coding Scheme[RS(255,127)]*Modulation Scheme[2ARY]	-0.000329	0.001779	-0.19	0.8531

Table 24. Strong Turbulence Regression Parameter Estimates

Parameter Estimates

Term	Estimate	Std Error	t Ratio	Prob>|t|
Intercept	0.1737028	0.000567	306.39	<.0001*
Coding Scheme[RepFull]	-0.085954	0.001134	-75.81	<.0001*
Coding Scheme[RepHalf]	-0.073432	0.001134	-64.76	<.0001*
Coding Scheme[RS(255,127)]	0.0524481	0.001134	46.26	<.0001*
Coding Scheme[RS(255,191)]	0.0534819	0.001134	47.17	<.0001*
SNR[SNR_15DB]	0.0820858	0.000802	102.38	<.0001*
SNR[SNR_30DB]	-0.041014	0.000802	-51.15	<.0001*
Coding Scheme[RepFull]*iT[0.125_iT]	0.0767908	0.001891	40.6	<.0001*
Coding Scheme[RepHalf]*SNR[SNR_15DB]	0.0626085	0.001544	40.54	<.0001*
iT[0.125_iT]*SNR[SNR_15DB]	0.1057844	0.001337	79.1	<.0001*
iT[0.125_iT]*SNR[SNR_30DB]	-0.052873	0.001337	-39.54	<.0001*
Coding Scheme[RepHalf]*iT[0.125_iT]	0.0739386	0.001891	39.09	<.0001*
iT[0.375_iT]*SNR[SNR_15DB]	-0.049847	0.001337	-37.27	<.0001*
Modulation Scheme[4ARY]*SNR[SNR_15DB]	0.0488408	0.001337	36.52	<.0001*
iT[0.125_iT]	-0.031279	0.000982	-31.85	<.0001*
Coding Scheme[RS(255,127)]*iT[0.125_iT]	-0.052309	0.001891	-27.66	<.0001*
Coding Scheme[RS(255,191)]*iT[0.125_iT]	-0.049237	0.001891	-26.03	<.0001*
Modulation Scheme[4ARY]	0.0233836	0.000982	23.81	<.0001*
numLasers*SNR[SNR_15DB]	0.0232415	0.001008	23.06	<.0001*
Coding Scheme[RepFull]*SNR[SNR_15DB]	0.0320475	0.001544	20.75	<.0001*
Coding Scheme[RS(255,191)]*SNR[SNR_15DB]	-0.031889	0.001544	-20.65	<.0001*
Coding Scheme[RepFull]*iT[0.375_iT]	-0.038644	0.001891	-20.43	<.0001*
Coding Scheme[RepHalf]*SNR[SNR_30DB]	-0.031185	0.001544	-20.19	<.0001*
Coding Scheme[RS(255,127)]*SNR[SNR_15DB]	-0.030882	0.001544	-20.00	<.0001*
iT[0.375_iT]*SNR[SNR_30DB]	0.0248998	0.001337	18.62	<.0001*
Modulation Scheme[4ARY]*SNR[SNR_30DB]	-0.024435	0.001337	-18.27	<.0001*
Modulation Scheme[BPPM]*SNR[SNR_15DB]	-0.023259	0.001337	-17.39	<.0001*
Laser WL[WL_855]	0.0092048	0.000567	16.24	<.0001*
Coding Scheme[RepHalf]*iT[0.375_iT]	-0.029565	0.001891	-15.63	<.0001*
numLasers*iT[0.125_iT]	0.0178419	0.001235	14.45	<.0001*
numLasers*iT[0.25_iT]	0.017493	0.001235	14.17	<.0001*
iT[0.25_iT]	-0.013108	0.000982	-13.35	<.0001*
Coding Scheme[RepHalf]*iT[0.25_iT]	0.0248888	0.001891	13.16	<.0001*
iT[0.25_iT]*SNR[SNR_15DB]	0.016842	0.001337	12.59	<.0001*
Coding Scheme[RS(255,127)]*iT[0.375_iT]	0.0233969	0.001891	12.37	<.0001*
Coding Scheme[RS(255,191)]*iT[0.375_iT]	0.0224244	0.001891	11.86	<.0001*
numLasers*SNR[SNR_30DB]	-0.011638	0.001008	-11.55	<.0001*
Modulation Scheme[BPPM]	-0.011262	0.000982	-11.47	<.0001*
Coding Scheme[RepFull]*SNR[SNR_30DB]	-0.016054	0.001544	-10.40	<.0001*
Coding Scheme[RS(255,191)]*SNR[SNR_30DB]	0.0159127	0.001544	10.3	<.0001*
Coding Scheme[RS(255,127)]*SNR[SNR_30DB]	0.015412	0.001544	9.98	<.0001*
Modulation Scheme[4ARY]*iT[0.125_iT]	0.0159183	0.001638	9.72	<.0001*
Modulation Scheme[BPPM]*SNR[SNR_30DB]	0.0116089	0.001337	8.68	<.0001*
Coding Scheme[RepFull]*iT[0.25_iT]	0.0150344	0.001891	7.95	<.0001*
numLasers(4,32)	-0.00533	0.000713	-7.48	<.0001*
Coding Scheme[RS(255,191)]*iT[0.25_iT]	-0.013662	0.001891	-7.22	<.0001*
Modulation Scheme[4ARY]*iT[0.25_iT]	0.0110809	0.001638	6.77	<.0001*

Parameter Estimates

Term	Estimate	Std Error	t Ratio	Prob>|t|
Coding Scheme[RS(255,127)]*iT[0.25_iT]	-0.012611	0.001891	-6.67	<.0001*
Coding Scheme[RepFull]*numLasers	-0.009466	0.001426	-6.64	<.0001*
iT[0.25_iT]*SNR[SNR_30DB]	-0.008452	0.001337	-6.32	<.0001*
iT[0.375_iT]	0.0054629	0.000982	5.56	<.0001*
Modulation Scheme[BPPM]*iT[0.125_iT]	-0.009038	0.001638	-5.52	<.0001*
Coding Scheme[RepHalf]*Laser WL[WL_855]	-0.005663	0.001092	-5.18	<.0001*
numLasers*iT[0.375_iT]	-0.006008	0.001235	-4.87	<.0001*
Coding Scheme[RepHalf]*numLasers	-0.006539	0.001426	-4.59	<.0001*
Coding Scheme[RepHalf]*Modulation Scheme[4ARY]	0.0085706	0.001891	4.53	<.0001*
Coding Scheme[RepFull]*Laser WL[WL_855]	-0.004887	0.001092	-4.48	<.0001*
Modulation Scheme[4ARY]*iT[0.375_iT]	-0.006625	0.001638	-4.04	<.0001*
Coding Scheme[RS(255,127)]*Laser WL[WL_855]	0.0042041	0.001092	3.85	0.0001*
Coding Scheme[RS(255,191)]*numLasers	0.0053515	0.001426	3.75	0.0002*
Coding Scheme[RS(255,127)]*numLasers	0.0053317	0.001426	3.74	0.0002*
Modulation Scheme[BPPM]*iT[0.25_iT]	-0.005061	0.001638	-3.09	0.0020*
Coding Scheme[RS(255,191)]*Laser WL[WL_855]	0.0031691	0.001092	2.9	0.0037*
numLasers*Laser WL[WL_855]	-0.001996	0.000713	-2.80	0.0051*
Coding Scheme[RepHalf]*Modulation Scheme[BPPM]	-0.004815	0.001891	-2.55	0.0109*
Modulation Scheme[BPPM]*iT[0.375_iT]	0.0040083	0.001638	2.45	0.0144*
Coding Scheme[RS(255,127)]*Modulation Scheme[4ARY]	-0.004464	0.001891	-2.36	0.0183*
Modulation Scheme[2ARY]*SNR[SNR_15DB]	-0.002348	0.001337	-1.76	0.0792
Laser WL[WL_855]*SNR[SNR_15DB]	-0.001172	0.000772	-1.52	0.129
Modulation Scheme[2ARY]*iT[0.125_iT]	0.0021518	0.001638	1.31	0.189
Coding Scheme[RS(255,127)]*Modulation Scheme[BPPM]	0.0022226	0.001891	1.18	0.24
Laser WL[WL_855]*iT[0.25_iT]	0.00092	0.000946	0.97	0.3306
Modulation Scheme[2ARY]*SNR[SNR_30DB]	0.0012454	0.001337	0.93	0.3518
Modulation Scheme[2ARY]	-0.000876	0.000982	-0.89	0.3723
Modulation Scheme[2ARY]*iT[0.375_iT]	-0.001373	0.001638	-0.84	0.4019
Laser WL[WL_855]*iT[0.125_iT]	-0.00076	0.000946	-0.80	0.4216
Coding Scheme[RepFull]*Modulation Scheme[4ARY]	-0.0014	0.001891	-0.74	0.4591
Laser WL[WL_855]*SNR[SNR_30DB]	0.0005666	0.000772	0.73	0.4631
Coding Scheme[RS(255,191)]*Modulation Scheme[4ARY]	-0.001352	0.001891	-0.72	0.4746
Laser WL[WL_855]*iT[0.375_iT]	0.0006426	0.000946	0.68	0.4968
Coding Scheme[RS(255,191)]*Modulation Scheme[BPPM]	0.0011888	0.001891	0.63	0.5297
Modulation Scheme[2ARY]*iT[0.25_iT]	-0.000961	0.001638	-0.59	0.5576
Coding Scheme[RepHalf]*Modulation Scheme[2ARY]	0.0010752	0.001893	0.57	0.57
Coding Scheme[RS(255,191)]*Modulation Scheme[2ARY]	-0.001045	0.001891	-0.55	0.5807
numLasers*Modulation Scheme[4ARY]	-0.000661	0.001235	-0.54	0.5924
Coding Scheme[RepFull]*Modulation Scheme[2ARY]	0.0009961	0.001891	0.53	0.5985
numLasers*Modulation Scheme[2ARY]	0.0002926	0.001235	0.24	0.8127
numLasers*Modulation Scheme[BPPM]	0.0001962	0.001235	0.16	0.8737
Coding Scheme[RepFull]*Modulation Scheme[BPPM]	0.0002115	0.001891	0.11	0.9109
Modulation Scheme[2ARY]*Laser WL[WL_855]	-9.736e-5	0.000946	-0.10	0.918
Modulation Scheme[BPPM]*Laser WL[WL_855]	0.0000929	0.000946	0.1	0.9217
Modulation Scheme[4ARY]*Laser WL[WL_855]	-8.426e-5	0.000946	-0.09	0.929
Coding Scheme[RS(255,127)]*Modulation Scheme[2ARY]	-8.397e-6	0.001891	-0.00	0.9965

D. TRANSMISSION RATE

The transmission rate is dependent on the number of lasers, the coding scheme, and the modulation scheme. The derivation of the transmission rate is presented in this section.

Each message word contains 8 bits. Each coding scheme implemented creates a 255-byte codeword. The coding rate is derived using Equation 21. The coding rate represents the ratio of message words in every block of codewords. The coding rates for the five coding schemes is presented in Table 25.

$$Rate_{Code} = \frac{MessageWords}{Codeword} = \frac{MessageWords}{255} \text{ [message word / codeword]} \qquad (21)$$

Table 25. Coding Rates and Error Correction Capacities

Coding Scheme	Message Words	Coding Rates	Error Correction Capacity
RS(255,233)	233	0.914	11
RS(255,191)	191	0.749	32
RS(255,127)	127	0.498	64
Repetition, Full	255	1.000	0
Repetition, Half	255	1.000	0

The modulation schemes determine how many time slots are required to transmit one 8-bit codeword. The summary of modulation schemes and the required time slots per 8-bit code word is presented in Table 26. The modulation rate is a ratio of the number of bits transmitted per time slot. The modulation rate is derived from Equation 23.

$$Rate_{Modulation} = \frac{Bits}{TimeSlot} \text{ [bits / time slot]} \qquad (22)$$

The modulation rate for the four modulation schemes is presented in Table 26.

Table 26. Modulation Rates

Modulation Scheme	Time Slots / Codeword	Modulation Rate (bits/time slot)
OOK	8	1
BPPM	16	0.5
2-Ary	16	0.5
4-Ary	32	0.25

Each architecture's transmission rate is derived from the size of the message word in bits, the coding rate, the number of lasers in the architecture, the modulation rate, and the laser modulation rate. To minimize the number of design decisions, the laser modulation rate was constant at 100 MHz which results in 100 million time slots per second. This modulation rate is well below high rate military programs and achievable by commercial products (Stotts 2008).

$$Rate_{Trans} = \frac{8bits}{MsgWord}\left(Rate_{Code}\right)\left(\#\,Lasers\right)\left(Rate_{Modulation}\right)\left(LaserMod_{Hz}\right)\text{[bits/sec]} \qquad (23)$$

E. POWER EFFICIENCY

The power required to transmit the message is dependent on the number of lasers, the coding scheme, and the modulation scheme. At this point in the architecture development, the laser transmitter does not have a required power in terms of Watts. To support further analysis, the proxy for power will be the required number of laser pulses per message bit. This is calculated using Equation 24. The dependent variables are the code rate, the number of lasers given the coding scheme and the power efficiency. The number of lasers given the coding scheme references the number of independent channels that are assigned data. The repetition codes suffer from increased power consumption because they transmit the same message information across multiple channels, while the RS codes do not.

$$Power = \left(Rate_{Code}\right)\left(NumLasers \mid CodeScheme\right)\left(Power_{Eff}\right) \qquad (24)$$

The power efficiency of the modulation scheme is dependent on the average number of pulses required to transmit a 8-bit codeword. The mean pulses per codeword for the modulation schemes are presented in Table 27.

Table 27. Modulation Scheme Pulses Per Codeword

Modulation Scheme	Pulses / Codeword
OOK	4
BPPM	8
2-Ary	4
4-Ary	2

F. TRADEOFF ANALYSIS

The tradeoff analysis will compare the transmission rates, the power efficiency, and the predicted BER. The previous sections have presented the effects that the architecture decisions have on the system MOEs. This section will provide a graphic presentation of the tension between achieving an acceptable BER and the costs incurred on the transmission rate and power efficiency.

The predicted BER for each turbulence level, transmission rate, and power efficiency for systems with four or eight lasers is presented in Table 28. The design space data for systems with 16-32 lasers is presented in Table 29.

Table 28. Design Space Data, Tradeoff Analysis, 4-8 Lasers

Coding Scheme	Number of Lasers	Modulation Scheme	Transmission Rate (Mbps)	Power Consumption (Pulses/Bit)	Bit Error Rate (Weak)	Bit Error Rate (Moderate)	Bit Error Rate (Strong)
RS(233,255)	4	OOK	365.4902	0.5472	0.0000	0.0345	0.0520
RS(233,255)	4	BPPM	182.7451	1.0944	0.0000	0.0257	0.0433
RS(233,255)	4	2-ARY	182.7451	0.5472	0.0000	0.0345	0.0520
RS(233,255)	4	4-ARY	91.3725	0.2736	0.0000	0.0494	0.0669
RS(191,255)	4	OOK	299.6078	0.6675	0.0000	0.0425	0.0936
RS(191,255)	4	BPPM	149.8039	1.3351	0.0000	0.0337	0.0849
RS(191,255)	4	2-ARY	149.8039	0.6675	0.0000	0.0425	0.0936
RS(191,255)	4	4-ARY	74.9020	0.3338	0.0000	0.0574	0.1085
RS(127,255)	4	OOK	199.2157	1.0039	0.0000	0.0295	0.0889
RS(127,255)	4	BPPM	99.6078	2.0079	0.0000	0.0206	0.0802
RS(127,255)	4	2-ARY	99.6078	1.0039	0.0000	0.0295	0.0889
RS(127,255)	4	4-ARY	49.8039	0.5020	0.0000	0.0443	0.0993
Repetition, Full	4	OOK	400.0000	2.0000	0.0000	0.0345	0.0520
Repetition, Full	4	BPPM	200.0000	4.0000	0.0000	0.0257	0.0433
Repetition, Full	4	2-ARY	200.0000	2.0000	0.0000	0.0345	0.0520
Repetition, Full	4	4-ARY	100.0000	1.0000	0.0000	0.0494	0.0669
Repetition, Half	4	OOK	400.0000	1.0000	0.0000	0.0345	0.0520
Repetition, Half	4	BPPM	200.0000	2.0000	0.0000	0.0257	0.0433
Repetition, Half	4	2-ARY	200.0000	1.0000	0.0000	0.0345	0.0520
Repetition, Half	4	4-ARY	100.0000	0.5000	0.0000	0.0494	0.0669
RS(233,255)	8	OOK	730.9804	0.5472	0.0000	0.0441	0.0555
RS(233,255)	8	BPPM	365.4902	1.0944	0.0000	0.0352	0.0468
RS(233,255)	8	2-ARY	365.4902	0.5472	0.0000	0.0441	0.0555
RS(233,255)	8	4-ARY	182.7451	0.2736	0.0000	0.0589	0.0704
RS(191,255)	8	OOK	599.2157	0.6675	0.0000	0.0520	0.1185
RS(191,255)	8	BPPM	299.6078	1.3351	0.0000	0.0432	0.1098
RS(191,255)	8	2-ARY	299.6078	0.6675	0.0000	0.0520	0.1185
RS(191,255)	8	4-ARY	149.8039	0.3338	0.0000	0.0669	0.1334
RS(127,255)	8	OOK	398.4314	1.0039	0.0000	0.0390	0.1137
RS(127,255)	8	BPPM	199.2157	2.0079	0.0000	0.0302	0.1050
RS(127,255)	8	2-ARY	199.2157	1.0039	0.0000	0.0390	0.1137
RS(127,255)	8	4-ARY	99.6078	0.5020	0.0000	0.0538	0.1241
Repetition, Full	8	OOK	800.0000	4.0000	0.0000	0.0441	0.0555
Repetition, Full	8	BPPM	400.0000	8.0000	0.0000	0.0352	0.0468
Repetition, Full	8	2-ARY	400.0000	4.0000	0.0000	0.0441	0.0555
Repetition, Full	8	4-ARY	200.0000	2.0000	0.0000	0.0589	0.0704
Repetition, Half	8	OOK	800.0000	2.0000	0.0000	0.0441	0.0555
Repetition, Half	8	BPPM	400.0000	4.0000	0.0000	0.0352	0.0468
Repetition, Half	8	2-ARY	400.0000	2.0000	0.0000	0.0441	0.0555
Repetition, Half	8	4-ARY	200.0000	1.0000	0.0000	0.0589	0.0704

Table 29. Design Space Data, Tradeoff Analysis, 16-32 Lasers

Coding Scheme	Number of Lasers	Modulation Scheme	Transmission Rate (Mbps)	Power Consumption (Pulses/Bit)	Bit Error Rate (Weak)	Bit Error Rate (Moderate)	Bit Error Rate (Strong)
RS(233,255)	16	OOK	1461.9608	0.5472	0.0000	0.0631	0.0625
RS(233,255)	16	BPPM	730.9804	1.0944	0.0000	0.0543	0.0538
RS(233,255)	16	2-ARY	730.9804	0.5472	0.0000	0.0631	0.0625
RS(233,255)	16	4-ARY	365.4902	0.2736	0.0184	0.0779	0.0774
RS(191,255)	16	OOK	1198.4314	0.6675	0.0000	0.0711	0.1683
RS(191,255)	16	BPPM	599.2157	1.3351	0.0000	0.0622	0.1596
RS(191,255)	16	2-ARY	599.2157	0.6675	0.0000	0.0711	0.1683
RS(191,255)	16	4-ARY	299.6078	0.3338	0.0000	0.0859	0.1832
RS(127,255)	16	OOK	796.8627	1.0039	0.0000	0.0580	0.1634
RS(127,255)	16	BPPM	398.4314	2.0079	0.0000	0.0492	0.1547
RS(127,255)	16	2-ARY	398.4314	1.0039	0.0000	0.0580	0.1634
RS(127,255)	16	4-ARY	199.2157	0.5020	0.0000	0.0729	0.1738
Repetition, Full	16	OOK	1600.0000	8.0000	0.0000	0.0631	0.0625
Repetition, Full	16	BPPM	800.0000	16.0000	0.0000	0.0543	0.0538
Repetition, Full	16	2-ARY	800.0000	8.0000	0.0000	0.0631	0.0625
Repetition, Full	16	4-ARY	400.0000	4.0000	0.0184	0.0779	0.0774
Repetition, Half	16	OOK	1600.0000	4.0000	0.0000	0.0631	0.0625
Repetition, Half	16	BPPM	800.0000	8.0000	0.0000	0.0543	0.0538
Repetition, Half	16	2-ARY	800.0000	4.0000	0.0000	0.0631	0.0625
Repetition, Half	16	4-ARY	400.0000	2.0000	0.0184	0.0779	0.0774
RS(233,255)	32	OOK	2923.9216	0.5472	0.0386	0.1011	0.0765
RS(233,255)	32	BPPM	1461.9608	1.0944	0.0280	0.0923	0.0678
RS(233,255)	32	2-ARY	1461.9608	0.5472	0.0369	0.1011	0.0765
RS(233,255)	32	4-ARY	730.9804	0.2736	0.0577	0.1160	0.0914
RS(191,255)	32	OOK	2396.8627	0.6675	0.0000	0.1091	0.2679
RS(191,255)	32	BPPM	1198.4314	1.3351	0.0000	0.1003	0.2592
RS(191,255)	32	2-ARY	1198.4314	0.6675	0.0000	0.1091	0.2679
RS(191,255)	32	4-ARY	599.2157	0.3338	0.0000	0.1240	0.2828
RS(127,255)	32	OOK	1593.7255	1.0039	0.0000	0.0960	0.2627
RS(127,255)	32	BPPM	796.8627	2.0079	0.0000	0.0872	0.2540
RS(127,255)	32	2-ARY	796.8627	1.0039	0.0000	0.0960	0.2627
RS(127,255)	32	4-ARY	398.4314	0.5020	0.0000	0.1109	0.2731
Repetition, Full	32	OOK	3200.0000	16.0000	0.0386	0.1011	0.0765
Repetition, Full	32	BPPM	1600.0000	32.0000	0.0280	0.0923	0.0678
Repetition, Full	32	2-ARY	1600.0000	16.0000	0.0369	0.1011	0.0765
Repetition, Full	32	4-ARY	800.0000	4.0000	0.0577	0.1160	0.0914
Repetition, Half	32	OOK	3200.0000	8.0000	0.0386	0.1011	0.0765
Repetition, Half	32	BPPM	1600.0000	16.0000	0.0280	0.0923	0.0678
Repetition, Half	32	2-ARY	1600.0000	8.0000	0.0369	0.1011	0.0765
Repetition, Half	32	4-ARY	800.0000	4.0000	0.0577	0.1160	0.0914

1. Methodology

This section presents the tradeoff analysis in each atmospheric condition. Several main effects were held constant throughout the tradeoff analysis. These effects were held constant to allow for consistent comparisons between the architectures. These values were chosen due to the main effects discussed in previous sections. The parameters are presented in Table 30.

Table 30. Tradeoff Analysis, Constant Parameters

Parameter	Value
Laser Wavelength	1550 nm
Irradiance Threshold	0.125
SNR	30 dB

The SNR was held constant at 30 decibels. Across the simulations at all three turbulence levels, the additional SNR did not provide a statistically significant improvement in mean BER response. The irradiance threshold of 0.125 was the highest performing threshold value across the three atmospheric conditions. Finally, the laser with a wavelength of 1550 nm consistently outperformed the 850 nm wavelength laser.

The candidate architectures are presented in 3D scatter plots. The three axes are the transmission rate in Mbps, the proxy for power consumption in pulses per bit, and the predicted BER from the least squares regression models. The ideal candidate will maximize the transmission rate, minimize power consumption, and have the smallest predicted BER. On the 3D scatter plot, the ideal candidate is as close to the bottom center of the plot as possible.

At this stage in the architecture development, there are no specific stakeholder requirements for minimum transmission rates, size limitations, or weight constraints. This precludes the use of threshold or objective performance levels associated with the MOEs. The analysis will focus first on minimizing the BER, then identifying the architecture that maximizes the transmission rate and minimizes power consumption.

2. Weak Turbulence

In the weak turbulence condition, there is a clustering of architectures that achieve similar BER. These architectures are clustered along the bottom of the scatter plot. The scatter plot of the three MOEs is presented in Figure 33.

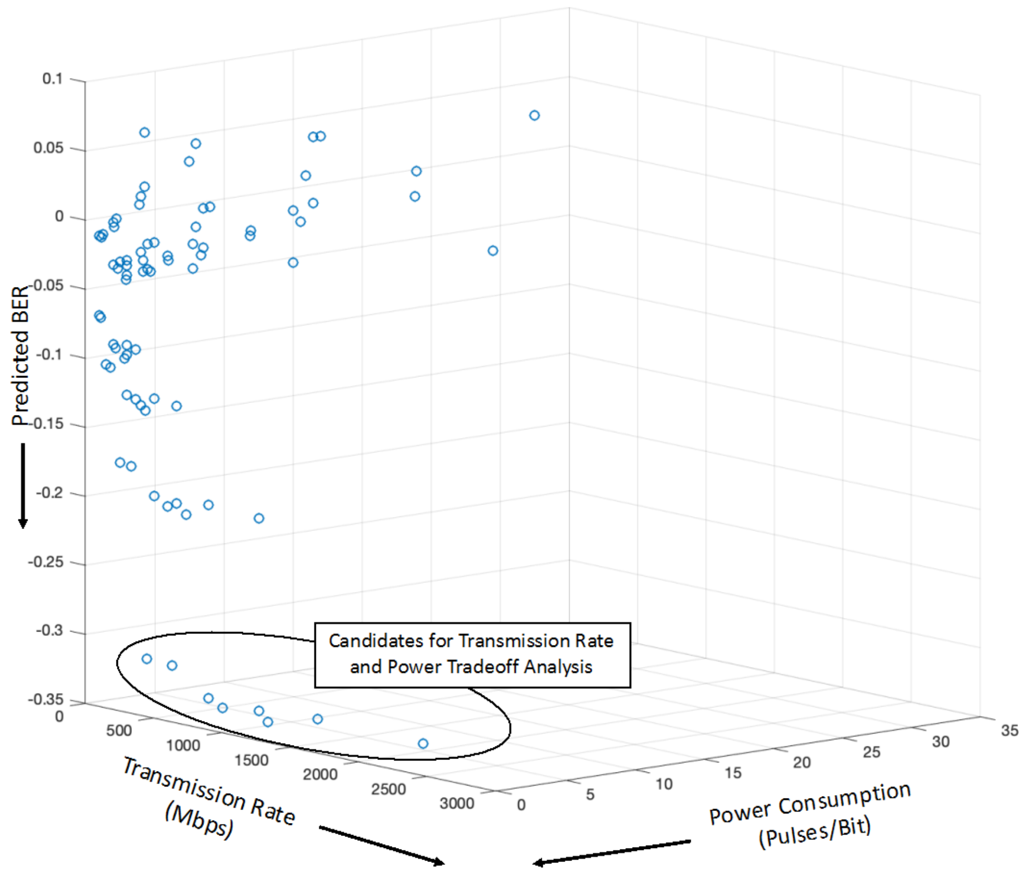

Figure 33. Weak Turbulence, 3D Scatter Plot, Tradeoff Analysis

The candidate architectures that have the lowest BER were selected for further comparison in terms of transmission rate and power efficiency. The top architectures are plotted with the transmission rate in Megabits per second along the horizontal axis and the power efficiency in pulses per bit along the vertical axis. The results are presented in Figure 34.

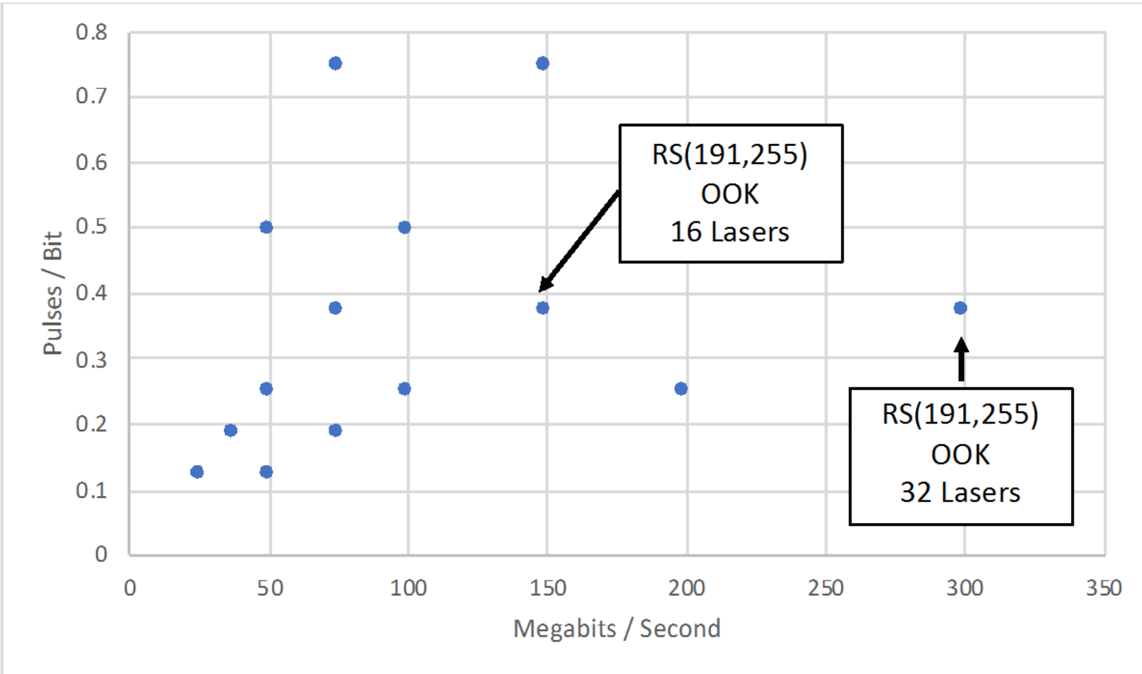

Figure 34. Candidate Architectures in Weak Turbulence, Transmission Rate Versus Power Efficiency

The maximum transmission rate with the lowest pulses per bit were selected as candidate architectures for the weak turbulence atmospheric condition. Both architectures employed the RS(191,255) code with the OOK modulation scheme.

3. Moderate Turbulence

There was a much more pronounced distribution in the system BER response. The architectures which were capable of achieving a low BER in weak turbulence conditions quickly deteriorated. The RS(127,255) code, in concert with the interactions amongst the architecture design decisions, was capable of handling the errors introduced by the atmospheric turbulence. Candidate architectures identified for further tradeoff analysis are encircled in the bottom left corner. The results are presented in Figure 35.

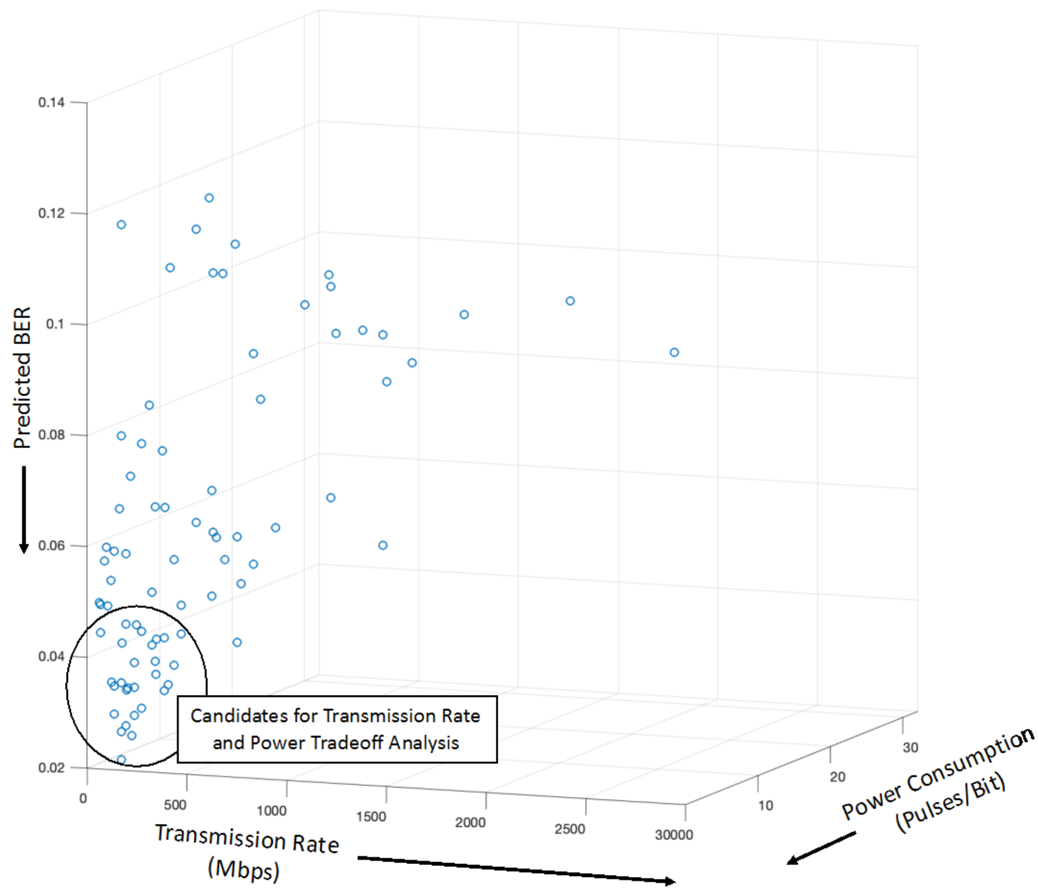

Figure 35. Moderate Turbulence, 3D Scatter Plot, Tradeoff Analysis

The cluster of architectures in the bottom left corner of the scatter plot represent the architectures with the best BER. The encircled candidate architectures are presented in a transmission rate versus power efficiency plot in Figure 36.

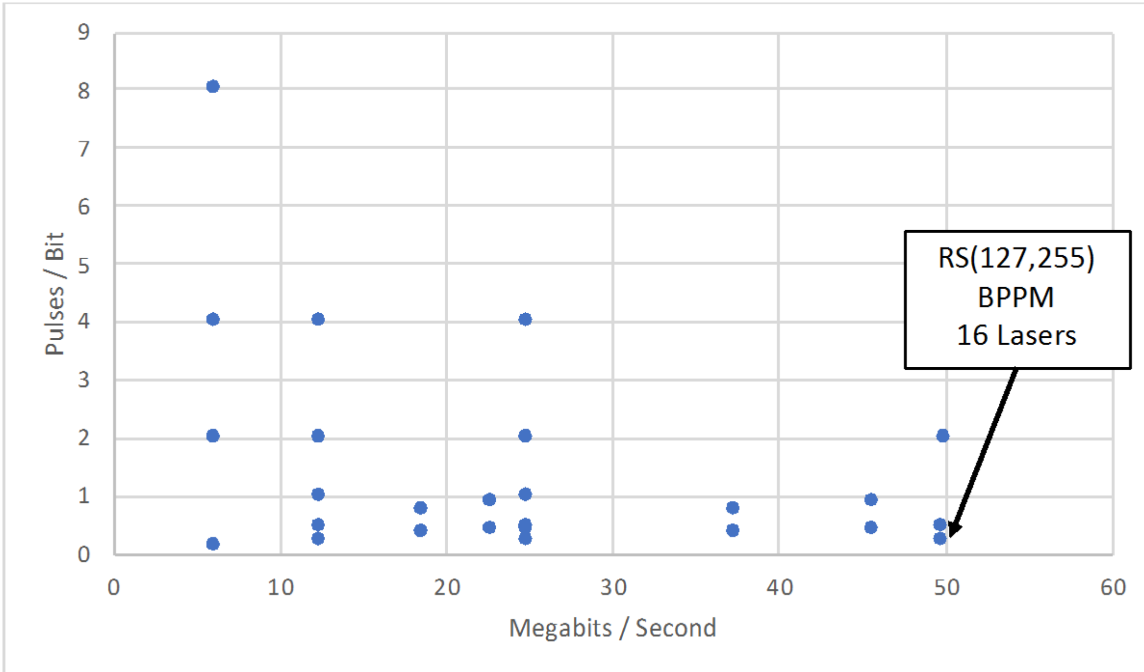

Figure 36. Candidate Architectures in Moderate Turbulence, Transmission Rate Versus Power Efficiency

The maximum transmission rate with the lowest pulses per bit were selected as candidate architectures for the moderate turbulence atmospheric condition. The highest performing architecture in terms of maximizing transmission rate and minimizing the number of pulses per bit was the 16 laser array with the RS(127,255) coding scheme and BPPM modulation.

4. Strong Turbulence

The same analysis steps were followed for the strong turbulence condition. The candidate architectures for further analysis were identified by their low predicted BER. The scatterplot is presented in Figure 37.

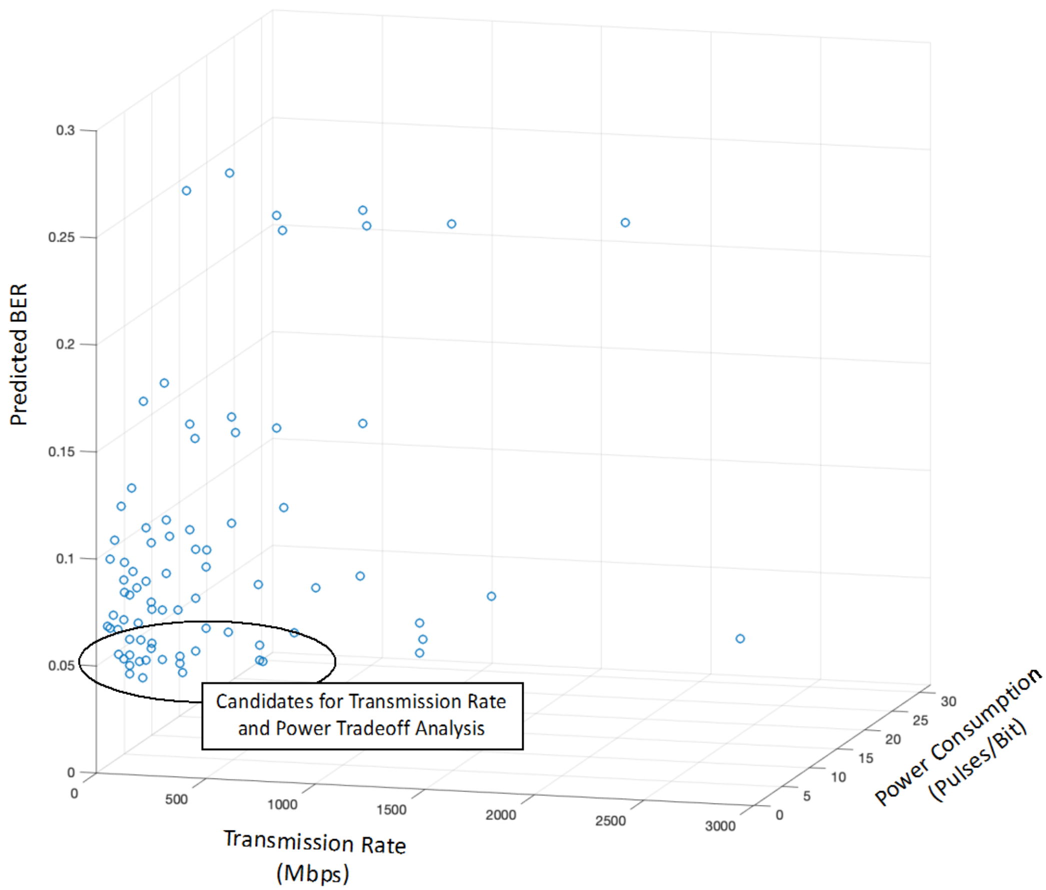

Figure 37. Strong Turbulence, 3D Scatter Plot, Tradeoff Analysis

The cluster of candidate architectures that achieve the best BER are encircled in the bottom left corner of the scatter plot. The encircled candidate architectures are presented in a transmission rate versus power efficiency plot in Figure 38.

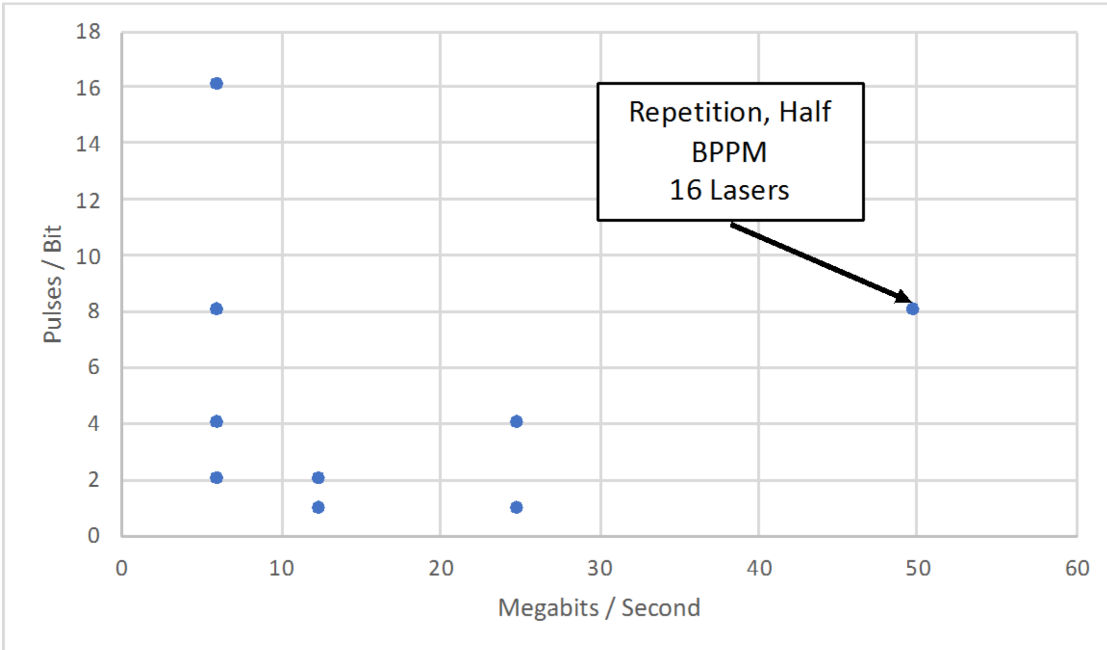

Figure 38. Candidate Architectures in Strong Turbulence, Transmission Rate Versus Power Efficiency

The candidate architectures are identified in the tradeoff analysis in Figure 38. The architecture design employs a 16-laser array, the half repetition coding scheme, and BPPM modulation.

5. Tradeoff Analysis Summary

The system architecture recommendation is an adaptive system that tunes its performance to the atmospheric conditions. As the atmospheric turbulence increases, the system requires a coding scheme with increased error correction capacity. In the weak turbulence regime, the RS(191,255) scheme provided an adequate level of error correction capacity to overcome the channel effects. In the moderate turbulence regime, the RS(127,255) is the candidate coding scheme. It provides the ability to correct 64 codeword errors in each 255-codeword block. In the strong turbulence regime, the repetition-half coding scheme provided the best performance while maximizing transmission rate. The proposed architecture decisions for each turbulence level are presented in Table 31.

Table 31. Summary of Candidate Architecture Results.

	Architecture
Weak	RS(191,255) OOK
Moderate	RS(127,255) BPPM
Strong	REP-HALF BPPM

The OOK modulation scheme worked well in weak and moderate turbulence conditions. As the atmospheric conditions become more challenging for FSOC systems, the BPPM modulation scheme provides extra protection against false alarms and missed detections. The final transmission rate requirements would guide the decision on the size of the laser array.

V. CONCLUSIONS AND RECOMMENDATIONS

This thesis followed a system engineering methodology to support the development of a functional architecture and development of final recommendations. The modeling and simulation provided an increased understanding of the complex interactions between the design decisions. This generated a set of candidate architectures to support future engineering prototype design and field testing.

A. SUMMARY

This project started with a review of the current US National Defense Strategy and supporting USN and USMC concepts. Chapter II outlined the current state of free space optical communication research and architectural design considerations. Chapter III defined the boundaries of the design space and the development of the architectural decisions. The FFBD was developed to provide structure for the design of the simulation. The full factorial design allowed for a thorough exploration of the design space.

The analysis identified significant main effects and second-degree interactions. Each of the architecture decisions had a statistically significant impact on the system's BER. The irradiance threshold had significant second-degree interactions in concert with the coding scheme, SNR, and the number of lasers. The repetition coding schemes were able to mitigate the negative effects on the detection and false alarm probabilities. The RS codes, however, suffered increased BER as the irradiance threshold increased. Once the system achieves 30 dB SNR, the system BER has a consistently increasing BER as the irradiance threshold increases. This is in contrast to the 15 dB SNR case where the BER decreased as the irradiance threshold increased. Finally, in the strong turbulence regime, the performance of the system with 4-lasers varies significantly between the different irradiance thresholds. As the number of lasers increases to 32, the interaction effect between the number of lasers and the irradiance threshold reveals a converging BER.

The two additional system MOPs are the transmission rate and the power efficiency. The transmission rate for the system is dependent on the coding rate, the number of lasers, the modulation rate, and the laser modulation rate. This provides a metric for how many bits of message information can be transmitted per second. The power efficiency is dependent on the coding rate, the number of independent channels with unique information, and the number of pulses per codeword required by the modulation scheme.

The tradeoff analysis identified the best performing architectures in terms of BER. Within this group, a tradeoff between transmission rate and power efficiency was analyzed to provide the recommended candidate architecture in each turbulence regime.

B. CONCLUSIONS

The goal of this thesis was to identify the significant architecture decisions. The architecture will support the development of engineering prototypes. There is a significant impact to the system performance from the atmospheric conditions. As the turbulence increases in the atmospheric channel, increased power from the transmitter cannot overcome the challenges imposed by deep fades. A laser array offers the opportunity to employ spatial diversity to achieve multiple independent channels.

The candidate architecture should have at least 16 lasers in the array. This size array minimized the effect of an independent channel being in a deep fade. With fewer lasers transmitting across the independent channels, the error correction capacity of the RS codes quickly becomes overwhelmed.

Under weak turbulence conditions, the RS(191,255) coding scheme paired with OOK modulation offers the best protection against the minimal effects of the optical channel while increasing the transmission rate beyond what the repetition codes are capable of attaining. When the turbulence increases into the moderate regime, the RS(127,255) code is required to overcome the increased number of errors incurred during transmission. In the strong turbulence regime, the error correction capacity of the three RS codes was not able to provide enough resiliency for the system. In strong turbulence, the repetition code is required to overcome the significant impairments in terms of reduced probability of detection, increased probability of the channel being in a fade, and the extended duration of the fades. The half repetition code provides an adequate level of resiliency while offering two times the transmission rate capability as the full repetition code.

The simulation explored the ability of modern block encoding algorithms to mitigate the devastating effects of deep fades. The development of an adaptive protocol is essential to leveraging this emerging technology. In addition to adaptive protocols at the physical layer, protocols controlling the upper layers of the OSI stack must be modified to increase resiliency.

C. SUGGESTIONS FOR FUTURE RESEARCH

The development of the simulation and the data analysis identified several opportunities for future research. Engineering prototype work to support field testing of this concept could offer the opportunity to explore the ability to employ FSOC systems at link distances of approximately 1000m. Field Programmable Gate Arrays (FPGAs) offer the flexibility to program and develop a system capable of operating at the transmission speeds required in the modern operating environment. Finally, the outcome of this report could be combined with the larger body of FSOC knowledge to meet emerging warfighter requirements.

THIS PAGE INTENTIONALLY LEFT BLANK

APPENDIX A. MATLAB SCRIPTS

A. FSOC PROBABILITY PARAMETERS

```
%
%%%%%%%%%%%%%%%%%%%%%%%%%%%%%%%%%%%%%%%%%%%%%%%%%%%%%%%%%%%
%%%%%%%%%%%%%%%%%%%%%%%
% Optical Channel Probability Parameters
% Eric R Stewart
% System Architecture of a MIMO FSO System
% Naval Postgraduate School
% 30 April 2019
%
%%%%%%%%%%%%%%%%%%%%%%%%%%%%%%%%%%%%%%%%%%%%%%%%%%%%%%%%%%%
%%%%%%%%%%%%%%%%%%%%%%%
% This function will derive critical probabilities for a FSOC System
function [probFade, probFA, probDetect_Out, probDetect_Avail, meanNumberFades] =
fsocParameters2(RyVar, SNR, i_T)

% Fundamental equations from
% Larry C. Andrews and Ronald L. Phillips. 2005.
% Laser Beam Propagation through Random Media, 2nd Edition.

i_S=1;      % Normalized Signal Irradiance
syms I;

alpha=1/(exp(0.49*RyVar/(1+1.11*RyVar^(6/5))^(7/6))-1);
beta=1/(exp(0.51*RyVar/(1+0.69*RyVar^(6/5))^(5/6))-1);
scintillationIndex = 1/alpha + 1/beta + 1/(alpha*beta);
v0=550; % 550 Hz constant quasi-frequency
p(I)=(2*(alpha*beta)^((alpha+beta)/2))/(gamma(alpha)*gamma(beta))*I^((alpha+beta)/2-
1)*besselk((alpha-beta),(2*((alpha*beta)*I)^(1/2)));


sigma_n=i_S/(10^(SNR/20));
probFade = double(vpaintegral(p(I), 0, i_T));
probFA=double(0.5*erfc(i_T/(sqrt(2)*sigma_n)));
probDetect_Out=probFA;
probDetect_Avail=double(vpaintegral(0.5*p(I)*erfc((i_T-i_S)/(sqrt(2)*sigma_n)),i_T,Inf));
meanNumberFades = (2*sqrt(2*pi*alpha*beta)*v0*sqrt(scintillationIndex)) /
(gamma(alpha)*gamma(beta)) * ( alpha*beta*i_T)^ ( (alpha+beta-1)/2) * besselk((alpha-beta),
2*sqrt(alpha*beta*i_T));
```

B. CHANNEL STATE BUILDS

```
function channelStatistics = channelBuilds();
%
%%%%%%%%%%%%%%%%%%%%%%%%%%%%%%%%%%%%%%%%%%%%%%%%%%%%%%%%%%%
%%%%%%%%%%%%%%%%%%%%%%%
% Channel State Builds
```

```
% Eric R Stewart
% System Architecture of a MIMO FSO System
% Naval Postgraduate School
% 30 April 2019
%
%%%%%%%%%%%%%%%%%%%%%%%%%%%%%%%%%%%%%%%%%%%%%%%%%%%%%%%%
%%%%%%%%%%%%%%%%%%%%
% Fundamental equations from
% Larry C. Andrews and Ronald L. Phillips. 2005.
% Laser Beam Propagation through Random Media, 2nd Edition.
structureIndex = [5e-15, 5e-14, 1e-13]; % Refractive Structure Index [m^-2/3]
SNR = [15, 30, 45]; % Signal-to-Noise Ratio [dB]
iT = [0.125, 0.250, 0.375, 0.500]; % Irradiance Threshold
waveLength = [850e-9; 1550e-9]; %Wavelength [m]
k = waveLength.^(-1)*2*pi; % Wave Number [m^-1]
L=1000; % Link length [m]
numStruct=length(structureIndex);
numSNR=length(SNR);
numiT=length(iT);
numWaveLength=length(waveLength);
rowNumber=1;

for ii = 1:numStruct
   Cn2=structureIndex(ii);
   for jj = 1:numSNR
      signalNoise=SNR(jj);
      for kk = 1:numiT
         irradianceThreshold = iT(kk);
         for ll = 1:numWaveLength
            wl = waveLength(ll);
            k = 2*pi/wl;
            rytovVariance = 1.23*structureIndex(ii)*k^(7/6)*L^(11/6);
            [probFade, probFA, probDetect_Out, probDetect_Avail,
meanFade]=fsocParameters2(rytovVariance,signalNoise,irradianceThreshold);
            channelStatistics(rowNumber,1) = Cn2;
            channelStatistics(rowNumber,2) = signalNoise;
            channelStatistics(rowNumber,3) = irradianceThreshold;
            channelStatistics(rowNumber,4) = wl;
            channelStatistics(rowNumber,5) = probFade;
            channelStatistics(rowNumber,6) = probFA;
            channelStatistics(rowNumber,7) = probDetect_Out;
            channelStatistics(rowNumber,8) = probDetect_Avail;
            channelStatistics(rowNumber,9) = meanFade;
            rowNumber = rowNumber+1;
         end
      end
   end
end
```

C. SIMULATION DESIGN

```
%
%%%%%%%%%%%%%%%%%%%%%%%%%%%%%%%%%%%%%%%%%%%%%%%%%%%%%%%%%%
%%%%%%%%%%%%%%%%%%%%%
% Experimental Design
% Eric R Stewart
% System Architecture of a MIMO FSO System
% Naval Postgraduate School
% 30 April 2019
%
%%%%%%%%%%%%%%%%%%%%%%%%%%%%%%%%%%%%%%%%%%%%%%%%%%%%%%%%%%
%%%%%%%%%%%%%%%%%%%%%
% Import Testing Information

testMachine = 1; % Test Machine Number
experimentParameters=buildExperiment(testMachine);
[numExperiments, numParameters]=size(experimentParameters);

% Build Channel Statistic Matrix
channelStatistics = channelBuilds(); % Build channel state matrix

laserModulation = 1/100e6;  % 100mbs laser modulation speed
totalBits = 2e6;    % 2 million bit message size
totalChars = totalBits / 8;

for experimentNumber = 1:numExperiments
   t=datetime()
   disp(experimentNumber);

   % Pull Parameters from the file into the experiment.
   codingScheme = experimentParameters(experimentNumber,1);
   numLasers = experimentParameters(experimentNumber,2);
   modulationScheme = experimentParameters(experimentNumber,3);
   Cn2 = experimentParameters(experimentNumber,4);
   waveLength = experimentParameters(experimentNumber,5);
   irradianceThreshold = experimentParameters(experimentNumber,6);
   SNR = experimentParameters(experimentNumber,7);

   % Assign Detection Statistics from System Architecture / Environment
   for ii = 1:length(channelStatistics)
      if (channelStatistics(ii,1)==Cn2)
         if (channelStatistics(ii,2)==SNR)
            if (channelStatistics(ii,3) == irradianceThreshold)
               if (channelStatistics(ii,4) == waveLength)
                     channelCharacter=channelStatistics(ii,5:9);
                     probFade = channelStatistics(ii,5);
                     probFA = channelStatistics(ii,6);
                     probDetect_Out = channelStatistics(ii,7);
                     probDetect_Avail = channelStatistics(ii,8);
                     meanFadeTime = floor(probFade/channelStatistics(ii,9));
                     % [probFade probFA probDetect_out probDetect_avail
                     % meanFadeTime]
               break;
```

```
            end
          end
        end
      end
    end

    timeStepAdjustment = floor(meanFadeTime/laserModulation);   % Duration of deep fades in
terms of laser modulation speed

    if codingScheme == 1
      % RS(255,233);
      messageLength=233;
      codeWordLength=255;
      rsEncoderObject= comm.RSEncoder(codeWordLength, messageLength);
      rsDecoderObject= comm.RSDecoder(codeWordLength, messageLength);
    elseif codingScheme == 2
      % RS(255,191)
      messageLength=191;
      codeWordLength=255;
      rsEncoderObject= comm.RSEncoder(codeWordLength, messageLength);
      rsDecoderObject= comm.RSDecoder(codeWordLength, messageLength);
    elseif codingScheme == 3
      % RS(255,127)
      messageLength=127;
      codeWordLength=255;
      rsEncoderObject= comm.RSEncoder(codeWordLength, messageLength);
      rsDecoderObject= comm.RSDecoder(codeWordLength, messageLength);
    elseif codingScheme == 4
      % Repetition 50%
      messageLength=255;
      codeWordLength=255;
    else
      messageLength=255;
      codeWordLength=255;
      % Repetition 100%
    end
    codeRate = messageLength/codeWordLength;    % Coding Rate
    messageWords = floor(totalChars/messageLength)+1;
    symbols = 255*messageWords;
    padding = mod(symbols,numLasers);   % Required number of symbol padding
    inputMessage = randi([0 255], messageLength, messageWords);

    % Assign 8-bit streams to lasers

    if codingScheme <= 3
      % RS Encoding Schemes
      for ii = 1:messageWords
        codeWord(:,ii) = rsEncoderObject(inputMessage(:,ii));
      end
      codeWord = reshape(codeWord, 1, messageWords*codeWordLength);
      codeWord = [codeWord randi([0 255], 1, padding)]; % Pad Codeword for Number of Lasers
      laserStream = reshape(codeWord, numLasers,
(codeWordLength*messageWords)/numLasers);
    elseif codingScheme == 4
      % 50% Repetition Encoding Scheme
```

```
        codeWord = reshape(inputMessage, 1, messageWords*codeWordLength);
        codeWord = [codeWord randi([0 255], 1, padding)]; % Pad Codeword for Number of Lasers
        laserStream = reshape(codeWord, numLasers,
(codeWordLength*messageWords)/numLasers);
        for ii = 1:2:numLasers
            laserStream(ii,:)=codeWord(1,:);
            laserStream(ii+1,:) = codeWord(2,:);
        end
    else
        % 100% repetition encoding scheme
        codeWord = reshape(inputMessage, 1, messageWords*codeWordLength);
        codeWord = [codeWord randi([0 255], 1, padding)]; % Pad Codeword for Number of Lasers
        for ii = 1:numLasers
            laserStream(ii,:) = codeWord;
        end
    end

    channelState = buildInitialChannelState(numLasers, probFade, timeStepAdjustment);

    currentTime = 0;
    totalPulses = 0;
    receivedLaserStream=[];

    for ii = 1:length(laserStream)

        % Modulation
        modulatedSignal = [];

        if modulationScheme == 1
            % OOK
            modulatedSignal = OOKmod(laserStream(:,ii));
        elseif modulationScheme == 2
            % BPPM
            modulatedSignal = bppmModulate(laserStream(:,ii));
        elseif modulationScheme == 3
            % 2-Ary
            modulatedSignal = mAryModulate(laserStream(:,ii),2);
        elseif modulationScheme == 4
            % 4-Ary
            modulatedSignal = mAryModulate(laserStream(:,ii),4);
        end

        % Transmission

        totalPulses = totalPulses + sum(sum(modulatedSignal));
        [receivedSignal, channelState, currentTime] = transmitFSOChannel(modulatedSignal,
probFade, probFA, probDetect_Out, probDetect_Avail, channelState, currentTime,
timeStepAdjustment, meanFadeTime);
        % Compress Repetition Codes

        if codingScheme == 4
            % 50% repetition coding
            receivedSignal = repetitionDecode(receivedSignal,codingScheme);
        elseif codingScheme == 5
            % Full repetition coding
```

```
        receivedSignal = repetitionDecode(receivedSignal,codingScheme);
    end

    % Demodulate Signal

    if modulationScheme == 1
        % OOK
        demodulatedSignal = OOKdemod(receivedSignal);
    elseif modulationScheme == 2
        % BPPM
        demodulatedSignal = bppmDemodulate(receivedSignal);
    elseif modulationScheme == 3
        % 2-Ary
        demodulatedSignal = mAryDemodulate(receivedSignal, 2);
    elseif modulationScheme == 4
        % 4-Ary
        demodulatedSignal = mAryDemodulate(receivedSignal, 4);
    end

    receivedLaserStream=[receivedLaserStream demodulatedSignal];
end

% Drop Padding

receivedCodeWord = reshape(receivedLaserStream, 1,
messageWords*codeWordLength+padding);
receivedCodeWord = receivedCodeWord(1:messageWords*codeWordLength);

% Reshape Matrix

receivedCodeWord = reshape(receivedCodeWord, codeWordLength, messageWords);
clear receivedLaserStream;

if codingScheme <= 3
    for ii = 1:messageWords
        receivedMessage(:,ii) = rsDecoderObject(receivedCodeWord(:,ii));
    end
    clear receivedCodeWord;
else
    receivedMessage = receivedCodeWord;
    clear receivedCodeWord;
end

receivedCodeWords = reshape(receivedMessage, messageLength, messageWords);

[systemErrors, systemBER] = biterr(inputMessage, receivedCodeWords);
totalTime = laserModulation*currentTime;
transmissionRate = totalBits / totalTime;
pulsesPerBit=totalPulses/2e6;

systemResults(experimentNumber,:)=[systemBER, transmissionRate, totalPulses];

clear codingScheme;
clear numLasers;
clear modulationScheme;
```

```
    clear Cn2;
    clear waveLength;
    clear irradianceThrehold;
    clear dataInput;
    clear messageLength;
    clear codeWordLength;
    clear rsEncoderObject;
    clear rsDecoderObject;
    clear messageWords;
    clear channelState;
    clear codeWord;
    clear receivedLaserStream;
    clear receivedCodeWord;
    clear laserStream;
    clear modulatedSignal;
    clear receivedSignal;
    clear channelCharacter;
    clear demodulatedSignal;
    clear totalPulses;
    clear irradianceThreshold;
    clear ii;
    clear jj;
    clear meanFadeTime;
    clear probDetect_Avail;
    clear probDetect_Out;
    clear probFA;
    clear probFade;
    clear SNR;
    clear systemBER;
    clear transmissionRate;
    clear systemErrors;
    clear receivedCodeWords;
    clear receivedMessage;
end
```

D. BPPM FUNCTIONS

```
function [modulatedSignal] = bppmModulate(codeWord)
% Binary Pulse-Position Modulation
%
%%%%%%%%%%%%%%%%%%%%%%%%%%%%%%%%%%%%%%%%%%%%%%%%%%%%%%%%
%%%%%%%%%%%%%%%%%%%%%
% BPPM Modulate
% Eric R Stewart
% System Architecture of a MIMO FSO System
% Naval Postgraduate School
% 30 April 2019
%
%%%%%%%%%%%%%%%%%%%%%%%%%%%%%%%%%%%%%%%%%%%%%%%%%%%%%%%%
%%%%%%%%%%%%%%%%%%%%%
% CodeWord is an integer
[numLasers, codeWordLength] = size(codeWord);
```

```
modulatedSignal = zeros(numLasers, 16*codeWordLength);
tempBitWindow = zeros(numLasers,16);

for codeWordIndex = 1:codeWordLength
   tempBitWindow = de2bi(codeWord(:,codeWordIndex),8,'left-msb');

   for bitLocation = 1:8

      for laserNumber = 1:numLasers

         if tempBitWindow(laserNumber, bitLocation) == 0

            modulatedSignal(laserNumber, (codeWordIndex-1)*16 + 2*bitLocation-1) = 0;
            modulatedSignal(laserNumber, (codeWordIndex-1)*16 + 2*bitLocation) = 1;
         else
            modulatedSignal(laserNumber, (codeWordIndex-1)*16 + 2*bitLocation-1) = 1;
            modulatedSignal(laserNumber, (codeWordIndex-1)*16 + 2*bitLocation) = 0;
         end
      end
   end
end

function [codeWord] = bppmDemodulate(receivedSignal)
%
%%%%%%%%%%%%%%%%%%%%%%%%%%%%%%%%%%%%%%%%%%%%%%%%%%%%%%
%%%%%%%%%%%%%%%%%%%%
% BPPM Demodulate Function
% Eric R Stewart
% System Architecture of a MIMO FSO System
% Naval Postgraduate School
% 30 April 2019
%
%%%%%%%%%%%%%%%%%%%%%%%%%%%%%%%%%%%%%%%%%%%%%%%%%%%%%%
%%%%%%%%%%%%%%%%%%%%
% Binary Pulse-Position Demodulation
% receivedSignal is binary
% codeWord are integers
[numLasers, signalLength] = size(receivedSignal);
numberCodeWords=signalLength/16;
codeWord = zeros(numLasers, signalLength/16);
signalBuffer = zeros(1,16);
receivedBit = zeros(1,8);
for codeWordIndex = 1:numberCodeWords
   for laserNumber = 1:numLasers
      bitIndex = (codeWordIndex-1)*16+1;
      signalBuffer = receivedSignal(laserNumber, bitIndex:(bitIndex+15));

      for bitLocation = 1:8
         startBit = (bitLocation-1)*2+1;
         if signalBuffer(startBit:startBit+1) == [0 1]
            receivedBit(bitLocation) = 0;
         elseif signalBuffer(startBit:startBit+1) == [1 0]
            receivedBit(bitLocation) = 1;
```

```
        elseif signalBuffer(startBit:startBit+1) == [0 0]
          receivedBit(bitLocation) = 0;
        else
          receivedBit(bitLocation) = 1;
        end
      end
      codeWord(laserNumber, codeWordIndex) = bi2de(receivedBit, 'left-msb');
  end
end
```

E. OOK FUNCTIONS

```
function OOK = OOKmod(laserStream)
%
%%%%%%%%%%%%%%%%%%%%%%%%%%%%%%%%%%%%%%%%%%%%%%%%%%%%%
%%%%%%%%%%%%%%%%%%%%
% OOK Modulate Function
% Eric R Stewart
% System Architecture of a MIMO FSO System
% Naval Postgraduate School
% 30 April 2019
%
%%%%%%%%%%%%%%%%%%%%%%%%%%%%%%%%%%%%%%%%%%%%%%%%%%%%%
%%%%%%%%%%%%%%%%%%%%

% Create a OOK modulated bitstream
numLasers = length(laserStream);
OOK = zeros(numLasers, 8);
for ii = 1:numLasers
  OOK(ii,:)=de2bi(laserStream(ii),8,'left-msb');
end
end

function demodulatedSignal = OOKdemod(receivedSignal)
%
%%%%%%%%%%%%%%%%%%%%%%%%%%%%%%%%%%%%%%%%%%%%%%%%%%%%%
%%%%%%%%%%%%%%%%%%%%
% OOK Demodulate Function
% Eric R Stewart
% System Architecture of a MIMO FSO System
% Naval Postgraduate School
% 30 April 2019
%
%%%%%%%%%%%%%%%%%%%%%%%%%%%%%%%%%%%%%%%%%%%%%%%%%%%%%
%%%%%%%%%%%%%%%%%%%%

% Demodulate a OOK modulated bitsteam
[numLasers, numBits] = size(receivedSignal);
demodulatedSignal=zeros(numLasers,1);
if numBits ~= 8
  return
end
for ii = 1:numLasers
```

```
    demodulatedSignal(ii) = bi2de(receivedSignal(ii,:),'left-msb');
end
end
```

F. M-ARY FUNCTIONS

```
function [modulatedSignal] = mAryModulate(codeWord,modLevel)
%
%%%%%%%%%%%%%%%%%%%%%%%%%%%%%%%%%%%%%%%%%%%%%%%%%%%%%%%%%%%%%%%%%%%%%%%%%%%%%%%%%%%
% M-ary pulse-position modulation
% Eric R Stewart
% System Architecture of a MIMO FSO System
% Naval Postgraduate School
% 30 April 2019
%
%%%%%%%%%%%%%%%%%%%%%%%%%%%%%%%%%%%%%%%%%%%%%%%%%%%%%%%%%%%%%%%%%%%%%%%%%%%%%%%%%%%

% codeWord is an integer matrix
% modulatedSignal is the pulse positions
[numLasers, codeWordLength] = size(codeWord);
modulatedSignal = [];
modsPerChar = 8 / modLevel;
% Build reference matrix to put pulse in proper Time Slot
referenceMatrix = zeros(modLevel^2,modLevel);
for ii = 1:(modLevel^2)
    referenceMatrix(ii,1:modLevel)=de2bi(ii-1,modLevel,'left-msb');
end
for codeWordIndex = 1:codeWordLength
    tempModSignal = zeros(numLasers, modsPerChar*modLevel^2);

    for laserNumber = 1:numLasers
        tempBitWindow = de2bi(codeWord(laserNumber, codeWordIndex),8,'left-msb');
        modBitWindow = [];
        for ii = 1:modsPerChar
            bitSlice = tempBitWindow( (ii-1)*modLevel + 1: (ii-1)*modLevel + modLevel);
            laserModSignal = zeros(1,modLevel^2);

            for timeSlot = 1:modLevel^2
                if bitSlice == referenceMatrix(timeSlot,:)
                    laserModSignal(timeSlot) = 1;
                    break
                end
            end
            modBitWindow = [modBitWindow laserModSignal];
        end
        tempModSignal(laserNumber,:)=modBitWindow;
    end
    modulatedSignal = [modulatedSignal tempModSignal];
end
```

```
function [demodulatedSignal] = mAryDemodulate(rxSignal, modLevel)
%
%%%%%%%%%%%%%%%%%%%%%%%%%%%%%%%%%%%%%%%%%%%%%%%%%%%%%%%%%%%%%
% M-ary pulse-position demodulation
% Eric R Stewart
% System Architecture of a MIMO FSO System
% Naval Postgraduate School
% 30 April 2019
%
%%%%%%%%%%%%%%%%%%%%%%%%%%%%%%%%%%%%%%%%%%%%%%%%%%%%%%%%%%%%%

% rxSignal is a matrix of binary received pulses
% DemodulatedSignal is an integer matrix
[numLasers, signalLength] = size(rxSignal);
sliceLength = modLevel^2;
slicesPerChar = 8 / modLevel;
charLength = slicesPerChar*sliceLength;
numberCodeWords = signalLength/charLength;
demodulatedSignal = zeros(numLasers, numberCodeWords);
% Build reference matrix to find proper integer from time slot
referenceMatrix = zeros(modLevel^2,modLevel);
for ii = 1:(modLevel^2)
   referenceMatrix(ii,1:modLevel)=de2bi(ii-1,modLevel,'left-msb');
end
for codeWordIndex = 1:numberCodeWords
   firstColumn=(codeWordIndex-1)*charLength + 1;
   lastColumn=codeWordIndex*charLength;
   tempModSignal=rxSignal(:,firstColumn:lastColumn); %All lasers, 1 modulated char
   for laserNumber = 1:numLasers
      bitBuild = [];
      laserModSignal = tempModSignal(laserNumber,:); % One laser's char
      for sliceNumber = 1:slicesPerChar
         firstBit = (sliceNumber-1)*sliceLength + 1;
         lastBit = sliceNumber*sliceLength;
         bitSlice = laserModSignal(firstBit:lastBit);
         timeSlot = 0;
         if sum(bitSlice) == 0
            % Signal is in a fade, no pulse received
            timeSlot = randi([1 sliceLength]);
         else
            for ii = 1:sliceLength
               if bitSlice(ii) == 1
                  timeSlot=ii;
                  break
               end
            end
         end
         bitBuild = [bitBuild referenceMatrix(timeSlot,:)];
      end
      demodulatedSignal(laserNumber, codeWordIndex) = bi2de(bitBuild, 'left-msb');
   end
end
```

G. REPETITION DECODING FUNCTION

```
function repetitionSignal = repetitionDecode(receivedSignal, codingScheme);
%
%%%%%%%%%%%%%%%%%%%%%%%%%%%%%%%%%%%%%%%%%%%%%%%%%%
%%%%%%%%%%%%%%%%%%%
% Repetition Decode Function
% Eric R Stewart
% System Architecture of a MIMO FSO System
% Naval Postgraduate School
% 30 April 2019
%
%%%%%%%%%%%%%%%%%%%%%%%%%%%%%%%%%%%%%%%%%%%%%%%%%%
%%%%%%%%%%%%%%%%%%%

[numLasers, numPulses]=size(receivedSignal);
threshold = 1.5/numLasers;
if codingScheme == 4
   % 1/2 repetition coding
   repetitionSignal=zeros(2,numPulses);
   for ii = 1:numLasers/2
      firstSignal(ii,:) = receivedSignal(2*ii-1,:);
      secondSignal(ii,:) = receivedSignal(2*ii,:);
   end
   for pulseNumber = 1:numPulses
      if mean(firstSignal(:,pulseNumber)) >= threshold
         repetitionSignal(1,pulseNumber) = 1;
      end
      if mean(secondSignal(:,pulseNumber)) >= threshold
         repetitionSignal(2,pulseNumber) = 1;
      end
   end
else
   % Full Repetition coding
   repetitionSignal=zeros(1,numPulses);
   for pulseNumber = 1:numPulses
      if mean(receivedSignal(:,pulseNumber)) >= threshold
         repetitionSignal(pulseNumber) = 1;
      end
   end
end
end
```

H. TRANSMIT FREE SPACE OPTICAL CHANNEL

```
function [receivedSignal, channelState, currentTime] = transmitClearChannel(modulatedSignal,
probFade, probFA, probDetect_Out, probDetect_Avail, channelState, currentTime,
modulationFactor, meanFadeTime)
%
%%%%%%%%%%%%%%%%%%%%%%%%%%%%%%%%%%%%%%%%%%%%%%%%%%
%%%%%%%%%%%%%%%%%%%
```

```
% Monte Carlo Simulation for optical channel transmission
% Eric R Stewart
% System Architecture of a MIMO FSO System
% Naval Postgraduate School
% 30 April 2019
%
%%%%%%%%%%%%%%%%%%%%%%%%%%%%%%%%%%%%%%%%%%%%%%%%%%%%%%%%%%%%%%%%%%%%%%%%%%%%%%
%%%%%%%%%%%%%%%%%%%%%%%%%%%%

[numLasers, signalLength] = size(modulatedSignal);
receivedSignal = zeros(numLasers,signalLength);
for timeSlot = 1:signalLength

   for laserNumber = 1:numLasers

      % Check for State Change
      if currentTime >= channelState(laserNumber,2)
         if rand() < probFade
            channelState(laserNumber,1) = 0;
         else
            channelState(laserNumber,1) = 1;
         end
         nextStep=modulationFactor * floor(meanFadeTime* (1-rand()));
         channelState(laserNumber,2) = currentTime + nextStep;
      end
      currentLaserState = channelState(laserNumber,1);
      if modulatedSignal(laserNumber, timeSlot) == 0
         % Transmitted '0' bit
         if rand() < probFA
            % False Alarm, Received 1
            receivedSignal(laserNumber, timeSlot) = 1;
         else
            receivedSignal(laserNumber, timeSlot) = 0;
         end
      else
         % Transmitted '1' bit
         if currentLaserState == 0
            % Channel is in a fade
            if rand() < probDetect_Out
                  receivedSignal(laserNumber, timeSlot) = 1;
            else
                  receivedSignal(laserNumber, timeSlot) = 0;
            end
         else
            % Channel is Available
            if rand() < probDetect_Avail
               receivedSignal(laserNumber, timeSlot) = 1;
            else
               receivedSignal(laserNumber, timeSlot) = 0;
            end
         end
      end
   end
   currentTime= currentTime + 1;
```

```
end
```

I. BUILD INITIAL CHANNEL STATES FUNCTION

```
function channelState = buildInitialChannelState(numLasers, probFade, timeStepAdjustment,
meanFadeTime)
%
%%%%%%%%%%%%%%%%%%%%%%%%%%%%%%%%%%%%%%%%%%%%%%%%%%%
%%%%%%%%%%%%%%%%%%%%
% Build Initial Channel States Function
% Eric R Stewart
% System Architecture of a MIMO FSO System
% Naval Postgraduate School
% 30 April 2019
%
%%%%%%%%%%%%%%%%%%%%%%%%%%%%%%%%%%%%%%%%%%%%%%%%%%%
%%%%%%%%%%%%%%%%%%%%

channelState = ones(numLasers, 2);
% Initialize Channel States

for jj = 1:numLasers
   if rand() < probFade
      channelState(jj,1) = 0; %Channel is in a fade
   end
   channelState(jj,2) = abs(floor(timeStepAdjustment*meanFadeTime(1-rand())));
end
```

APPENDIX B. SYSTEM BER ANALYSIS

The initial analysis of the system BER response variable did not categorize the results by atmospheric turbulence levels. The least squares regression analysis was conducted for the main effects from the architecture decisions and second-degree interactions. The regression model explained 87.5% of the variability. The summary of fit is presented in Figure 39.

Summary of Fit	
RSquare	0.8758
RSquare Adj	0.875139
Root Mean Square Error	0.046541
Mean of Response	0.125068
Observations (or Sum Wgts)	23039

Figure 39. Summary of Fit, BER.

The main effects were identified for the regression model. The effects that have a significance of greater than 0.05 are outlined with a dashed black line. The effect summary is presented in Figure 40. The significant influence of the atmospheric turbulence was not helpful in developing candidate architectures. The architecture must be able to operate in the range of turbulence conditions, but the system performance should not be dictated significantly by the environment.

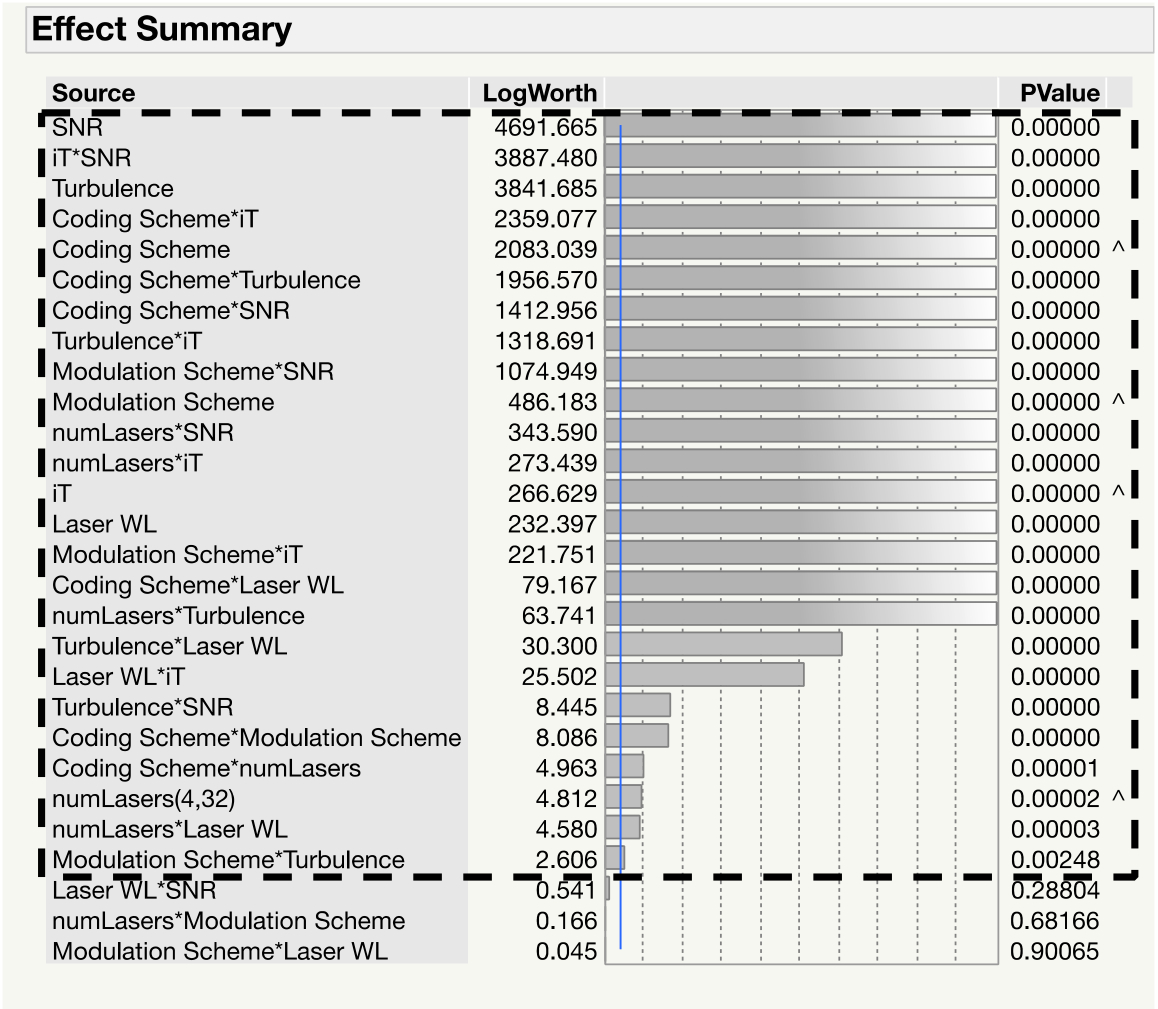

Effect Summary

Source	LogWorth	PValue
SNR	4691.665	0.00000
iT*SNR	3887.480	0.00000
Turbulence	3841.685	0.00000
Coding Scheme*iT	2359.077	0.00000
Coding Scheme	2083.039	0.00000 ^
Coding Scheme*Turbulence	1956.570	0.00000
Coding Scheme*SNR	1412.956	0.00000
Turbulence*iT	1318.691	0.00000
Modulation Scheme*SNR	1074.949	0.00000
Modulation Scheme	486.183	0.00000 ^
numLasers*SNR	343.590	0.00000
numLasers*iT	273.439	0.00000
iT	266.629	0.00000 ^
Laser WL	232.397	0.00000
Modulation Scheme*iT	221.751	0.00000
Coding Scheme*Laser WL	79.167	0.00000
numLasers*Turbulence	63.741	0.00000
Turbulence*Laser WL	30.300	0.00000
Laser WL*iT	25.502	0.00000
Turbulence*SNR	8.445	0.00000
Coding Scheme*Modulation Scheme	8.086	0.00000
Coding Scheme*numLasers	4.963	0.00001
numLasers(4,32)	4.812	0.00002 ^
numLasers*Laser WL	4.580	0.00003
Modulation Scheme*Turbulence	2.606	0.00248
Laser WL*SNR	0.541	0.28804
numLasers*Modulation Scheme	0.166	0.68166
Modulation Scheme*Laser WL	0.045	0.90065

Figure 40. Effect Summary, BER.

LIST OF REFERENCES

Andrews, Larry C., and R. L. Phillips. 2001. *Laser Beam Scintillation with Applications.* Bellingham, WA.: SPIE Press.

———. 2005. *Laser Beam Propagation through Random Media*. 2nd ed. Bellingham, WA.: SPIE Press.

Baumert, Leonard D., Robert McEliece, and H.C. Rumsey, Jr. 1978. *Coding for Optical Channel in The Deep Space Network Progress Report.* Report No. 42–49.

Blanchard, Benjamin S., and Fabrycky, W. J. 2001. *Systems Engineering and Analysis.* 5th ed. Boston, MA: Prentice Hall.

Buede, Dennis M. 2009. *The Engineering Design of Systems Models and Methods*. 2nd ed. Hoboken, NJ: John Wiley & Sons.

Chan, V. W. S. 2006. "Free-Space Optical Communications." *Journal of Lightwave Technology* 24, no. 12 (December): 4750–62.

Chief of Naval Operations and Headquarters, U.S. Marine Corps. 2017. *Littoral Operations in a Contested Environment*. Washington, DC: Office of the Chief of Naval Operations and Headquarters, U.S. Marine Corps.

———. 2018. *Expeditionary Advanced Base Operations*. Washington, DC: Office of the Chief of Naval Operations and Headquarters, U.S. Marine Corps.

Crawley, Edward, Olivier de Weck, Steven Eppinger, Christopher Magee, Joel Moses, Warren Seering, Joel Schindall et al. 2004. *The Influence Of Architecture In Engineering Systems.* Boston, MA. MIT.

Crawley, Edward, Bruce Cameron, and Daniel Selva. 2015. *System Architecture: Strategy and Product Development for Complex Systems*. Boston, MA: Pearson.

Defense Acquisition University. 2011. *Defense Acquisition University Guidebook.* Alexandria, VA: DAU.

Djordjevic, Ivan, William Ryan, and Bane Vasic. 2010. *Coding for Optical Channels*. Boston, MA: Springer US.

Fath, Thilo, Falk Schubert, and Harald Haas. 2014. "Wireless Data Transmission Using Visual Codes." *Photonics Research* 2, no. 5 (May): 150–60.

Felder, Adrian W. 2018. "Array based free space optic system for tactical communications." Master's thesis. Naval Postgraduate School.

Frederick, G. W., A. N. George, S. Michael, R. Parenti, J. Roth, J. Taylor, W. Wilcox et al. 2010. “Air-to-Ground Lasercom System Demonstration.” In *2010 Military Communications Conference*, 1594–1600.

Fricke, Ernst, and Armin P. Schulz. 2005. “Design for Changeability (DfC): Principles to Enable Changes in Systems throughout Their Entire Life cycle.” *Systems Engineering* 8, no. 4 (April).

Ghassemlooy, Zabih, W. Popoola, and S. Rajbhandari. 2013. *Optical Wireless Communications: System and Channel Modeling with MATLAB*. Boca Raton, FL: CRC Press.

Haveman, Steven P., and G. Maarten Bonnema. 2013. “Requirements for High Level Models Supporting Design Space Exploration in Model-Based Systems Engineering.” *Procedia Computer Science* 16: 293–302.

Haykin, Simon, and Michael Moher. 2007. *Introduction to Analog and Digital Communications*. 2nd ed. Hoboken, NJ: John Wiley & Sons.

Headquarters United States Marine Corps. 2009. *Employment of the Light Armored Reconnaissance Battalion.* MCWP 3-14. Washington, DC: Headquarters United States Marine Corps.

Hebert, James L., Thomas H. Holzer, Timothy J. Eveleigh, and Shahryar Sarkani. 2016. “Use of Multifidelity and Surrogate Models in the Design and Development of Physics-Based Systems.” Systems Engineering 19, no. 4 (April): 375–91.

Huffman, W. Cary, and Vera Pless. 2003. *Fundamentals of Error-Correcting Codes*. New York, NY: Cambridge University Press.

Joint Chiefs of Staff. 2012. *Joint Electromagnetic Spectrum Management Operations.* JP 6-01. Washington, DC: Joint Chiefs of Staff.

Kang, Eunsuk, Ethan Jackson, and Wolfram Schulte. 2011. “An Approach for Effective Design Space Exploration.” In *Foundations of Computer Software. Modeling, Development, and Verification of Adaptive Systems*. Heidelberg, Germany: Springer Berlin: 33–54.

Karp, Sherman, and Larry B. Stotts. 2012. *Fundamentals of Electro-Optic Systems Design: Communications, Lidar, and Imaging*. Cambridge, United Kingdom: Cambridge University Press.

Kartalopoulous, Stamatios V. 2011. *Free Space Optical Networks for Ultra-Broad Band Services*. Hoboken, NJ: John Wiley & Sons.

Law, Averill M. 2014. *Simulation Modeling and Analysis.* 5th edition. New York, NY: McGraw-Hill Education.

Levis, Alexander H., and Lee W. Wagenhals. 2000. “C4ISR Architectures: Developing a Process for C4ISR Architecture Design.” *Systems Engineering* 3, no. 4 (April): 225–47.

Li, G. Y., Z. Xu, C. Xiong, C. Yang, S. Zhang, Y. Chen, and S. Xu. 2011. “Energy-Efficient Wireless Communications: Tutorial, Survey, and Open Issues.” *IEEE Wireless Communications* 18, no. 6 (June): 28–35.

Lucas, Andrew R. 2013. “Digital Semaphore: Technical Feasibility of QR Code Optical Signaling For Fleet Communications.” Master’s thesis, Naval Postgraduate School.

Maier, Mark W., and Eberhardt Rechtin. 2009. *The Art of Systems Architecting*. 3rd ed. Boca Raton, FL: CRC Press.

Majumdar, Arun K. 2015. *Advanced Free Space Optics: A Systems Approach.* New York, NY: Springer Science.

Muhammad, S. S., T. Javornik, I. Jelovcan, E. Leitgeb, and O. Koudelka. 2007. “Reed Solomon Coded PPM for Terrestrial FSO Links.” In *2007 International Conference on Electrical Engineering*: 1–5.

Nakagami, M. 1960. "The *m* Distribution - A General Formula of Intensity Distribution of Rapid Fading." In *Statistical Methods in Radio Wave Propagation*. New York, NY: Pergamon: 3-36.

Olanrewaju, H. G., J. Thompson, and W. O. Popoola. 2016. “On Spatial Pulse Position Modulation for Optical Wireless Communications.” In *2016 IEEE Photonics Society Summer Topical Meeting Series (SUM)*: 44–45.

Popoola, W. O., E. Poves, and H. Haas. 2012. “Spatial Pulse Position Modulation for Optical Communications.” *Journal of Lightwave Technology* 30 (18): 2948–54.

Raz, Ali K., C. Robert Kenley, and Daniel A. DeLaurentis. 2018. “System Architecting and Design Space Characterization.” Systems Engineering 21, no. 3 (March): 227–42.

Renzo, M. Di, H. Haas, A. Ghrayeb, S. Sugiura, and L. Hanzo. 2014. “Spatial Modulation for Generalized MIMO: Challenges, Opportunities, and Implementation.” In *Proceedings of the IEEE* 102 (1): 56–103.

Richter, Stephen P. 2013. “Digital Semaphore: Tactical Implications Of QR Code Optical Signaling For Fleet Communications.” Master’s thesis, Naval Postgraduate School.

Sanchez, Susan M., and Hong Wan. 2015. “Work Smarter, Not Harder: A Tutorial on Designing and Conducting Simulation Experiments.” In *Proceedings of the 2015 Winter Simulation Conference:* 1795-1809.

Secretary of Defense. 2018. *National Defense Strategy of The United States of America*. Washington, DC: Secretary of Defense.

Schmidt, Jason D. 2010. *Numerical Simulation of Optical Wave Propagation with Examples in MATLAB*. Bellingham, WA: SPIE.

Selva, Daniel, Bruce Cameron, and Ed Crawley. 2016. “Patterns in System Architecture Decisions.” Systems Engineering 19, no. 6 (June): 477–97.

Shannon, Claude Elwood. 1948. A Mathematical Theory of Communication. In *Bell System Technical Journal*. 27, no. 3 (March): 379–423.

Stotts, Larry B. 2017. *Free Space Optical Systems Engineering: Design and Analysis*. Hoboken, NJ: John Wiley & Sons, Inc.

Stotts, Larry B, Paul Kolodzy, Alan Pike, Buzz Graves, Dave Dougherty, and Jeff Douglass. 2010. “Free-Space Optical Communications Link Budget Estimation.” Applied Optics 49, no. 28.

Stotts, Larry B., Brian Stadler, and Gary Lee. 2008. “Free Space Optical Communications: Coming of Age.” In *Atmospheric Propagation V*, 6951:69510W. International Society for Optics and Photonics.

Tatarskii, V.I. 1961. *Wave Propagation in a Turbulent Medium*. New York, NY: McGraw-Hill.

Ulrich, Karl T., and Steven D. Eppinger. 2012. *Product Design and Development.* New York, NY: McGraw-Hill.

United States Marine Corps. 2016. *Marine Corps Operating Concept*. Washington, DC: Headquarters, U.S. Marine Corps.

Woodward, T. K. 2017. “What to Do When There’s No Fiber: The DARPA 100Gb/s RF Backbone Program.” In *2017 Optical Fiber Communications Conference and Exhibition (OFC)*: 1–3.

INITIAL DISTRIBUTION LIST

1. Defense Technical Information Center
   Ft. Belvoir, Virginia

2. Dudley Knox Library
   Naval Postgraduate School
   Monterey, California